NASA CR - 72332

LAC ER- 9757

FINAL REPORT

EFFECT OF NUCLEAR RADIATION ON MATERIALS AT CRYOGENIC TEMPERATURES

by

LOCKHEED NUCLEAR PRODUCTS

C. A. Schwanbeck, Project Manager

prepared for

NATIONAL AERONAUTICS AND SPACE ADMINISTRATION

August 1967

Contract NAS 3-7985

Technical Management
NASA Lewis Research Center
Cleveland, Ohio
Nuclear Systems Division
Charles L. Younger, Project Manager
Advanced Systems Division
John C. Liwosz, Jr.

LOCKHEED NUCLEAR PRODUCTS
LOCKHEED-GEORGIA COMPANY

A DIVISION OF LOCKHEED AIRCRAFT CORPORATION

Contract: NAS 3-7985	Code: U

FOREWORD

This report is submitted to the National Aeronautics and Space Administration, Lewis Research Center, by the Lockheed-Georgia Company in accordance with the requirements of NASA Contract NAS 3-7985.

PRECEDING PAGE BLANK NOT FILMED.

TABLE OF CONTENTS

LIST OF TABLES

LIST OF FIGURES

PRECEDING PAGE BLANK NOT FILMED.

LIST OF SYMBOLS

°K	Degree Kelvin
MeV	Million electron Volts
fJ	femtoJoule
n/cm^2	Neutrons per square centimeter
ϕ	Fast Neutron Flux, energies over 0.5 MeV (80 fJ)
F_{tu}	Ultimate Tensile Strength
F_{ty}	Tensile Yield Strength
psi	Pounds per square inch
N/cm^2	Newtons per square centimeter
E	Modulus of elasticity in tension
σ_e	Elastic Strain
σ_p	Plastic Strain
σ^p	Strain
N	Newton
Hz	Hertz (cycles per second)

EFFECT OF NUCLEAR RADIATION ON MATERIALS AT CRYOGENIC TEMPERATURES

by

LOCKHEED NUCLEAR PRODUCTS

C. A. Schwanbeck, Project Manager

1 SUMMARY

This report describes the result of a test program investigating the effects of cryogenic and combined nuclear-cryogenic environments on the mechanical properties of several metals and alloys. The effects on tensile properties of strain hardened poly-crystalline high purity aluminum, commercially pure titanium, Titanium - 5 aluminum - 2.5 tin, and Titanium - 6 aluminum - 4 vanadium are reported in detail. The Titanium - 5 aluminum - 2.5 tin was tested at two levels of interstitial content; the Titanium - 6 aluminum - 4 vanadium was tested in both the annealed and the aged conditions. Effects on the fatigue behavior under high load, low cycle rate loading conditions are reported for commercially pure titanium and Titanium - 5 aluminum - 2.5 tin. In all cases, unirradiated room temperature control specimen were tested and the results are herein reported as reference data.

The most noticeable effect of cryogenic temperature on the high purity aluminum was a sharp decrease in the yield strength/ultimate strength ratio at low temperatures. Irradiation at cryogenic temperatures produced an increase in yield strength which caused a pronounced recovery in the value of this ratio. The results of irradiation temperature, and post-irradiation annealing studies show that the effects induced by irradiation to 10^{17} neutrons per square centimeter with energies greater than 0.5 MeV (80 femtojoule), at 17 degrees Kelvin appear to be completely annealed out when tested at much lower temperatures. However, testing the irradiated material at 17 degrees Kelvin following annealing at various temperatures including 300 degrees Kelvin, indicates considerable residual irradiation effects

For titanium and titanium alloys, increasing levels of irradiation produced an essentially linear increase in the strength parameters measurable in tensile testing, although increased interstitial content appears to increase data scatter.

Fatigue test data indicated the cryogenic increase in fatigue life is markedly less than the similar increase in ultimate tensile strength for unalloyed titanium. For the solid solution of aluminum and tin in alpha titanium, the cryogenic increases in fatigue life and ultimate tensile strength are about the same. Irradiation effects in all cases seem more pronounced at higher load levels. The higher interstitial content in Titanium - 5 aluminum - 2.5 tin alloy seems to increase the fatigue life in all conditions.

PRECEDING PAGE BLANK NOT FILMED.

2 INTRODUCTION

The need for engineering evaluation of the combined neutron-irradiation cryogenic effects on structural materials has long been recognized by people responsible for advanced design in the aero-space program. Both low temperature environments and neutron bombardment produce embrittlement in many metals and alloys. Defects introduced by neutron irradiation are mobile even at the boiling point of liquid-hydrogen (20.5 degrees Kelvin). Tests must, therefore, be conducted with the specimens held at the temperature of interest during the entire irradiation and testing period.

A screening program on selected engineering alloys was previously conducted (ref. 1). Test results from the screening program indicated that titanium alloys were not markedly affected by irradiation to 1×10^{17} neutrons per square centimeter (n/cm^2)* at 17 degrees Kelvin (°K). On the other hand, moderately strain-hardened poly-crystalline high purity aluminum (Aluminum 1099-H14) was found to be very sensitive to low temperature irradiation.

An in-pile test program was initiated to investigate in greater detail the effects of a combined nuclear-cryogenic environment on the mechanical properties of these metals. The scope of the program consists of three general phases:

(1) The effects of cryogenic irradiation and annealing on tensile properties of poly-crystalline high purity aluminum.

(2) The effects of cryogenic irradiation on tensile properties of unalloyed titanium and alpha titanium alloys.

(3) The effect of cryogenic irradiation on low-cycle fatigue properties of unalloyed titanium and Titanium - 5 aluminum - 2.5 tin (Ti-5Al-2.5 Sn) alloy.

Test results for each of these phases are reported and discussed in the following sections of this report.

*Neutron energies are greater than 0.5 million electron volts (80 femtojoule).

3 TEST MATERIALS AND SPECIMENS

All test specimens for each material were made from one special lot of the material with a common melting and fabrication history. The complete history has been published previously (ref. 2); a summary of the mechanical properties and chemical composition is given in tables I and II. The same material lots were used in a previous test program (ref. 1).

Space and refrigeration capacity limitations in the available reactor access port require the use of miniature test specimens in this experimental hardware. The tensile specimens used (figure 1) are geometrically similar miniaturizations of the standard 0.500 in (1.27 cm) round specimen of ASTM E 8-66 (ref. 3) with the gage diameter reduced to a nominal 1/8 inch (0.318 cm).

Fatigue specimen design is much less standardized than that for tensile specimens. The actual specimen design may be varied to accommodate individual test parameters, such as load control through stress amplitude or strain amplitude. The test program consisted of low cycle - high load fatigue testing conducted within the load range where appreciable plastic behavior may be expected. The specimen design shown in figure 2 was a modification of several widely used forms designed to minimize bending during the compressive position of the load cycle.

PRECEDING PAGE BLANK NOT FILMED.

4 TEST PROCEDURE

All testing was performed at the NASA Plum Brook Reactor Facility using testing equipment specially designed and built by the Lockheed-Georgia Company. Temperature control was maintained with an 1150 watt helium refrigerator designed by the A. D. Little Company. Design and operating features of this equipment have been discussed in a previous report (ref. 1).

4.1 TENSILE TESTING

The tensile testing phase of the program was conducted, as nearly as feasible, in accordance with the provisions of the applicable ASTM specifications, ASTM E 8-66 and ASTM E 184-62 (ref. 3). The tensile load was applied at a strain rate which did not exceed 9×10^{-2} per second during elastic behavior. The load was monitored with a proving ring type dynamometer calibrated to within two percent of National Bureau of Standards certified reed type proving ring. The extensometer used was classified as ASTM E 83-64T, class B-2 under actual operational conditions. The accuracy and calibration of the test system is discussed in detail in Appendix A.

4.2 FATIGUE TESTING

Fatigue testing practice is much less standardized than tensile testing; indeed the only ASTM standard relating to fatigue testing of metallic materials, ASTM E 206-66 (ref. 3), is limited in scope to the definition of terms and description of statistical treatments. A wide variety of specimen designs and load methods are in current use for special applications. For this program, fatigue testing consisted of low cyclic rate - high loading patterns with a test run-out of 10^4 cyclic reversals from compression to tension with a test ratio of -1. Coffin (ref. 4) and Manson (ref. 5) have prepared review articles on low cyclic fatigue which provide good background sources in this area of interest.

For fatigue testing, the existing tension/compression system was modified to permit conducting fatigue tests in-pile. The modified system is shown schematically in figure 3 and permits axial loading, not over 5000 pounds (22,240 newtons) in tension and/or compression at cyclic rates up to 0.5 Hz. This system is essentially a closed loop electro-hydraulic servo system which automatically applies a sinusoidal cyclic load to the specimen. The maximum tensile load is equal to the maximum compression load and is predetermined by the specimen dimension (at its minimum diameter) and by the stress load to be employed in the test. (Strain was not monitored in this test program.) The load sensing element used by the servo system is the test loop proving ring type dynamometer, which is also used for tensile testing. Through error detector circuitry the system amplifies small differences between the load and a sinusoical input signal and matches the load to the signal by way of a servo valve in the hydraulic loading system.

At the beginning of a test, the cyclic load amplitude is gradually increased, in about 10 cycles at 0.1 Hz, to the test load amplitude. This ramp is required to accurately set the test load amplitude without overshooting. At the end of the ramp, the cyclic rate is increased to 0.25 Hz and automatic cycle counting is started. A few tests were also conducted at cyclic rates of 0.1 Hz and 0.5 Hz.

The cyclic load is recorded versus time during the ramp and at intervals during the testing as a check on the performance of the control system. The test stops automatically on reaching 10,000 cycles or when the specimen fails.

A more detailed discussion of the equipment modifications and operating characteristics is given in Appendix B.

All fatigue tests, regardless of temperature and irradiation condition were conducted in a gaseous helium atmosphere to preclude the possibility of an environmental effect, such as described by Shen, et al (ref. 6) influencing the test data.

4.3 MEASUREMENT AND CONTROL OF SPECIMEN TEMPERATURE

Direct measurement of the specimen temperature during exposure and testing was not feasible. Therefore, platinum resistance thermometers, located some thirty feet from the test zone, were calibrated to monitor and control test specimen temperature. These temperature sensors were positioned in the helium gas streams in the inlet and return legs of the refrigeration manifold.

For calibration, both tensile and fatigue specimens were prepared with copper-constantan thermocouples welded or soldered at each end and the mid-point of the specimen gage length. These instrumented test specimens were calibrated and then installed in the normal test position in a test loop. Calibration curves for each thermal environment were then preoared for use in the test program.

A more detailed discussion of the temperature calibration technique is contained in Appendix C.

The calibration technique and curves obtained for the platinum resistance thermometers assures the maintenance of specimen temperature within $\pm$ 0.5°K during exposure in-pile or out-of-pile.

4.4 DETERMINATION OF NEUTRON ENVIRONMENT

Fast neutron dose rates in the test location in HB-2 were determined during performance of the screening program (ref. 1) using foil measurement techniques. The resultant flux curve versus reactor control rod bank position is shown in the upper portion of figure 4.

During performance of the test program reported herein, seven additional foil packages were irradiated and evaluated. Sets of foils, as shown in Table III, were placed in the test specimen location of a test loop in an aluminum foil holder. The foils were then irradiated for thirty minutes with sufficient refrigeration provided to prevent the melting of the sulfur foil from gamma heating. Reactor operational parameters were recorded at the time of irradiation. The activities of the irradiated foils were measured using standard counting techniques. The resultant spectral curves are shown in the lower portion of figure 4.

Examination of the family of spectral curves in figure 4 shows the new measurements to be somewhat lower at high rod bank positions than the screening program (ref. 1) measurements. The difference, however, is within the uncertainty of measurement using this technique.

During irradiation of test specimens in the present program, the accumulated neutron flux dosage with energies greater than 0.5 MeV ($E > 80$ fJ) was calculated hourly using reactor operational parameters and the flux curve shown in the upper portion of figure 4.

4.5 STRUCTURAL STUDIES

Structural studies in conjunction with the test program consisted of:

(1) Optical metallography of failed tensile specimens;
(2) X-ray diffraction on failed tensile specimens;
(3) Electron metallography of failed fatigue specimens.

Optical metallography of failed tensile specimens was performed by remote techniques in the PBRF hot laboratory. Fractured specimens were sectioned, mounted in bakelite, ground, vibratory polished (using Linde A and B), and then etched. For aluminum, Keller's etch was used, and for titanium a mixed acid (1% HF - 2% HNO_3 - 97% H_2O) etchant was used. Photomicrographs were made of the fracture zone, the strained region near the gage mark, and the unstrained region near the specimen end section.

X-ray diffraction of failed tensile specimens consisted of both back-reflection Laue patterns and diffractometer traces. Specimens mounted for optical metallography were also used for X-ray diffraction studies.

Back-reflection Laue patterns were obtained for both the strained region near the fracture and the unstrained region near the end section. Diffractometer traces were obtained from only the end section of the test specimen due to the small size of the gage section.

Electron microstructures of Titanium 55A fatigue specimens were obtained using replication techniques. The fractured face and the strained region along the side of the fracture were replicated and processed as follows:

- Replication using Fax-Film,
- Two-directional gold shadowing of replicas,
- Carbon coating gold shadowed replicas,
- Refluxing carbon-coated replicas with acetone,
- Examination of refluxed samples using Phillip's EM-100-B and photographing selected areas using Ilford 5B11 film.

Representative electron fractographs are presented in Appendix K.

5 TEST RESULTS AND DISCUSSION

Evaluation and interpretation of irradiation effects test data requires a combination of evaluation in the context of physical metallurgy, interpretive considerations in the solid state level and a limited statistical analysis of the values involved. The test results generated in the testing program are reported and discussed in the following sections according to the program objectives which were previously defined and consist of three general phases of investigation:

(1) The effects of cryogenic irradiation and annealing on tensile properties of high-purity aluminum.

(2) The effect of cryogenic irradiation on tensile properties of unalloyed titanium and alpha titanium alloys.

(3) The effect of cryogenic irradiation on low-cycle fatigue properties of unalloyed titanium and titanium - 5 aluminum - 2.5 tin alloy.

5.1 TENSILE PROPERTIES OF HIGH-PURITY ALUMINUM

Aluminum 1099-H14 is a high-purity, poly-crystalline aluminum and, from the view of the physical metallurgist, would be considered as essentially elemental face-centered-cubic aluminum. It is a rather low strength material with limited aerospace structural application. The material had earlier (ref. 1) been observed to exhibit large cryogenic effects and significant irradiation effects at relatively low fast neutron fluences. It was selected for study in this program primarily as a tool for investigation of cryogenic irradiation effect mechanisms. However, the poly-crystalline form of this material, the presence of trace impurities, and the strain hardened condition (-H14) in its initial test condition result in much greater structural complexity than is found in single crystal studies.

The scope of the tensile testing of aluminum 1099-H14 in this program consists of the following four studies:

(1) Effects of irradiation at 17°K
(2) Effects of irradiation temperature
(3) Effects of annealing and test temperature following irradiation
(4) Effects of annealing following irradiation

For each of these investigations, unirradiated test data were generated which duplicated the thermal environment of the corresponding irradiated test data with the exception of time at temperature during irradiation. The unirradiated test data were held for one hour at the temperature of interest; the irradiated specimens required from 4 to 20 kiloseconds of irradiation at temperature of interest. Post-irradiation thermal treatments were the same for both irradiated and unirradiated material.

5.1.1 Effects of Irradiation at 17°K

This study is to determine the effects of neutron irradiations up to 3×10^{17} n/cm^2 at 17°K. The specimens are held at 17°K throughout irradiation and tensile testing. Test results are shown graphically in Figure 5 and are compiled in detail in Appendix D.

Examination of Figure 5 shows that the net change in the strength and ductility functions is dependent on irradiation level, with no evidence of saturation effects at these irradiation levels. Note also the effect on the F_{ty}/F_{tu} ratio which is clearly dependent on the level of irradiation. The cryogenic depression of this ratio at 3×10^{17} n/cm^2, evident in the unirradiated control specimens tested at 17°K, (see figure 6), has virtually been eliminated by interaction between neutrons and lattice atoms. In this instance, the irradiation effect seems to resemble the effect of cold working on the intracrystalline critical shear stress.

The optical micrographs proved to be of little interpretive value due, in part, to the difficulty of assessing the effect of gamma irradiation on the attack rate of etchants on irradiated specimens.

The X-ray diffraction data on the Aluminum 1099-H14 was in no way inconsistent with the difference between low temperature yielding and initiation of plastic behavior at normal temperatures. However, no conclusive observations could be made to support the explanation for the observed property changes. The random variations in intercrystallite lattice orientations normally present in strain deformed, fairly coarse grained materials might be expected to obscure definitive interpretations of subsequent lattice distortions.

5.1.2 Effects of Irradiation Temperature

This phase of the testing program is for the purpose of studying the magnitude of the irradiation effect as a function of irradiation temperature. The specimens are irradiated to 1 x 10^{17} n/cm^2 at 78°K, 178°K, or 300°K, then tested in tension at the irradiation temperature. Unirradiated control specimens were stabilized and held one hour at temperature of interest prior to testing. The test data for 17°K is the same as that discussed in section 5.1.1. Test results are shown graphically in figure 7 and are reported in detail in Appendix E.

Comparison of figures 6 and 7 shows a marked similarity in geometric form in all functions except the yield strength (F_{ty}) and, naturally, the F_{ty}/F_{tu} ratio. The effect of irradiation at or near room temperatures is slight at levels of 10^{17} n/cm^2; the effect of cryogenic irradiation is observable particularly in the changes induced in the yield strength (F_{ty}) and, obviously, the F_{ty}/F_{tu} ratio.

The optical micrographs and X-ray diffraction data, as noted previously (section 5.1.1) were of little interpretive value. The small physical dimension of residual effects of neutron irradiation also contributes to this lack of interpretive value.

5.1.3 Effects of Annealing and Test Temperature Following Irradiation

This study is to determine the magnitude of irradiation effects remaining at various temperatures following irradiation at 17°K. The specimens were irradiated to 1 x 10^{17} n/cm^2 at 17°K, warmed to 78°K, 178°K or 300°K, annealed at that temperature for 3.6 kiloseconds and tested at that temperature. Unirradiated control specimens had an identical thermal history during the test cycle with one exception; the time at 17°K was 3.6 kiloseconds compared to a nominal 50 kiloseconds for the irradiated specimens. Test results are shown graphically in figure 8 and are reported in detail in Appendix F.

Comparison of figures 7 and 8 indicates that the net effects of annealing and testing at temperatures above the irradiation temperature of 17°K are quite similar to those resulting from irradiation at the "annealing" temperature. Annealing and testing at near room temperature results in essentially complete removal of irradiation induced effects. Annealing and testing at lower temperatures leaves a significant irradiation induced effect on the F_{ty} and the F_{ty}/F_{tu} ratio, with a lesser residual effect on the F_{tu}.

The optical micrographs and X-ray diffraction data, as in previous discussions, proved to be of little use in interpreting radiation effects.

5.1.4 Effects of Annealing Following Irradiation

This study is to determine the magnitude of recovery at various temperatures of irradiation effects occuring at 17°K. The specimens are irradiated to 1×10^{17} n/cm^2 at 17°K, then warmed to 78°K, 178°K, or 300°K, annealed at that temperature for 3.6 kiloseconds, cooled to and stabilized at 17°K and then tested at 17°K. Unirradiated control specimens were given the same thermal treatment with one exception; the initial 17°K holding period was 3.6 kiloseconds of temperature rather than the nominal 50 kiloseconds of irradiation exposure at 17°K. Test data for 17°K without annealing was previously presented in section 5.1.1. Test results are shown graphically in figure 9 and are reported in detail in Appendix G.

Since a direct comparison with the annealing studies discussed in section 5.1.3 is desirable, a sumation of test data in both sections is given in figure 10 with the data reduced to a common set of ordinates. Due to the large variation of the magnitudes in the individual function between the different test conditions, this plot is based on test value ratios (V) as a function of temperature. The test value ratio was determined as follows:

For anneal at T and test at 17°K

$$V_{17} = \frac{F_t \text{ @ 17°K after irradiation to } 10^{17} \text{ at 17°K and 3.6 kiloseconds anneal at T}}{F_t \text{ @ 17°K, no irradiation}}$$

For anneal and test at T

$$V_T = \frac{F_t \text{ @ T after irradiation at 17°K to } 10^{17} \text{ and 3.6 kiloseconds anneal at T}}{F_t \text{ @ T, no irradiation}}$$

where V = TEST VALUE RATIO
T = Annealing temperature
F_t = Tensile Test Value obtained at described condition

In the interest of clarity, only the F_{tu} and F_{ty} have been included in the plot shown in figure 10 Examination of this plot shows that an effect of irradiation at 17°K on F_{ty} appears to anneal out if tested at higher temperatures but is still observable through post-annealing testing at 17°K.

Optical micrographs and X-ray diffraction data were again of little interpretive value.

in work hardening during fabrication because of the lack of similar differences in the ultimate strength and ductility values. Although little work has been done at extremely low temperatures on this material, test data from other laboratories (ref. 7) indicates the probability of a cold-work dependent divergence of F_{ty} at temperatures below 80°K for commercially pure aluminum (Aluminum 1100).

Therefore it is concluded that the noted differences can be attributed to stock variation and fabrication variables rather than to differences in test conditions.

Examination of the data shown in figure 6 shows the significant effect of cryogenic environments, without irradiation, on the strain hardened aluminum. The F_{ty} is relatively insensitive to temperature variation while the F_{tu} is strongly temperature dependent, particularly below 78°K. This, naturally, produces a profound effect on the F_{ty}/F_{tu} ratio, which drops from near unity, at room temperature, to 0.32 at 17°K. The elongation in 0.5 inch (1.27 cm) is markedly increased by reduction in temperature while the reduction of area shows a sharp decrease below 78°K. The relatively high reduction of area to elongation ratio at temperatures above 78°K indicates a large degree of necking down during late plastic behavior while a value near unity for this ratio at lower temperatures is indicative of uniform plastic strain.

The overall effect on mechanical properties of cryogenic exposure, in the absence of irradiation, would seem to resemble annealing. Comparison of tensile test data for other strain-hardened aluminum alloys tested at room temperature with data obtained at or below liquid nitrogen temperatures, obtained with the experimental equipment used in this program (ref. 1) and in other laboratories (ref. 7), also indicate a cryogenic influence on the mechanical properties which resembles thermal annealing in the mitigation of strain-hardening effects. The ductility parameters for Aluminum 1099-H14 at 17°K are similar to those of Aluminum 1099-0 at room temperature and the strength functions have a similar relationship, with the 17°K values showing a cryogenicly induced increase in magnitude by about a factor of three. As figure 6 shows these effects are slight above 170°K, moderate in the region of 78°K and quite marked at lower temperatures.

Although the range of the data for the F_{ty} obscures the magnitude of a specific effect, the overall relationship of the several tensile test parameters justifies the general validity of the previously reported (ref. 1) hypothesis that the intragranular critical shear stress of this material is below the microscopic elastic limit at very low temperatures and early plastic strain is produced through the formation of mechanical twins.

The effect of fast neutron irradiation at 17°K shown by the data presented in figure 5, appears similar to that of the initial cold work which provides the H14 temper. Even at quite low irradiation exposures, 5×10^{15} n/cm^2, the hardening effect is observable through a slight increase in the F_{ty} and the F_{ty}/F_{tu} ratio. The net increases in both F_{ty} and F_{tu} are essentially linear functions of irradiation level to 3×10^{17} n/cm^2; however, the greater slope of the F_{ty} shown in figure 5 indicates an irradiation hardening effect similar to cold work. The increase in F_{ty}/F_{tu} ratio as a function of irradiation level is shown in the same figure. The inter-relationship of the mechanical properties at 17°K with increasing irradiation levels approachs that of the unirradiated material at room temperature with but two notable exceptions: the much greater tendency for necking-down immediately prior to failure (shown by the reduction of area) and the lower fracture stress for the unirradiated material. Since the data required to provide a correction for the tri-axial loading conditions during fracture of the unirradiated material are not available these fracture stress values are likely to be in error (ref. 8). The greater instability in tension of the unirradiated material might be attributed to a difference in the nature of void nucleation sites between irradiated and unirradiated aluminum. Grain boundry dislocation pile-ups large enough to produce cavity dislocations would appear more probable as a source of fracture initiation in irradiated material, the failure would be more likely to originate at foreign particle sites in the unirradiated stock. However, since the formation of a neck under tensile stresses occurs after maximum load during deformation, the engineering importance of this difference in behavior seems limited.

A rapid evaluation of the effects of test temperature of Aluminum 1099-H14 with various irradiation histories can be made by comparing figures 6 through 9. The data plotted in figure 7, was obtained from specimens irradiated to 10^{17} n/cm^2 at the test temperature; that plotted in figure 8, from specimens irradiated to 10^{17} n/cm^2 at 17°K and held at the test temperature for one hour prior to testing. Comparison of figures 7 and 8 shows no essential difference in the data; apparently the irradiation temperature is not significant if the specimens are annealed and tested at temperatures at or above the irradiation temperature. At temperatures above 178°K the curves shown in figures 7 and 8 are similar to those of figures 6 and 8. The effect of irradiation to 10^{17} n/cm^2 at and above this temperature is negligable. Below 178°K, the effect of the level of irradiation on the F_{ty} is pronounced and the F_{ty}/F_{tu} ratio remains reasonably constant and the degree of specimen necking is reduced.

In examination of figure 10, a comparison of the mitigation of the effects of irradiation to 10^{17} n/cm^2 at 17°K through annealing as measured at the annealing temperature and at the irradiation temperature, shows that a marked residual irradiation effect is observable by post-annealing testing at 17°K which is not discernable through testing at annealing temperatures.

5.1.5 Discussion

Examination of the several figures referenced in the preceding sections (5.1.1 through 5.1.4) reveals an inter-relationship of the test data generated under varying conditions for Aluminum 1099-H14

The material was tested at 17°K, 78°K, 178°K, and 300°K without irradiation to obtain control test data for the nuclear cryogenic irradiation and annealing studies. These data appear in appendicies D through G and are represented graphically in figures 5 and 6. The 17°K control data shown in figure 5 is from reference 1. To allow ready comparison of the test data, mean values of all results obtained in the aluminum tensile testing program are presented in table IV.

Extra test values were obtained for control purposes at the various temperatures to determine if there were any possible systematic effects of temperature changes prior to testing. If existant, such changes could be attributed to differential thermal contraction in the specimen loading components of the test loop and would have to be considered in the evaluation of the annealing data taken with the test loop components subjected to the same temperature changes. It should be noted that special precautions during insertion of the specimen and preparation for testing are meant to exclude this possibility. If observed at all, such effects would be observed in the yield strength values. Evaluation of the data indicates that in nearly all cases, there are no statistically significant differences (at the 90% confidence level).

At 178°K there is a significant difference, however, this difference is attributable to location in the stock from which the specimens were taken. The test specimens are numbered according to the location from which they were taken in the plate stock and are generally chosen at random for a particular test condition. This results in effects due to variations in the material and tensile properties within the stock being averaged out. However, in this particular case there was an error in the choice of specimens with the resulting nonrandom location which could easily account for the small but statistically significant difference between the yield strength values from the two groups of tests at 178°K. This conclusion is confirmed by differences in ultimate strength and ductility values which can also be attributable to location in the stock.

Although there are no significant differences between the various groups of tests at 17°K, there is a significant difference between these values as a group obtained in the current program and the values obtained at the same temperature in the screening program (ref. 1). These differences have to be attributed to differences

A summary of the test data presented in this section indicates that the most pronounced effect is the depression of the F_{ty}/F_{tu} ratio at low temperatures, coupled with an essentially linear recovery of this parameter with increasing irradiation levels. At room temperature, it appears the grain boundaries block the travel of dislocation movement. Due to the relatively large amplitude of the thermal oscillation of the lattice atoms at this temperature, annihilation of strain induced Frenkel pairs through recombination limits the intra-crystallite defect generation at locii of maximum point stresses, preventing twinning at stresses below the macroscopic yield stress. The reduction of the thermal vibration at low temperatures allows development of point stresses above the intragranular critical shear stress and twinning occurs. Since the individual crystallites are elongated and oriented parallel to the direction of stress by cold work, the resultant twinning produces departure of the stress-strain curve from linearity. Irradiation produces large populations of solid state defects and the action of the grain boundary, considered as an array of dislocations, becomes less important as an obstical to travel. As a result, the macroscopic critical shear stress again governs plastic behavior. The effect of test temperature on the mitigation of annealing effects, shown in figure 10, might also be considered as indicative of the importance of thermal vibrations of lattice atoms in the evaluation of irradiation effects in light metals.

5.2 THE EFFECT OF CRYOGENIC IRRADIATION ON TENSILE PROPERTIES OF UNALLOYED TITANIUM AND ALPHA TITANIUM ALLOYS

The titanium alloys of primary alpha structure usually exhibit good cryogenic properties due to the hexagonal close-packed structure of this phase. They have a high modulus of rigidity and a strength-weight ratio which is comparable with the best aluminum alloys. Screening program test results (ref. 1) indicated that titanium alloys were not markedly affected by irradiation to 1×10^{17} n/cm^2 at 17°K. To investigate the radiation resistance of these alloys, the following investigations were undertaken:

- Effects of irradiation at 17°K on commercially pure titanium (Titanium -55A).
- Effects of interstitial content in Titanium - 5 Al - 2.5 Sn on changes due to irradiation at 17°K.
- Effects of initial heat treatment of Titanium - 6 Al - 4 V on changes due to irradiation at 17°K.

Mean values of the test results for the titanium tensile testing program are shown in figure V.

Out-of-pile test data and in-pile test data for irradiations to $1 \times 10^{17} n/cm^2$ were obtained in the screening program (ref. 1).

5.2.1 Effects of Irradiation at 17°K on commercially pure Titanium (Titanium - 55A)

Titanium 55A is essentially commercially pure elemental titanium and exhibited a small but measurable increase in yield strength due to fast neutron irradiation of 10^{17} n/cm^2 at 17°K in earlier test program (ref. 1). Additional test data for irradiation at 17°K to 6×10^{17} and 1×10^{18} n/cm^2 and tensile testing at 17°K without interim warming were obtained during performance of this program. Test results are shown in figure 11 and are reported in detail in Appendix H.

The data plotted in figure 11 show that there is a direct dependence of F_{tu} and F_{ty} on irradiation level (to 10^{18} n/cm^2) accompanied by a significant but not critical reduction in ductility parameters. No degradation of any mechanical property of sufficient magnitude to compromise engineering integrity after exposures to 10^{18} n/cm^2 was observed.

Titanium 55A is essentially a polycrystalline titanium of commercial purity. This material was tested in the annealed condition, but with standard interstitial content; therefore, the population of "foreign" substitutional solute atoms should be small but the number and distribution of interstitial atoms should be similar to the interstitial populations in alloyed materials. Since alpha titanium is a hexagonal close packed lattice material, slip might be expected to be fairly laminar--particularly with a relatively small population of substitional atoms. The presence of interstitials might be expected to increase turbulence of the flow during slip. Since the reported F_{ty} is based on 0.2% offset rather than on divergence from Hookes Law, the relatively low (for titanium alloys) F_{ty}/F_{tu} ratio of about 0.7 at 17°K, both unirradiated and at 1×10^{17} n/cm^2, indicate a rather laminar behavior, the increase of this parameter to 0.75 at 6×10^{17} n/cm^2 and 0.78 at 1×10^{18} n/cm^2 indicates an increase in turbulence resultant from lattice imperfections induced by increased irradiation levels.

Optical micrographs proved, as was the case for Aluminum 1099, to be of little interpretive value due, in part to the difficulty of assessing the effect of gamma irradiation on the attack rate of etchants on irradiated specimens. The X-ray diffraction patterns obtained show no distinctive pattern of irradiation effects.

5.2.2 Effects of Interstitial Content in Ti-5 Al-2.5 Sn on Changes Due to Irradiation at 17°K

Titanium - 5 Al - 2.5 Sn is a fairly high strength alpha phase alloy ($F_{tu} \approx$ 120 Ksi at room temperature) and is commercially available in standard and extra low interstitial (less than 0.125% interstitials, and designated ELI) grades. Screening program (ref. 1) nuclear cryogenic tests to 10^{17} n/cm^2 at 17°K, indicate that the ultimate strength of the ELI material may be adversely affected by the neutron irradiation. It is conceivable that higher irradiations might cause adverse effects on various properties, including fatigue strength, which would negate any inherent advantages of the ELI material.

During this program, both standard interstitial and extra low interstitial grades of Ti-5 Al-2.5 Sn were irradiated at 17°K to 1 x 10^{18} n/cm^2 and tested at 17°K without interim warming. Test results are shown in figures 12 and 13 and are reported in detail in Appendix I. Unirradiated test data and values for 1 x 10^{17} n/cm^2 are results from the screening program (ref. 1).

Comparison of the data plotted in figures 12 and 13 show that both interstitial grades of Ti-5 Al-2.5 Sn are increased in strength with an accompanying decrease in ductilities as a result of irradiation to 1 x 10^{18} n/cm^2 at 17°K. The magnitude of change is about the same for both grades, however the standard interstitial grade was subject to extremely large scatter in test data (figure 12). Examination of the material composition shown in table 1 shows a rather high hydrogen content (0.57 atomic %). The possibility of an interaction between fast neutrons and interstitial hydrogen atoms is suggested in the case of the standard interstitial material. The presence of similar consistent relationship between strength and ductility parameters in conjunction with an apparently random variation in the magnitude of the irradiation effects seems to support this premise.

Optical micrographs did not provide interpretive assistance, but examination of the Laue rings in the back-reflection X-ray photographs showed a systematic difference between the extra low interstitial material and the standard alloy. A typical set of these patterns, obtained from specimens tested in tension at 17°K after irradiation to 10^{18} n/cm^2, are shown in figure 14. The difference in these patterns was consistent for all test environment observed, and appears dependent solely on interstitial content.

Obviously, since the diffraction of X-rays is a function of the atomic number of the diffracting atom, these observed differences are not a direct result of interstitial content but, rather, a record of a physical result of straining altered by the interstitial atom population density.

Examination of the patterns obtained from the unstrained portions of the specimen reveals essential similarity for both interstitial grades. However, after cold work the rings obtained from the ELI material are of a grainier nature; the individual points which form each ring are less numerous but of greater intensity. This is indicative of a somewhat greater deformation within individual crystallites in the ELI stock after failure. It appears that the ELI material received a larger amount of actual plastic strain.

The difference in the degree of actual plastic strain is slight and, apparently, not of practical significance in tensile behavior. In fact, it is not detectable from the relatively insensitive tensile parameters; 0.2% off-set yield strength, elongation, and reduction of area, normally used as measured of tensile plastic strain. However, this difference in the material response to load may be of increasing importance in cyclic loading at high unit stresses and may help explain the observed increase in fatigue life with increased interstitial content discussed in section 5.3.2 of this report.

5.2.3 Effects of Initial Heat Treatment of Ti-6 Al-4 V on Changes Due to Irradiation at 17°K

Titanium - 6 Al - 4V is an alpha-beta alloy. In the annealed condition the microstructure contains the metastable beta phase in an alpha matrix. Solution treating and aging largely transforms this metastable beta phase into alpha during the aging treatment. Irradiation to 10^{17} n/cm^2 at 17°K (ref. 1) showed measurable increases in the strength of the aged material but not the annealed materials. High irradiations at the same temperature may confirm this effect and may possibly yield fundamental information regarding the effects of nuclear irradiation on precipitation processes. Such effects are still not very well understood although they are of wide general interest to both basic researchers and applications people.

Additional test data for irradiations to 1×10^{18} n/cm^2 at 17°K were obtained for both annealed and aged conditions of Ti-6 Al-4 V. Test results are plotted in figures 15 and 16 and are reported in detail in Appendix J.

An examination of figures 15 and 16 shows that irradiation to 10^{18} n/cm^2 at 17°K caused an increase in strength of both the annealed and aged material without significant effect on ductilities. The magnitudes of the strength increases are about the same for both material conditions, however the test data for the aged material exhibits a large scatter in 10^{18} n/cm^2 strength values. This effect is probably similar to that occurring in Ti-5 Al-2.5 Sn (standard interstitial grade). Examination of the material compositions shown in table 1 shows a notable similarity in the hydrogen content for the two materials with large data scatter.

The optical micrographs and x-ray diffraction data were of little interpretive value for the Ti-6 Al-4 V alloy.

The changes in the mechanical properties of both conditions of Titanium 6 Al-4 V, observable by comparison of figures 15 and 16 are similar to the effects previously noted in Titanium 5 Al-2.5 Sn in two interstitial grades (figures 12 and 13). These changes seem consistent with an increase in the turbulence pattern of internal flow during the transition from elastic behavior resulting from an increase in foreign precipitate populations and the introduction of additional lattice perturbations through fast neutron-lattice atom interaction.

5.2.4 Discussion

From the view of the physical metallurgist, Titanium 55A would be considered as essentially elemental form. However, the polycrystalline form of this material and the presence of trace impurities, complicate model formation based on solid state theory. The alloyed titaniums are somewhat more complex structurally than the unalloyed material. Examination of the binary equalibrium diagrams of titanium with each of the alloying elements shown in table I shows that aluminum is a strong alpha stabilizer, while the negative slope of the alpha-beta transus on the Ti-Sn and Ti-V curves indicates that they tend to promote beta retention under non-equilibrium conditions.

However, the beta transus for commercially pure titanium is about 1173°K for Titanium 5% Al-2.5% Sn it is about 1311°K, and for 6% Al-4% V, about 1266°K. Alpha stability should be sufficient to prevent irradiation induced phase transformations at cryogenic temperatures in all the materials tested. The alloying elements, from a solid state view, may be considered as substitutional solute atoms in a metastable hexagonal close packed lattice. The presence of "foreign" atoms with different atomic radii also tend to generate Frenkel pairs of vacancies and interstitials* which serve as generators of dislocations. Grain boundaries may be considered as arrays of dislocations.

The hexagonal close packed structure of the titanium alloys provides a great number of planes which accommodate dislocation movement and may be expected to have a large laminar component, and smaller turbulent component, in plastic flow.

Comparison of the sets of data presented in figures 11 through 16 indicates that the presence of interstitial hydrogen and, to a lesser degree, the other gaseous interstitials may exert a rather unpredictable effect on preferential displacements and defect generation during neutron irradiation. Slip in hexagonal lattices, such as these alpha generated by "foreign" constituents such as interstitials, substitutional solute atoms and intermetallic or second phase precipitates. This increase in turbulence is shown by increased in the F_{ty}/F_{tu} ratio caused by alloying, irradiation, or aging treatments. Since the gaseous interstitials, particularly hydrogen, are within a few orders of the neutron mass, the neutron interstitial atom interaction might be expected to vary the turbulent component of flow during slip. Since this interaction is a random event, it apparently causes an increase in the data randomization observable in a wider data scatter band at high fluences.

An effect on the commercially pure titanium, somewhat similar to that observed in pure aluminum, of F_{ty}/F_{tu} reduction at low temperatures with radiation induced recovery, may be observed from the test data. This effect is of a much smaller magnitude due to the annealed state of the material and the absence of long oriented grains. The mechanism may differ extensively with that described for aluminum due to the prior cold-work and thermal histories of the materials and to the inherent lack of crystallographic similarity. Further studies in this area might prove rewarding.

The materials, as expected, generally showed an increase in strength parameters accompanied by a reduction in ductility as a result of increased irradiation levels. An increase in gaseous interstitials (of the solute-solid solution type). particularly hydrogen, appear to increase the scatter of the data points. This phenomenon, attributable to the randomness of neutron-interstitial interaction and the mutual energy

*In this case, the interstitial is a displaced lattice atom and should not be confused with the interstitial solid solute atoms, C, N, O and H, discussed elsewhere. The interstitial which is a displaced lattice atom may be annihilated by combination with a vacancy. This can occur during plastic straining of the material, or as a result of energy absorption due to collision with a neutron of suitable energy level. However, they may also serve as locii of thermal spikes or displacement spikes as a result of fast neutron bombardment.

change due to the similarity of mass, might be an important consideration in the use of this material in engineering design in areas of intense fast neutron activity.

5.3 FATIGUE TESTING

Fatigue testing is broadly divided into two general classes: conventional fatigue testing, using loads within the elastic limit applied at high cyclic rates, with a test runout of at least 10^7 cycles to establish an engineering endurance limit; and low cycle fatigue testing, using test loads with an appreciable plastic strain component at low cyclic rates, with a test runout in the order of 10^4 cycles. Due to the requirements of high load rates and rather severe thermal cycling inherent in space hardware, the low cycle fatigue properties were investigated in this program as being of greater interest to design engineers in the field. The fatigue testing phase of this program was limited to two materials, commercially pure titanium (Ti-55A) and Ti-5 Al-2.5 Sn. The Ti-5 Al-2.5 Sn included testing of both standard interstitial and extra low interstitial grades. Test specimens were fabricated from the same pedigreed materiel used in the tensile program and described in Tables I and II. The specimen design is shown in figure 2.

Fatigue testing was conducted under three test conditions: 300°K, unirradiated; 17°K, unirradiated; and 17°K, irradiated to 1×10^{17} n/cm^2 at 17°K. The test run out was 10^4 cyclic reversals of load. The load was controlled through calculated stress amplitudes; strain was not monitored. The applied load was computed to represent a specified percentage of the nominal F_{tu} obtained from reference 1. The load was applied axially to the test specimen and cycled to full amplitude between compression and tension with a test ratio of -1. The compressive component was applied in the initial loading and the full load was reached using an incremental ramp approach over ten full cycles to reduce the possibility of shock loading or specimen buckling in the first full-load cycle.

To assess the effect of strain hardening during the ramp loading coupled with the effect the specimen geometry might have on the nominal F_{tu}, specimens of each test material were ramp loaded at 17°K to full amplitude and then failed in axial tension. The results of these tests, shown in table VI, indicate an increase of about 18% over the nominal values from reference 1.

The cyclic load rate used during the fatigue program was 0.251 Hz. Additional tests were conducted at 0.10 Hz and 0.50 Hz on Titanium 55A specimens loaded to 90% of the nominal F_{tu} at 17°K. These data, plotted in figure 17, show no statistically discernable systematic variation due to cyclic rate variation within these limits.

5.3.1 Fatigue Testing of Commercially Pure Titanium (Titanium 55A)

The test results obtained for this material are plotted in figure 18 and presented in full in Appendix K.

Examination of the data in figure 18 shows that the cryogenic increase in ultimate tensile strength is greater than the accompanying increase in fatigue life. Irradiation to 10^{17} n/cm^2 appears to increase the fatigue life at higher load ranges but seems to have little effect at load levels below 85% of the F_{tu}.

In addition to the normal three test conditions, three additional Titanium 55A specimens were tested at different load levels during irradiation. This was accomplished by inserting a specimen at 17°K into the high flux zone of the reactor and applying the initial cyclic load immediately. This was performed to investigate a possible effect on fatigue properties through an interaction between load energy and the neutron flux. The limited data generated, shown in table VII along with corresponding unirradiated and postirradiation test data, indicates the possibility that such an effect might increase the fatigue life at high load levels; however, due to the paucity of data, any conclusions on this effect would be premature.

An atlas of electron fractographs of this material, with brief description of each fractograph, appears in Appendix K.

5.3.2 Fatigue Testing of Ti-5 Al-2.5 Sn Alloy

Fatigue testing of Titanium-5 Al-2.5 Sn was conducted for 300°K, unirradiated; 17°K, unirradiated; and 17°K irradiated to 1 x 10^{17} n/cm^2 at 17°K exposure conditions. Both standard interstitial and extra low interstitial grades were investigated. Test results are plotted as S-N diagrams in figure 19 for the standard interstitial material and in figure 20 for the extra low interstitial material.

Examination of figures 19 and 20 show that, unlike the unalloyed material, the cryogenic strengthening effect is at least as great in fatigue as in tensile properties. In the standard interstitial grade, the observed influence of low temperature is somewhat more evident in fatigue testing. Specimens of the standard interstitial material withstood between 2000 and 3000 cyclic reversals of stress at a level of 112.5 percent of the nominal F_{tu} at 17°K. At stress levels of 105% of the nominal F_{tu} the material withstood from 2500 to 6400 cyclic reversals as compared to less than 1200 for the ELI grade in all cases at the load. One standard interstitial specimen was tested at 115% of the nominal F_{tu}; it failed on the ramp as the load reached the full amplitude. While this is not surprising since the actual breaking stress of a fatigue specimen after ramp loading is of that order, the fatigue life at 112.5% of the nominal F_{tu} is surprisingly long.

It would appear from figures 19 and 20 that the interstitial content exerts a large effect on fatigue properties of this titanium alloy. As table I shows, the standard interstitial material has a total interstitial content of 1.1 atomic percent and the ELI grade has a 0.6 atomic percent. The major difference is in the gaseous elements, the carbon content being about constant for both materials. This large effect of interstitial content on the fatigue life of Titanium-5 Al-2.5 Sn was unexpected. As figures 19 and 20 show, the standard interstitial grade has appreciably greater fatigue life at all three test conditions than the ELI material. Additional specimens were prepared from a lot of material, supplied by NASA, Lewis Research Center, with a different interstitial content. The chemical analyses of this lot, TMCA Heat No. D-6123, is given below for comparison with the composition of the regular test material given in table I.

TMCA Heat #D-6123   1" Diameter Bar   Annealed and Centerless Ground

Fe	Al	Sn	C		N		H		O	
wt%	wt%	wt%	wt%	At%	wt%	At%	wt%	At%	wt%	At%
0.16	5.0	2.6	0.023	0.11	0.010	0.04	0.0133	0.63	0.173	0.52

Comparison of this analysis with that of the regular Titanium 5% Al-2.5% Sn (Std. I) test material shows the total interstitial contents to be about the same, but the special lot has 1.30 atomic % interstitials with lower carbon and nitrogen contents offset by higher quantities of hydrogen and oxygen.

The Goldschmidt atomic radii of the interstitial elements are: C = 0.77, N = 0.71, H = 0.46, and O = 0.60.

Specimens from this special heat of material were tested at 300°K at stress levels of 90%, 85% and 80% of the nominal F_{tu} for this material. The results of these tests, together with the germane data from the regular test program, are shown in figure 21.

Examination of figure 21 shows that not only does the total interstitial content influence the fatigue life; the degree of effect is dependent on the type of interstitial atom present.

The material difference is probably attributable to blocking by interstitial atoms reducing the mobility, and thus the ability to pile-up, of dislocations generated by cyclic loading. This would tend to increase the number of constant amplitude cycles required to produce crack nucleation. Not surprisingly, the elements with larger atomic radii provide a greater blocking action, causing a larger loss of dislocation mobility than smaller atoms.

As with the Titanium 55A, the principal irradiation effects in the Ti-5 Al-2.5 Sn alloy are more pronounced at high load levels. Both grades of Ti-5 Al-2.5 Sn exhibit what appears to be an upper knee at high loads after irradiation. However, there is considerable data scatter at these load levels and the small population makes speculation on the validity of this observation questionable.

5.3.3 Discussion

The fatigue testing program was limited to polycrystalline commercially pure titanium (Ti-55A, annealed) and Ti-5 Al-2.5 Sn alloy in two interstitial grades; except that a few tests, at 300°K, unirradiated, were run on a special lot of material of a third interstitial content. For convenience in assessing the relative cryogenic and irradiation effects on these materials, the data have been replotted in figures 22, 23, and 24 to show the test results for each of the materials at a common test environment. The ordinate in each case is the test load expressed as the percentage of the nominal F_{tu}. The actual load on the Ti-55A specimens is much lower than on the alloyed material.

In evaluating these data, it should be borne in mind that fatigue test parameters are statistical quantities, and considerable deviation from an average curve may be expected (ref. 8). This is probably due to the nature of the origin of fatigue cracks. Recent investigations of crack nucleation (ref. 9) by Wilkov and Shield indicate the probability that these points of origin begin as sequences of small cavities oriented along slip traces which unite to form continuous microcracks or surface intrusions. This model might be expected particularly in a randomly oriented hexagonal close packed polycrystal, to result in the rather broad scatter band of data points normally observed in fatigue testing. The rather small sample size used in this experiment would not tend to provide a Gaussian distribution apparent in data by inspection. Also, the test loads used make accurate determination of the actual plastic component difficult and might be expected to increase scatter. As far as feasible, additional data points were run to increase the confidence level in the test data.

Examination of figures 22, 23 and 24 shows that the curve for Ti-55A is above both grades of Titanium 5 Al-2.5 Sn at room temperature and below them for both conditions at 17°K. This is understandable on the basis of the cryogenic effect on the F_{ty}/F_{tu} ratio for these materials. This parameter is depressed significantly at 17°K for the unalloyed material; in the case of the substitutional alloy this effect is negligable or, possibly, reversed. Thus, the plastic component of the total strain is increased in the Titanium 55A, resulting in a reduction of the fatigue limit.

The specimen configuration, shown in figure 2, was designed to minimize the possibility of generating inaccurate test data through specimen distortion during high compressive loading or minor equipment misalignment. However, the specimen used is not conducive for accurate measurement of axial strain. The combined effects of the specimen geometry and ramp loading on the actual strength of the specimen at the time of the initial application of the full fatigue locd were determined by failing fatigue specimens in axial tension after ramp loading.

The results of these tests indicate that the actual breaking stress of the specimens as tested is about 118% of the nominal F_{tu} obtained in testing cylindrical specimens of annealed stock. Tests to assess these effects on the F_{ty} were impractical due to the above mentioned difficulty in strain determination. These factors would seem to make determination of plastic vs. elastic stress or strain components of flow rather uncertain. However, this difficulty is not unique to this experiment. Examination of load-elongation curves confirms the gradual transition from essentially elastic to essentially plastic behavior in Titanium 55A tensile specimens at 17°K. Determination of the F_{ty} by the 0.2% offset method includes, by definition, 0.002 in/in of plastic strain in this important engineering parameter; the true elastic limit is difficult to obtain at normal temperatures with conventional equipment, without introducing the additional complications of cryogenic-irradiation environments and remote handling techniques. Monitoring strain during cyclic loading does not automatically separate the plastic from the elastic modes; this can be done rigorously only by precise determination of the elastic limit and, unfortunately, this parameter changes during cyclic loading as it is influenced by strain-hardening. Therefore, any practical division of actual specimen behavior into plastic and elastic components must be of a somewhat arbitrary nature.

However, for the evaluation of cyclic loads in the plastic-elastic interface range some attempt must be made to provide an arbitrary division below which the stress/strain pattern is assumed to be principally elastic and above which primarily plastic flow is postulated. Since only stress was directly measured in this experiment, rationalizations to divide strain into separate components appear tenuous. Since the nominal F_{ty} obtained in tensile testing can be assumed to be about 20% below the actual yield strength of the fatigue specimen at the end of the ramp function and the nominal F_{ty} can be assumed to be about 20% above the actual elastic limit for titanium alloys, the use of the nominal F_{ty} from the tensile program seems justified as a defined upper limit of elastic stress and lower limit of plastic behavior. The percentages of elastic stress and plastic stress for the several test conditions, computed on these bases, are given in table VIII.

It has been demonstrated that, in samples with a sufficiently large specimen population, the distribution of fatigue data follows a normal Gausian distribution when the fatigue life is expressed as the logarithm of the number of cycles to failure (ref. 8). For this reason S-N curves are drawn on semi-logarithm paper. The points used as the N value in the curves presented in figures 18 through 24 are the mean of the logarithm N values rather than the logarithm of the mean N values, to provide a more reliable parameter from a limited number of test points with the rather high data scatter expected in fatigue test work. These mean values have been charted, for all load conditions at which failures occurred uniformly before 10^4 cycles, against the plastic stress component as defined above in table IX. Even allowing for the rather dubious definition of plastic behavior, examination of the data in table VIII indicate no usable relationship between plastic stress and endurance limit in these materials. The large effect of the large radii interstitials, shown in figure 21, indicates that solid state effects on fatigue properties in the titanium alloys are of sufficient magnitude to overshadow macroscopic mechanical parameters. Further investigation of this interstitial effects would appear warranted.

PAGE BLANK NOT FILMED.

6 CONCLUSIONS AND RECOMMENDATIONS

Several observations of interest were made during the test program which, to the best knowledge of the authors, have not been previously published. These are discussed briefly in the following paragraphs.

The mechanical properties of Aluminum 1099-H14 under a wide variety of nuclear cryogenic test conditions have been determined. The interrelationship of the test data can be examined to arrive at certain important conclusions with regard to both similarities and differences in the data from various test conditions.

The most prominent observable effect of cryogenic temperatures on Aluminum 1099-H14 in the absence of irradiation is in a reduction of the yield to tensile ratio (F_{ty}/F_{tu}) with decreasing temperatures. This is accompanied by a sharp increase in the uniform strain, as contrasted with necking down, occurring during plastic deformation. The notable increase in elongation indicates a mitigation of the effect, at room temperature, due to cold work in the H14 material. The reduction of area values confirm this trend, although this parameter usually shows a greater range of values than the other functions, since it is the most structure sensitive of those values measured in tensile testing.

The effect of fast neutron bombardment on Aluminum 1099-H14 at 17°K is to increase the strength values and reduce the ductility values. There is a tendency for the F_{ty}/F_{tu} ratio and the elongation to assume their approximate levels for the unirradiated material tested at room temperature. The data shows that this recovery is primarily due to an increase in the F_{ty} and the hardening mechanism resulting from the irradiation appears to resemble that resulting from cold work.

Comparison of the F_{ty}/F_{tu} and elongation values for Aluminum 1099-H14 at room temperature, unirradiated, with those at 17°K after irradiation (at 17°K) show a remarkable similarity. Although there is an increase in the strength values (F_{tu} and F_{ty}) by approximately a factor of 3, accompanied by a decrease of about 50 percent in the reduction of area, the elongations are essentially the same for the two test conditions. This indicates that any combined nuclear-cryogenic induced embrittlement accompanying the increase in strength values effects only the necking-down portion of the plastic behavior. The only instance in which the behavior of the irradiated material at 17°K resembles that of the unirradiated material at 17°K more closely than that of the unirradiated material at room temperature is in the relative uniformity of plastic strain.

Thus, in a very important respect, the cryogenic (unirradiated) induced mitigation of the effects of cold work in Aluminum 1099 in the H14 condition can be overcome by neutron irradiation.

A comparison of the data from irradiating Aluminum 1099-H14 and testing at various temperatures to that from irradiating at 17°K and then annealing and testing at various temperatures indicates an essential similarity, with no significant differences at particular test temperatures between the data from the two test conditions.

Comparison of the data indicates that in the normal temperature range (above about 200°K) the effects of irradiation to 10^{17} n/cm^2 are slight and the effects of irradiation at cryogenic temperatures tend to anneal out if the material is warmed to room temperature. At lower temperatures the effects persist to a much greater degree. At temperatures below 180°K, the F_{ty}/F_{tu} ratio remains about constant with irradiation or annealing temperature while necking down during plastic deformation is reduced, accompanied by an irradiation induced increase in the strength values. This confirms the similarity of irradiation effects and work-hardening.

To facilitate an analysis of annealing of nuclear cryogenic effects in Aluminum 1099-H14, the data was reduced to ratios of strengths at test conditions to strengths without irradiation at corresponding test temperatures. The results show that the effects induced by irradiation to 10^{17} n/cm^2 at 17°K appear to be completely annealed out when tested at 300°K and essentially annealed when tested at much lower temperatures. However, testing the material at 17°K following annealing at various temperatures, including 300°K indicates considerable residual irradiation effects. The difference in behavior is, not unexpectedly, more pronounced in the F_{ty} than in F_{tu} values. This effect is even more pronounced in the increase in the uniform strain component of the plastic deformation with increasing annealing temperatures.

Irradiation at 17°K produces moderate strengthening in all the titanium alloys up to fluence levels of 10^{18} n/cm^2. This is accompanied by a moderate decrease in ductility parameters. The effect is apparently similar in nature to increase of the foreign substitutional solute atoms population or to second phase precipitation within the structure. No indications of saturation of these irradiation levels was observed. The observed effects are attributed to an increase in the turbulent component during the early stages of local plastic strain. The light interstitial atoms appear to increase the scatter of the test data at the higher fluences.

The cryogenic increase in the fatigue strength for a given endurance limit was of less magnitude than the similar increase in tensile strength in the unalloyed material;

this effect is not observed in the alloyed grades. This is attributed to a greater cryogenically induced effect on the F_{tu}, in pure metals, than on the F_{ty}. The resultant reduction of the F_{ty}/F_{tu} ratio introduces a larger plastic strain component at high load levels, at cryogenic temperatures, which adversely affects the endurance limit. In all materials tested, the irradiation effects on fatigue behavior were more readily observable at high load levels.

A large and rather unexpected increase in fatigue life resulting from increased interstitial content was observed in the alloyed material. This effect is more pronounced in materials higher in atomic percentages of the interstitial atoms with relatively large atomic radii. The introduction of a controlled test variable of atomic dimensions appears to introduce solid state mechanisms which complicate the relationship between fatigue and tensile test parameters on the metallurgical level. Thus, the emperical established interrelation between tensile plastic strain ductility and fatigue life established by other observers (ref. 10) is somewhat obscured in these data due to the large relevance of dislocation-interstitial interaction of sub-microscopic dimensions on the fatigue life of materials with essentially similar tensile properties. The emperical relationship was established in tests using strain amplitude as the mode of load control, the data reported herein was obtained controlling stress amplitude. Therefore caution should be exercised in making direct comparison between the data sets.

The data randomization reported in tensile properties of high interstitial material was not observable in fatigue data due to the relatively low (10^{17} n/cm^2) irradiation level prior to fatigue testing. However, this effect should be noted in evaluating interstitial content of titanium alloys to be subjected to high fluences.

These tensile and fatigue results suggest further studies which would lead to a better knowledge of irradiation effects in structural materials as well as to a better understanding of the fundamental mechanisms occuring in solids under fast neutron irradiation.

There is a practical need for data at higher irradiation levels at 17°K and data on annealing of the irradiation effects produced at 17°K, since it can be expected that structural materials in aerospace hardware might be highly stressed after reactor operation and shutdown as well as during operation. Such work should include representative strain hardenable, precipitation hardenable, austenitic stainless steel, and super alloy compositions.

The fatigue studies should be expanded to include high irradiation levels, other structural alloys and possible effects of the surrounding atmosphere. Also, when suitable strain gages are available, fatigue studies should be made under controlled strain conditions rather than controlled stress conditions, to more nearly duplicate the thermal cycling which will occur in operating nuclear reactors. This would also make a different specimen design more desirable. Post-irradiation studies could then include plastic deformation measurements on specimens failed under cyclic loading.

Temperature of irradiation studies might be expanded to pure metals heavier than aluminum since different effects would be expected from metals with lower self-diffusion coefficients (ref. 11). Titanium would be a good candidate for such studies and could be obtained in single crystal form for fundamental studies.

The cryogenic irradiation facility described in this report is uniquely capable of producing valuable fundamental information on irradiation effects associated with changes in internal stress. Low irradiation temperatures can isolate effects due to diffusion controlled metallurgical changes (thermal mechanisms) from effects due to dynamical mixing. Proper choice of experiments and materials for study might isolate dynamical effects associated with vacancy zone formation from those associated with interstitial clustering and also might isolate focussing effects from channeling effects (ref. 12).

With strain rate control capability, strain rate sensitivities of yield stresses can be measured for determinations of size distribution of obstacles to dislocation motion. Also, with this capability, stress relaxation experiments can be performed.

An experiment of interest to applications people as well as to theoreticians would apply various stresses to metals during irradiation at low temperatures, maintain constant strain and look for a decrease in the stress. Even though such a decrease may not be observed, removing the load and reapplying to yield and failure would likely show changes in the deformation characteristics resulting from the irradiation. The stress during irradiation should be a source of energy and cause changes in the clustering of vacancies which would not ordinarily occur at low temperatures (ref. 13). Conceivably this could cause the clusters to become too large to have an effect on the yield strength and be equivalent to irradiating at elevated temperatures. This is an experiment which might be particularly valuable if performed with single crystals.

7 TABLES

TABLE I MATERIAL COMPOSITIONS (PEDIGREE DATA)

Aluminum Alloys:

Alloy and Temper	Lockheed Code	PERCENT OF ELEMENT Al	Cu	Fe	Si	(Mn, Mg, Zn, Ni, Cr, Ti, V, Z, Zn)
1099-H14	8 Ba	99.99	0.003	0.001	0.001	each 0.0006 total 0.005

Titanium Alloys:

Alloy and Temper	Lockheed Code	Percent of Element (remainder: Titanium) Fe	Al	Other	C		N		H		O	
		wt%	wt%	wt%	wt%	At%	wt%	At%	wt%	At%	wt%	At%
55A Annealed	1 Aa	0.19	-	-	0.032	0.13	0.023	0.08	0.006	0.29	0.218	0.65
5 Al-2.5 Sn (ELI) Annealed	3 Aa	0.028	5.43	2.41 Sn	0.033	0.13	0.011	0.04	0.006	0.29	0.053	0.16
5 Al-2.5 Sn (Std) Annealed	8 Aa	0.110	5.10	2.50 Sn	0.032	0.13	0.019	0.07	0.012	0.57	0.116	0.35
6 Al - 4 V Annealed	2 Ac	0.170	5.95	4.00 V	0.010	0.040	0.022	0.08	0.006	0.29	0.065	0.19
6 Al - 4 V Sol. Treated Aged	2 Aa	0.150	5.80	3.90 V	0.010	0.040	0.035	0.12	0.010	0.48	0.102	0.31

TABLE II MATERIAL PHYSICAL CHARACTERISTICS (PEDIGREE DATA)

Alloy / Temper	Lockheed Code	Form	Spec.	Vendor Code / Vendor Lot or Heat No.	F_{tu} Ksi	F_{tu} $\frac{kN}{cm^2}$	F_{ty} 0.2% offset Ksi	F_{ty} 0.2% offset $\frac{kN}{cm^2}$	Elongation in 4D (%)	Hardness	Grain Size *
Aluminum 1088 H14	8 Ba	0.5" Plate	Vendor	(1) 199352	13.5	9.31	12.9	8.89	20.5	BHN 26	**
Titanium 55A Annealed	1 Aa	0.5" Round Bar	Mil-T-7993A Class II	(2) M-9186	70.5	48.6	60.5	41.7	35	Rockwell B 87	5
Ti-5Al-2.5 Sn (ELI) Annealed	8 Aa	0.5" Round Bar	Vendor 49021-1	(2) V-2402	119.3	82.5	101.2	69.8	17	Rockwell C 24.9	**
Ti-5Al-2.5 Sn (Std. I) Annealed	3 Aa	0.5" Round Bar	AMS-4910	(2) M-7888	131.0	90.3	127.0	87.5	22	Rockwell C 31-33	8
Ti-6Al-4V Annealed	2 Ac	0.5" Round Bar	Mil-T 9047C	(2) M8574	146.0	100.7	138.0	95.1	15.5	Rockwell C 30-33	**
Ti-6Al-4V Solution Treated And Aged	2 Aa	0.5" Round Bar	Mil-T 9047C	(2) M-9812	173.0	119.3	165.0	113.8	13	Rockwell C 33-36	**

* ASTM No. E112-58T
** Not Measured

(1) Aluminum Company of America
(2) Titanium Metals Corporation of America

TABLE III FLUX MAPPING FOILS

Type of Foil	Nuclear Reaction	Threshold Energy, E_T		Cross Section ($\times 10^{-24}$ cm^2)
		MeV	fJ	
Indium	$In^{115}(n,n')In^{115m}$	0.45	72	0.20
Neptunium	$Np^{237}(n,f)Ba^{140}$	0.75	120	1.52
Uranium	$U^{238}(n,f)Ba^{140}$	1.45	232	0.54
Sulfur	$S^{32}(n,p)P^{32}$	2.9	464	0.284
Nickel	$Ni^{58}(n,p)Co^{58}$	5.0	300	1.67
Magnesium	$Mg^{24}(n,p)Na^{24}$	6.3	1008	0.0715
Aluminum	$Al^{27}(n,\alpha)Na^{24}$	8.6	1376	0.23

TABLE IV EFFECTS OF TEMPERATURE AND IRRADIATION ON ALUMINUM 1099-H14

Fluence	TEST CONDITIONS Temperature, °K Irradiation	Anneal	Test	Ultimate Tensile F_{tu} Ksi	F_{tu} kN/cm^2	Tensile Yield F_{ty} Ksi	F_{ty} kN/cm^2	F_{ty}/F_{tu}	Elong. in 4D %	Red. of Area %	Fracture Stress Ksi	Fracture Stress kN/cm^2	Modulus # E 10^3 Ksi	Modulus # E MN/cm^2
0	-	-	17	37.25	25.68	12.00	8.27	0.319	57.9	65.4	92.6	63.8	10	7
0	-	-	78	21.73	14.98	13.98	9.64	0.643	47.3	79.3	79.5	54.8	8	6
0	-	-	178	14.52	10.01	12.93	8.92	0.890	27.7	82.3	36.2	25.0	9	6
0	-	-	300	13.10	9.03	12.41	8.56	0.945	21.9	73.2	23.5	16.2	9	6
5×10^{15}	17	-	17	46.10	31.78	20.27	13.98	0.440	54.7	66.0	106.0	73.1	12	8
5×10^{16}	17	-	17	49.67	34.25	34.07	23.49	0.687	42.0	52.7	81.7	56.3	15	10
10^{17}	17	-	17	52.25	36.03	40.02	27.59	0.770	35.0	54.5	87.0	60.0	13	9
3×10^{17}	17	-	17	56.50	38.96	49.53	34.15	0.873	24.0	38.3	72.3	49.8	13	9
10^{17}	78	-	78	25.43	17.53	18.57	12.80	0.730	42.0	74.0	55.0	37.9	7	5
10^{17}	178	-	178	15.97	11.01	14.57	10.05	0.910	27.7	78.3	28.0	19.3	8	6
10^{17}	300	-	300	12.17	8.39	11.10	7.65	0.913	17.7	14.0	-	-	-	-
10^{17}	17	78	78	27.40	18.89	20.80	14.34	0.757	38.0	70.0	39.0	26.9	16	11
10^{17}	17	178	178	16.60	11.45	15.03	10.36	0.907	26.7	81.3	-	-	9	6
10^{17}	17	300	300	11.87	8.18	11.30	7.79	0.953	20.7	75.7	29.0	20.0	8	6
10^{17}	17	78	17	48.60	33.51	30.60	21.10	0.630	42.7	56.3	80.3	55.4	15	10
10^{17}	17	178	17	42.00	28.96	21.50	14.82	0.507	49.3	61.0	79.7	55.0	11	8
10^{17}	17	300	17	43.10	29.72	14.17	9.77	0.330	59.7	59.3	83.3	57.4	6	4

Values are arithmetic means of test data points

Modulus of Elasticity Values for comparison purposes only.

TABLE V EFFECT OF IRRADIATION AT 17°K ON TITANIUM ALLOYS

ALLOY	TEST CONDITIONS Fluence	Temp. °K	Ultimate Tensile F_{tu} Ksi	F_{tu} kN/cm²	Tensile Yield F_{ty} Ksi	F_{ty} kN/cm²	F_{ty}/F_{tu}	Elong in 4D %	Red. of Area %	Fracture Stress Ksi	Fracture Stress kN/cm²	Modulus # E 10^3 Ksi	Modulus # E MN/cm²
55A Annealed	0	300	67.0	46.2	53.5	36.9	0.798	30.0	62.3	-	-	14	10
	0	17	169.4	116.8	122.0	84.1	0.722	33.3	53.0	-	-	18	12
	10^{17}	17	192.3	132.6	131.7	90.8	0.690	34.0	53.0	-	-	18	12
	6×10^{17}	17	206.0	142.0	155.3	107.1	0.753	28.3	43.0	363.7	250.8	18	12
	10^{18}	17	217.3	149.8	170.3	117.4	0.780	26.0	43.7	388.3	267.5	17	12
5 Al-2.5 Sn (ELI) Annealed	0	300	126.4	87.2	113.4	78.2	0.896	16.0	42.2	170.0	117.2	15	10
	0	17	228.4	157.5	214.2	147.7	0.948	9.7	32.3	-	-	-	-
	10^{17}	17	223.3	150.0	213.0	146.9	0.953	11.0	31.0	-	-	18	12
	10^{18}	17	263.8	181.9	258.4	178.2	0.980	6.0	24.7	353.0	243.4	22	15
5 Al-2.5 Sn (Std. I) Annealed	0	300	125.2	86.3	114.8	79.2	0.920	23.3	50.7	-	-	15	10
	0	17	224.8	155.0	205.2	141.5	0.915	13.8	30.0	298.0	205.5	18	12
	10^{17}	17	239.0	164.8	218.0	150.3	0.913	11.5	36.0	-	-	18	12
	10^{18}*	17	250.0	172.4	243.4	167.8	0.974	7.4	29.8	352.4	243.0	21	14
6 Al-4V Annealed	0	300	144.0	99.3	137.8	95.0	0.957	13.8	45.0	-	-	15	10
	0	17	260.4	179.5	243.2	167.7	0.934	7.6	30.4	-	-	17	12
	10^{17}	17	273.7	188.7	254.0	175.1	0.950	5.7	37.3	-	-	-	-
	10^{18}	17	320.2	220.8	299.5	206.5	0.940	4.7	34.0	485.3	334.6	26	18
6 Al-4V Aged	0	300	167.6	115.6	158.6	109.4	0.946	16.5	54.0	-	-	16	11
	0	17	282.2	194.6	275.0	189.6	0.976	6.4	25.4	-	-	18	12
	10^{17}	17	302.3	208.4	293.3	202.2	0.970	5.0	22.4	-	-	20	14
	10^{18}	17	329.5	227.2	324.0	223.4	0.983	4.4	15.4	380.0	262.0	19	13

Values are arithmetic means of test data points

Modulus of Elasticity value for comparison purposes only.

* Caution should be exercised in engineering use of these values since considerable scatter was observed in the data. See section 5.2 for discussion.

TABLE VI

EFFECT OF RAMP LOADING AND SPECIMEN GEOMETRY ON BREAKING STRESS OF FATIGUE SPECIMENS AT 17°K, UNIRRADIATED

Specimen	Breaking Load		Breaking Stress		Change from Nominal F_{tu}	
	lbf	N	Ksi	kN/cm^2	Absolute	Relative
Titanium 55A; Nominal F_{tu} 169.4 Ksi, 116.8 kN/cm^2 (ref. 1):						
1 Aa 294	2425	335	197.2	136.0	-	-
1 Aa 295	2460	340	198.4	136.8	-	-
1 Aa 296	2480	343	200.0	137.9	-	-
MEAN	2455	339	198.5	136.7	+ 29.1 Ksi +20.0 kN/cm^2	+ 17.2%
Titanium 5% Al-2.5% Sn (ELI); Nominal F_{tu} 228.4 Ksi 157.5 kN/cm^2 (ref. 1):						
8 Aa 102	NR*		NR*		-	-
8 Aa 103	3360	464	271.0	186.9	-	-
8 Aa 104	3340	462	271.5	187.2	-	-
MEAN	3350	463	271.2	187.0	+ 42.8 Ksi +29.5 kN/cm^2	+ 18.7%
Titanium 5% Al-2.5% Sn (Std. I); Nominal F_{tu} 224.8 Ksi 155.0 kN/cm^2 (ref. 1):						
3 Aa 112	3192	441	257.4	177.5	-	-
3 Aa 115	3150	435	254.0	175.1	-	-
3 Aa 116	3360	465	271.0	186.9	-	-
MEAN	3234	447	260.8	179.8	+ 36.0 Ksi +25.8 kN/cm^2	+ 16.0%

* Test load interrupted due to hydraulic pressure surge during test - invalid test data produced

TABLE VII FATIGUE TEST RESULTS AT 17°K, TITANIUM 55A, COMPARISON OF IN-PILE FATIGUE TESTING AND POST-IRRADIATION FATIGUE TESTING

STRESS Ksi	kN/cm^2	%F_{tu}*	EXPOSURE n/cm^2		SPECIMEN NUMBER	CYCLES TO FAILURE
160.9	111.0	95	0		1 Aa 256	1619
			0		1 Aa 267	1260
			0		1 Aa 268	903
			1×10^{17}	(a)	1 Aa 280	2401
			1×10^{17}	(a)	1 Aa 253	1748
			1×10^{17}	(a)	1 Aa 271	1568
			2.7×10^{16}	(b)	1 Aa 313	2105
152.5	105.1	90	0		1 Aa 248	3589
			0		1 Aa 250	1322
			0		1 Aa 266	1001
			1×10^{17}	(a)	1 Aa 270	5498
			1×10^{17}	(a)	1 Aa 244	3436
			1×10^{17}	(a)	1 Aa 252	2329
			2.5×10^{16}	(c)	1 Aa 254	2709
135.5	93.4	80	0		1 Aa 249	10,000 (not failed)
			1×10^{17}	(a)	1 Aa 259	10,000 (not failed)
			1×10^{17}	(a)	1 Aa 289	10,000 (not failed)
			1×10^{17}	(a)	1 Aa 291	10,000 (not failed)
			5.2×10^{16}	(d)	1 Aa 281	5762

(a) Fatigued following irradiation exposure
(b) Fatigued during irradiation: rate 2.4×10^{12} n/cm^2/sec.
(c) Fatigued during irradiation: rate 2.2×10^{12} n/cm^2/sec.
(d) Fatigued during irradiation: rate 2.1×10^{12} n/cm^2/sec.

TABLE VIII PLASTIC AND ELASTIC STRESS COMPONENTS AT VARIOUS TEST LOAD LEVELS

Nominal Test Load % F_{tu}	Titanium 55A				Ti 5-2.5 (ELI)				Ti 5-2.5 (Std. I)			
	300°K		17°K		300°K		17°K		300°K		17°K	
	σ_e	σ_p	σ_e	σ_p	σ_e	σ_p	σ_e	σ_p	σ_e	σ_p	σ_e	σ_p
115	-	-	-	-	-	-	-	-	-	-	80	20
110	-	-	-	-	-	-	86	24	-	-	84	16
105	-	-	-	-	-	-	90	10	-	-	88	12
100	80	20	72	28	90	10	95	5	92	8	92	8
95	84	16	76	24	95	5	100	0	97	3	97	3
90	89	11	80	20	100	0	100	0	100	0	-	-
85	94	6	85	15	100	0	100	0	100	0	-	-
80	100	0	90	10	100	0	100	0	100	0	-	-
75	100	0	96	4	100	0	100	0	100	0	-	-

σ e = % of total strain in elastic component

σ p = % of total strain in plastic component

– = tests not performed at this load

TABLE IX RELATIONSHIP BETWEEN PLASTIC STRESS COMPONENT AND MEAN OF LOGARITHM, NUMBER OF CYCLES TO FAILURE

Material	Test Condition Temp	Test Condition ϕ	Test Load $\%F_{tu}$	σ_p % Test Load	Cycles to Failure (anti-log of mean of log)
55A	300°K	0	100	20	1500
			95	16	3066
			90	11	2622
			85	6	6729
			82.5	3	one specimen not failed
55A	17°K	0	95	24	1226
			90	20	1680
			85	15	4376
			80	10	one specimen not failed
55A	17°K	10^{17}	100	28	1012
			95	24	1874
			90	20	3530
			85	15	one specimen not failed
5-2.5 ELI	300°K	0	90	0	551
			85	0	1790
			80	0	2423
			75	0	one specimen not failed
5-2.5 ELI	17°K	0	105	5	671
			100	0	1334
			95	0	4054
			90	0	one specimen not failed
5-2.5 ELI	17°K	10^{17}	110	24	187
			105	10	2083
			100	5	2466
			95	0	4832
			90	0	one specimen not failed
5-2.5 Std.I	300°K	0	100	8	911
			95	3	2024
			90	0	3684
			85	0	6802
			80	0	one specimen not failed
5-2.5 Std.I	17°K	0	112.5	18	2186
			110	16	3109
			105	12	4233
			100	8	one specimen not failed
5-2.5 Std.I	17°K	10^{17}	115	20	1529
			110	16	2374
			105	12	4280
			100	8	one specimen not failed

8 FIGURES

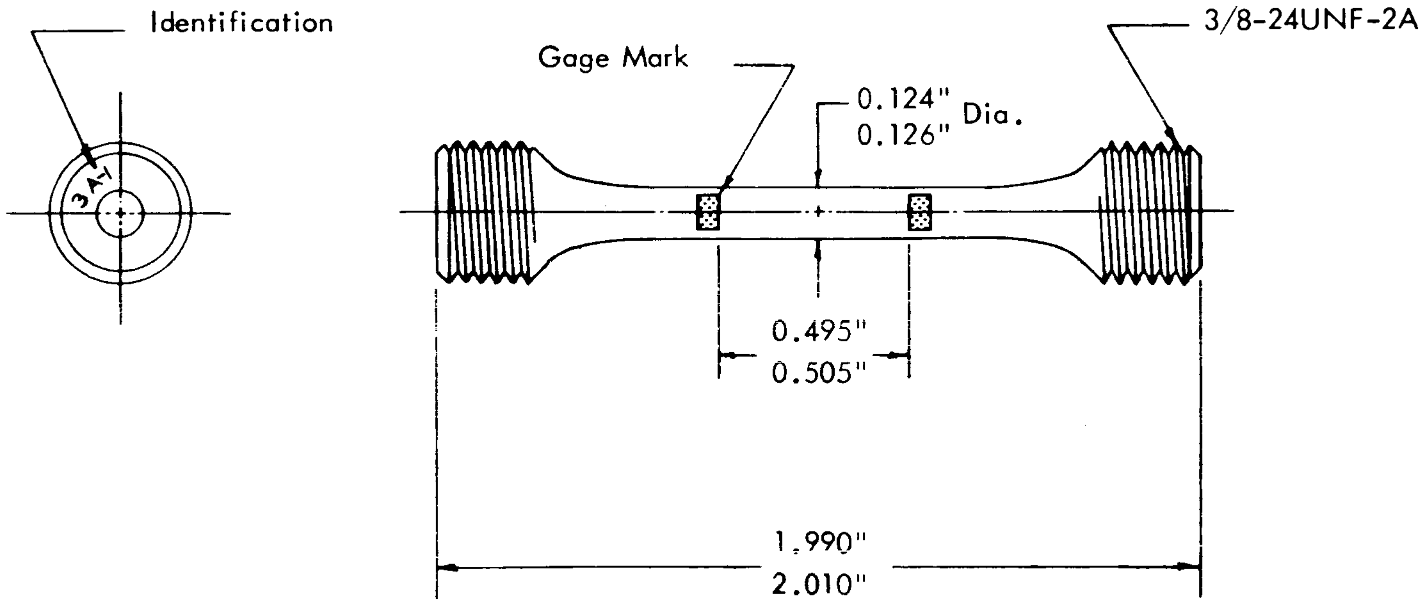

Note: Diameter at gage marks shall be center diameter + $\genfrac{}{}{0pt}{}{0.002"}{0.004"}$.

FIGURE 1 TENSILE SPECIMEN

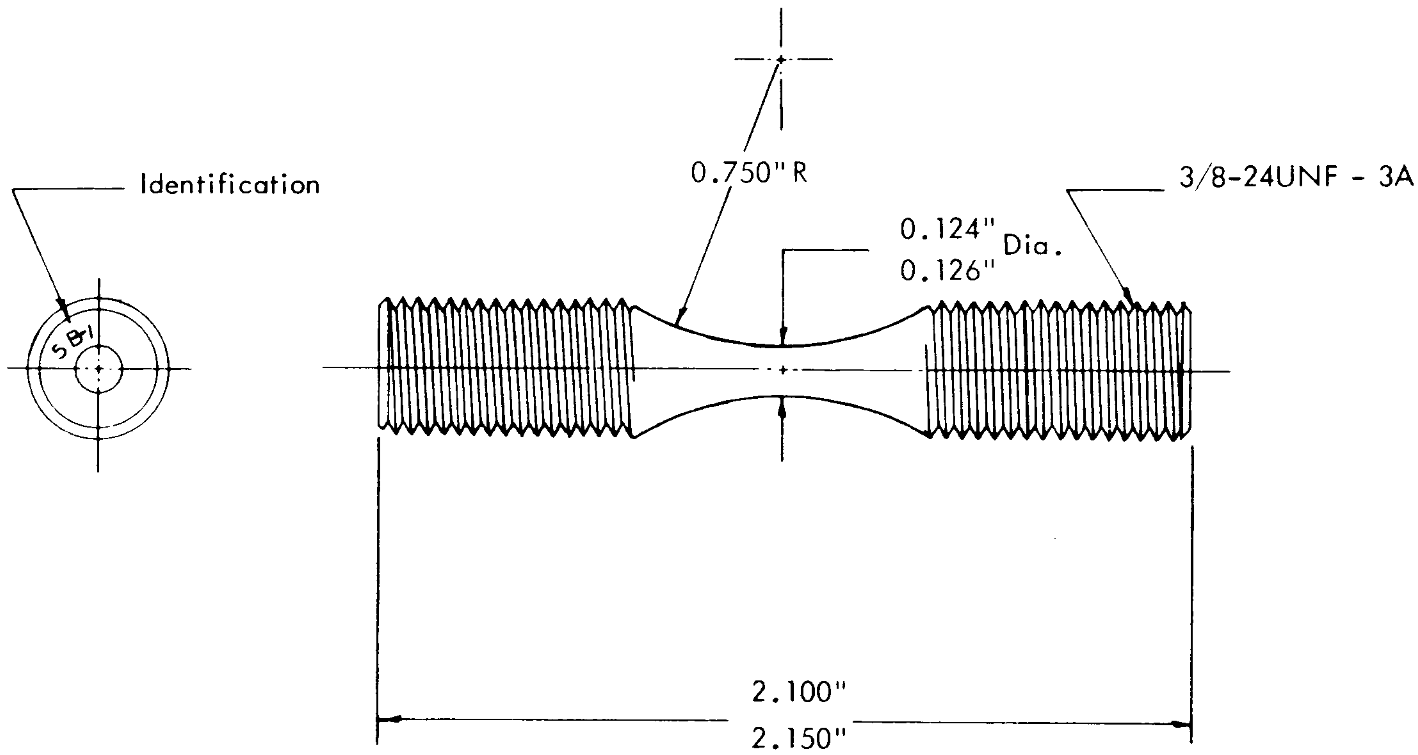

FIGURE 2 FATIGUE SPECIMEN

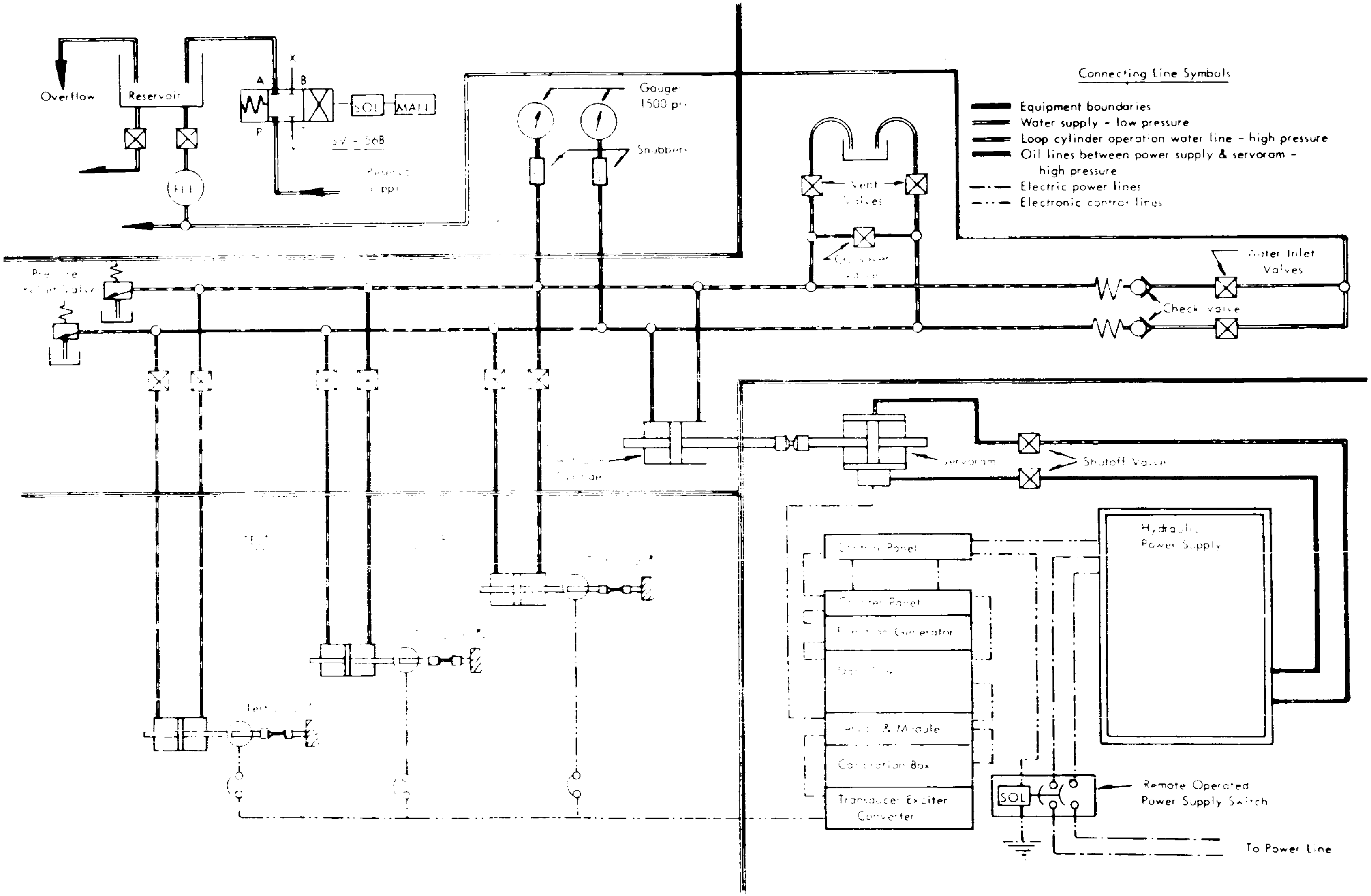

FIGURE 3 LOAD CONTROL SYSTEM (SCHEMATIC)

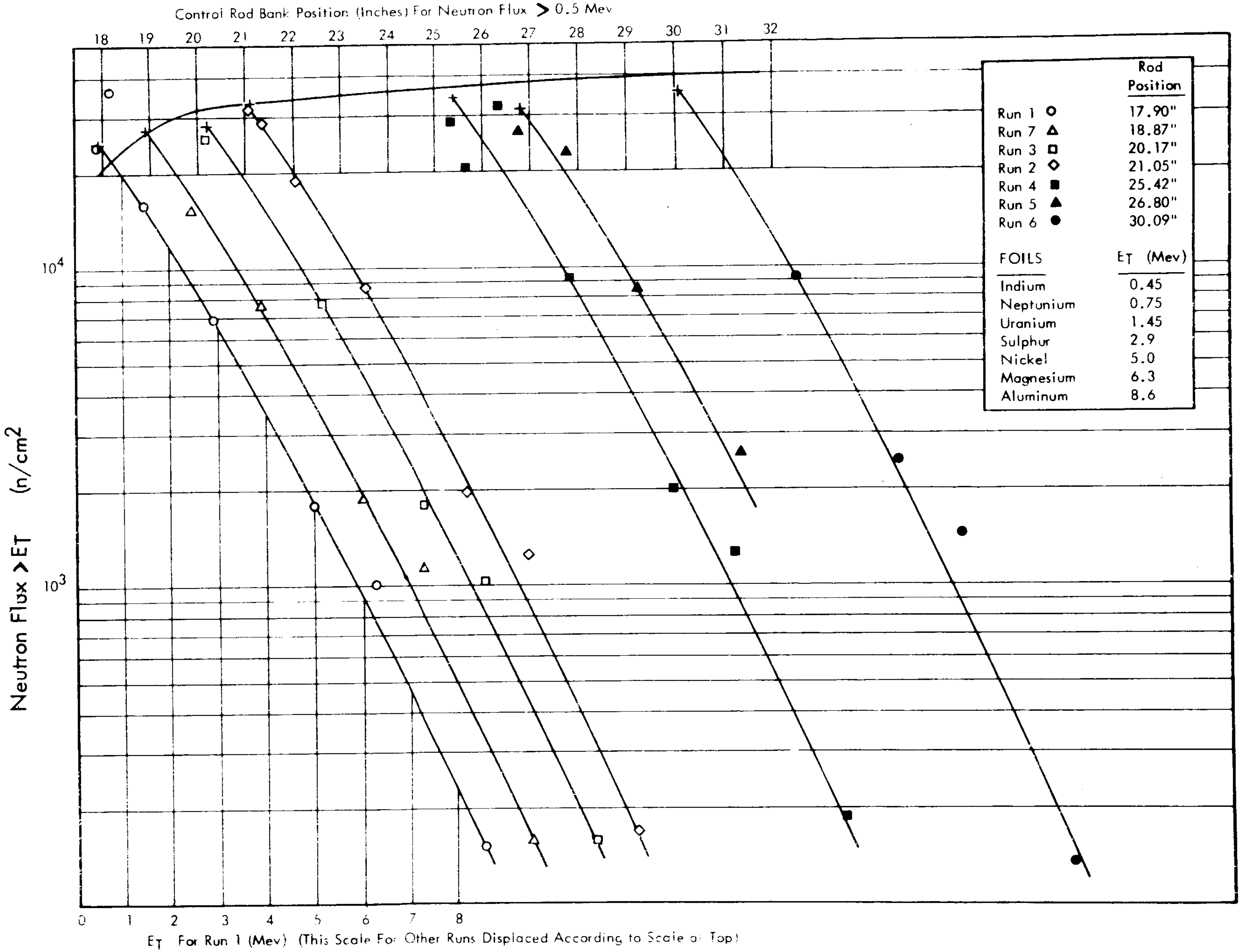

FIGURE 4 NEUTRON FLUX>E_T VS. E_T AND NEUTRON FLUX >0.5 MEV VS. CONTROL ROD BANK POSITION

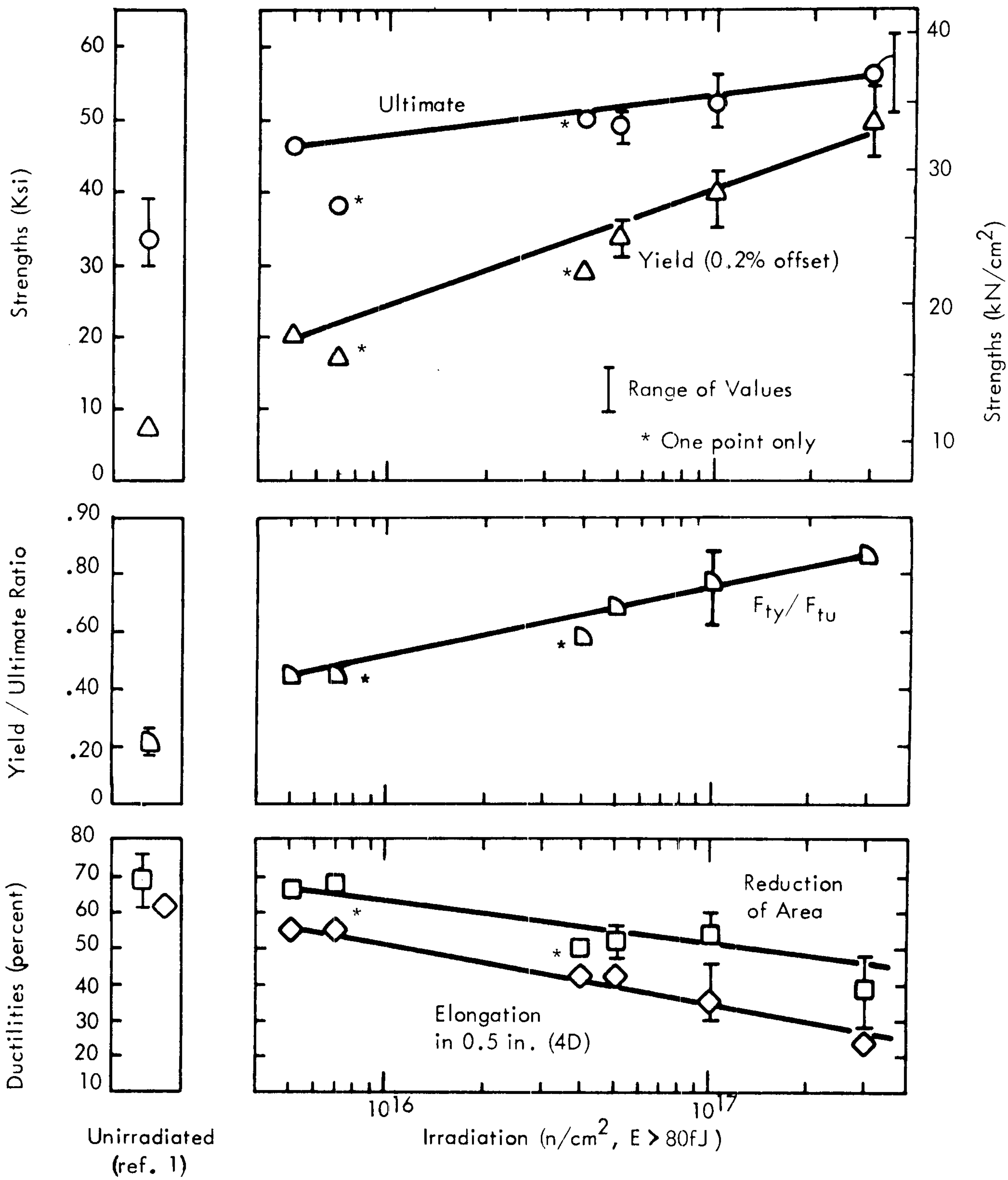

FIGURE 5 EFFECTS OF IRRADIATION AT 17°K ON ALUMINUM 1099-H14

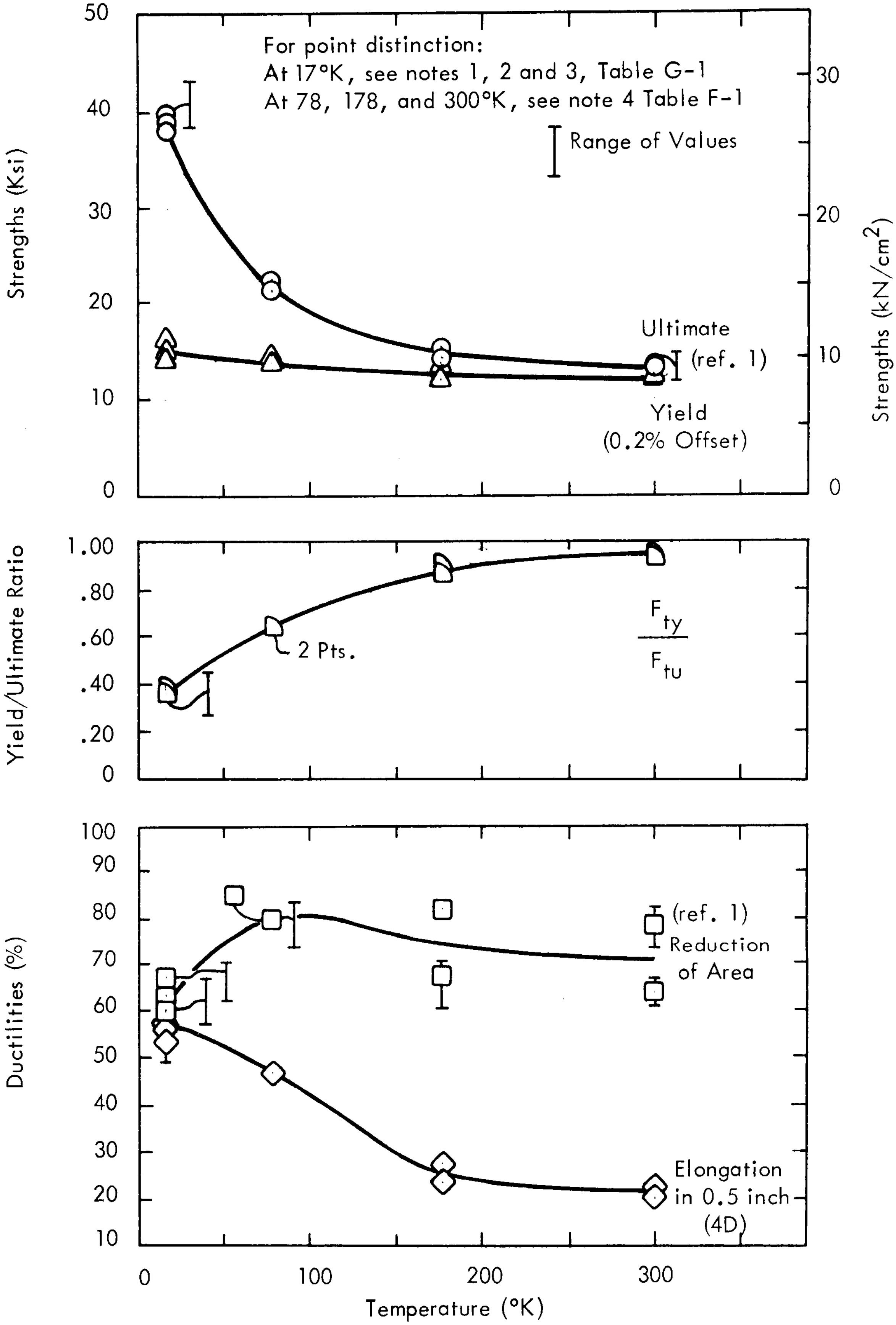

FIGURE 6 TEMPERATURE DEPENDENCE OF TENSILE PROPERTIES ALUMINUM 1099-H14 , UNIRRADIATED

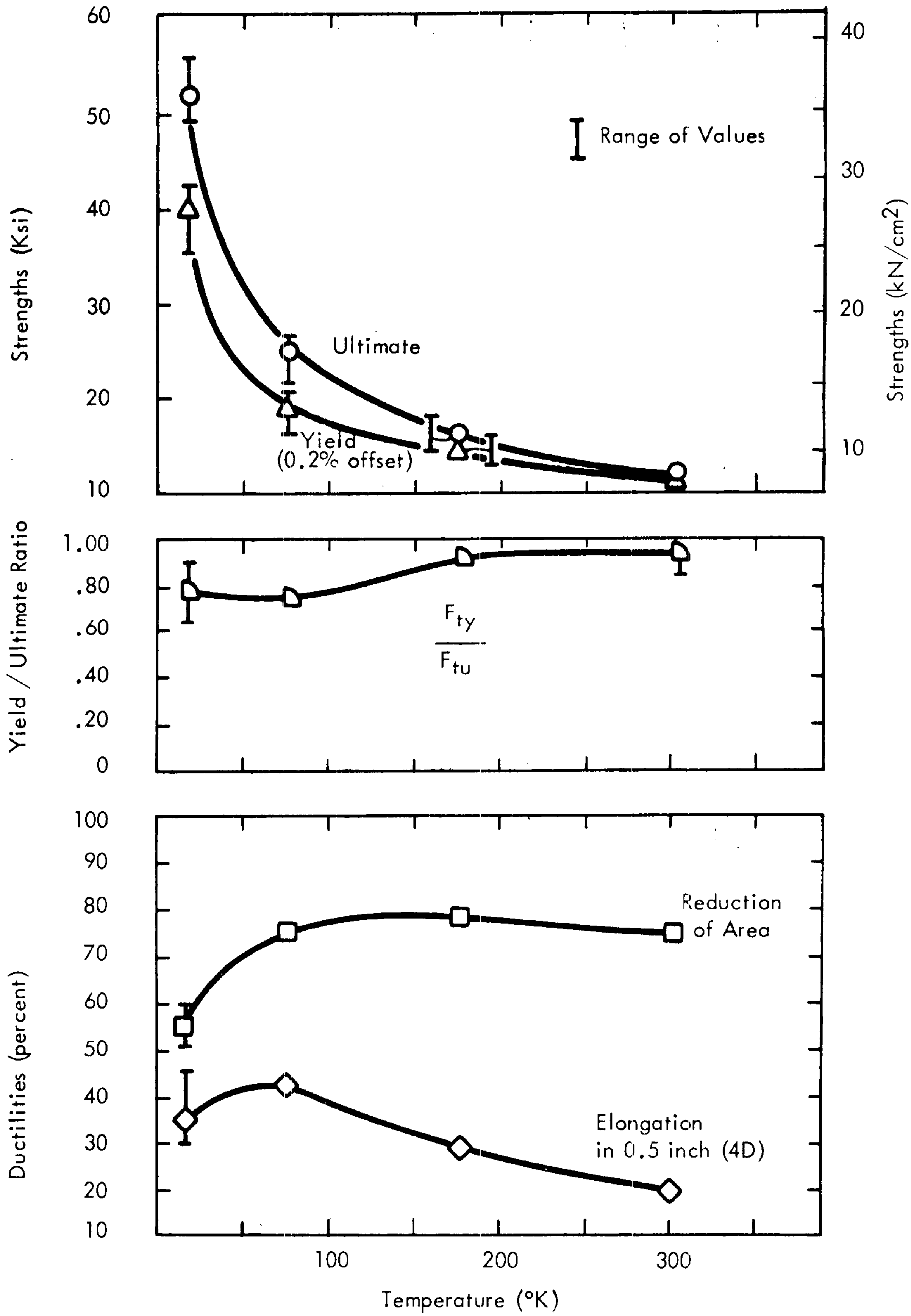

FIGURE 7 EFFECTS OF IRRADIATION TEMPERATURE, IRRADIATED TO 10^{17} n/cm^2 AT INDICATED TEMPERATURE, TESTED AT IRRADIATION TEMPERATURE, ALUMINUM 1099-H14

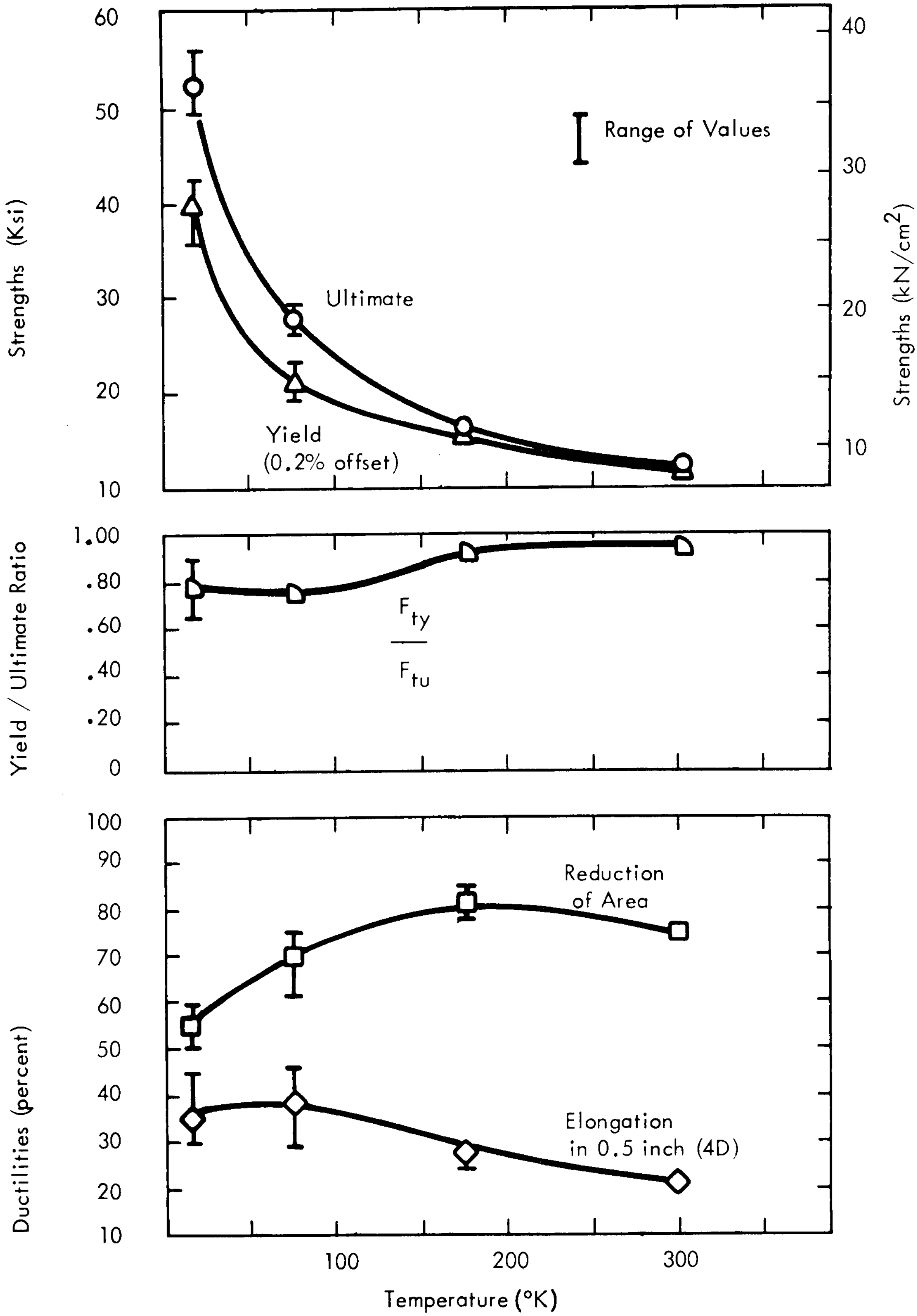

FIGURE 8 EFFECTS OF ANNEALING AND TEST TEMPERATURE, IRRADIATED TO 10^{17} n/cm^2 AT 17°K, ANNEALED AND TESTED AT INDICATED TEMPERATURE, ALUMINUM 1099-H14

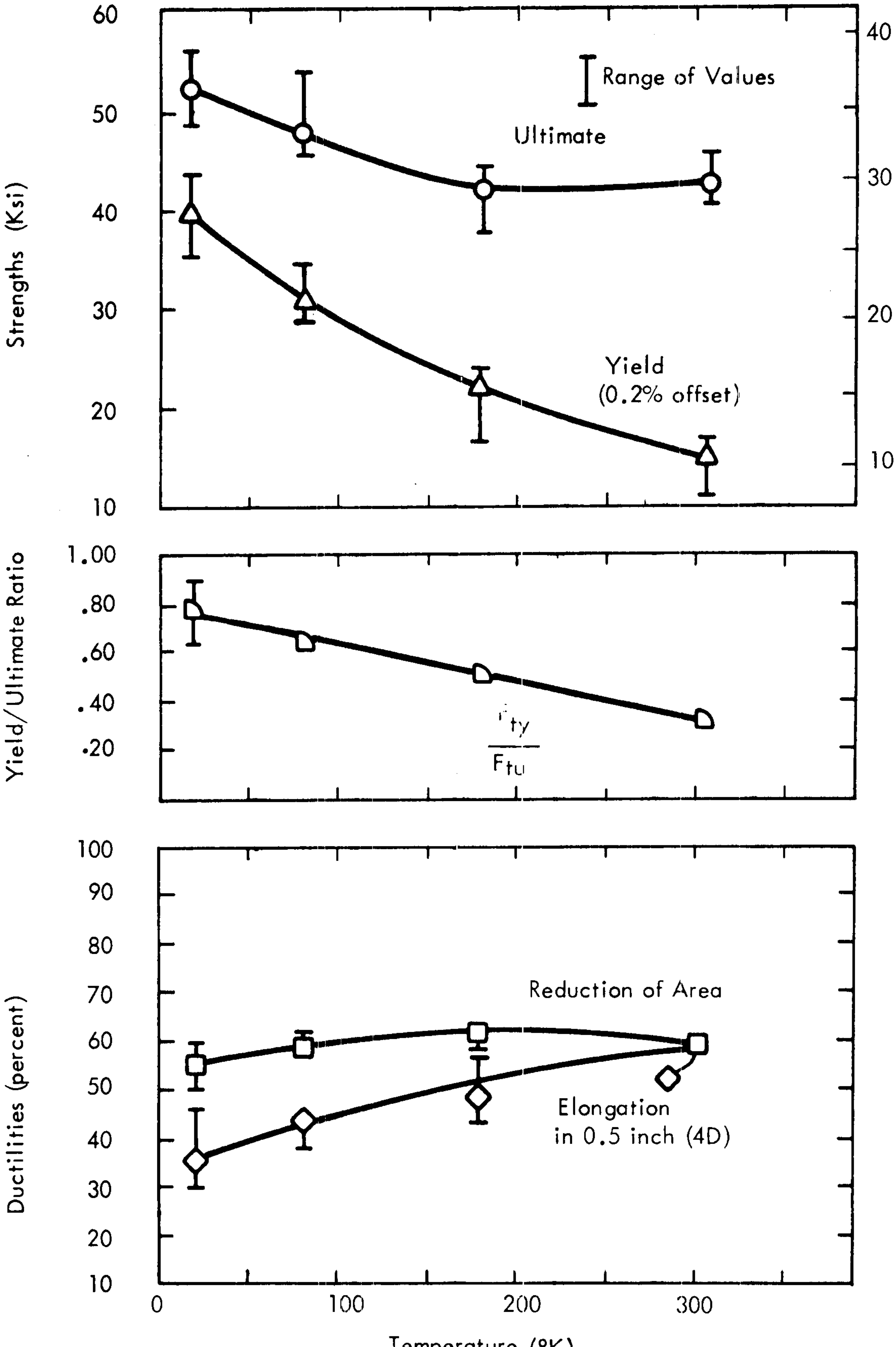

FIGURE 9 EFFECTS OF ANNEALING TEMPERATURE, IRRADIATED TO 10^{17} n/cm^2 AT 17°K, ANNEALED AT INDICATED TEMPERATURE, TESTED AT 17°K, ALUMINUM 1099-H14

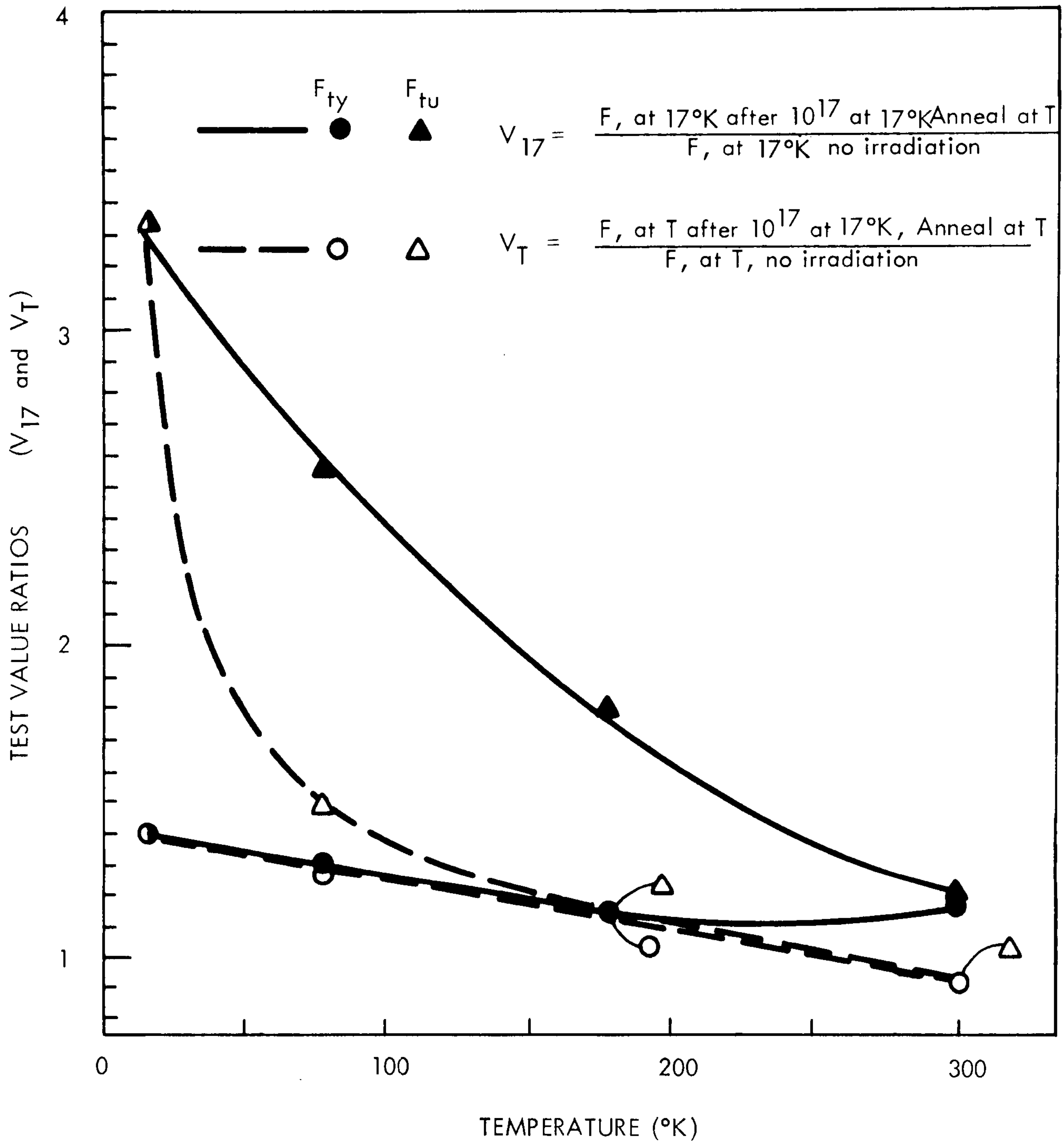

FIGURE 10 COMPARISON OF TEST RESULTS, ALUMINUM 1099-H14, ANNEALED AND TESTED AT INDICATED TEMPERATURE VS. ANNEALED AT INDICATED TEMPERATURE, TESTED AT 17°K

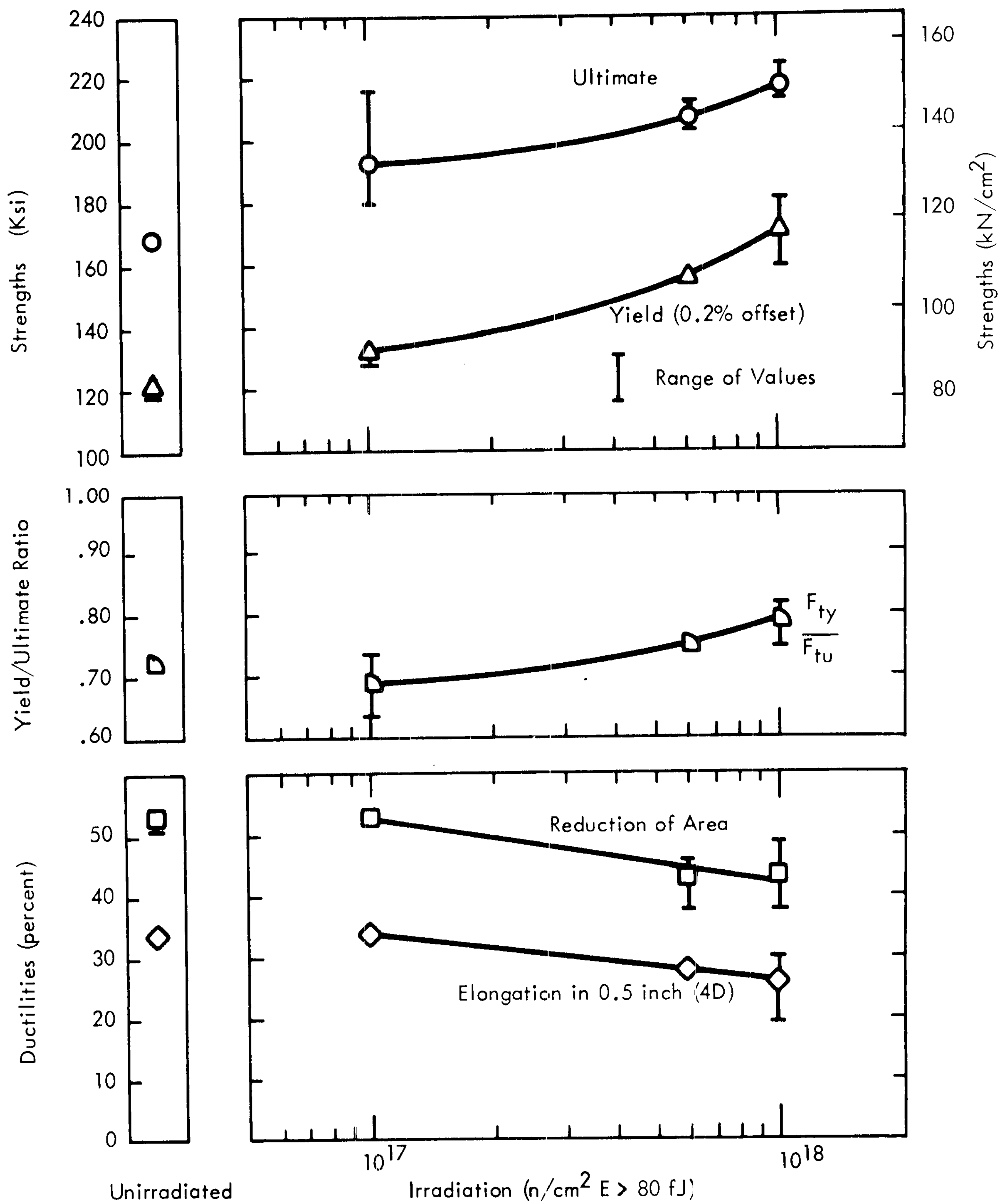

FIGURE 11 EFFECTS OF IRRADIATION AT 17°K ON TITANIUM 55A (ANNEALED)

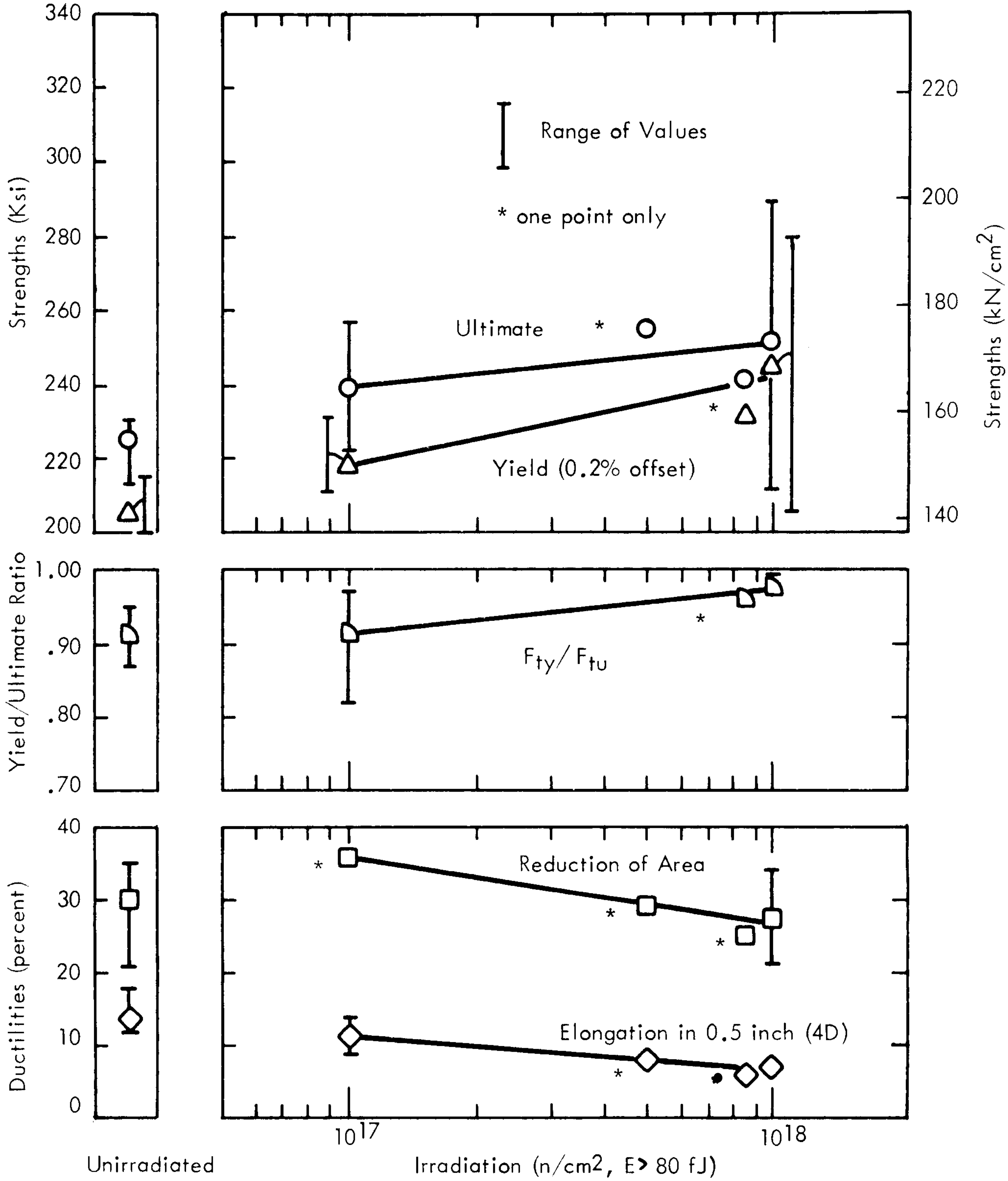

FIGURE 12 EFFECTS OF IRRADIATION AT 17°K ON TITANIUM 5 Al-2.5 Sn (Std. I) (ANNEALED)

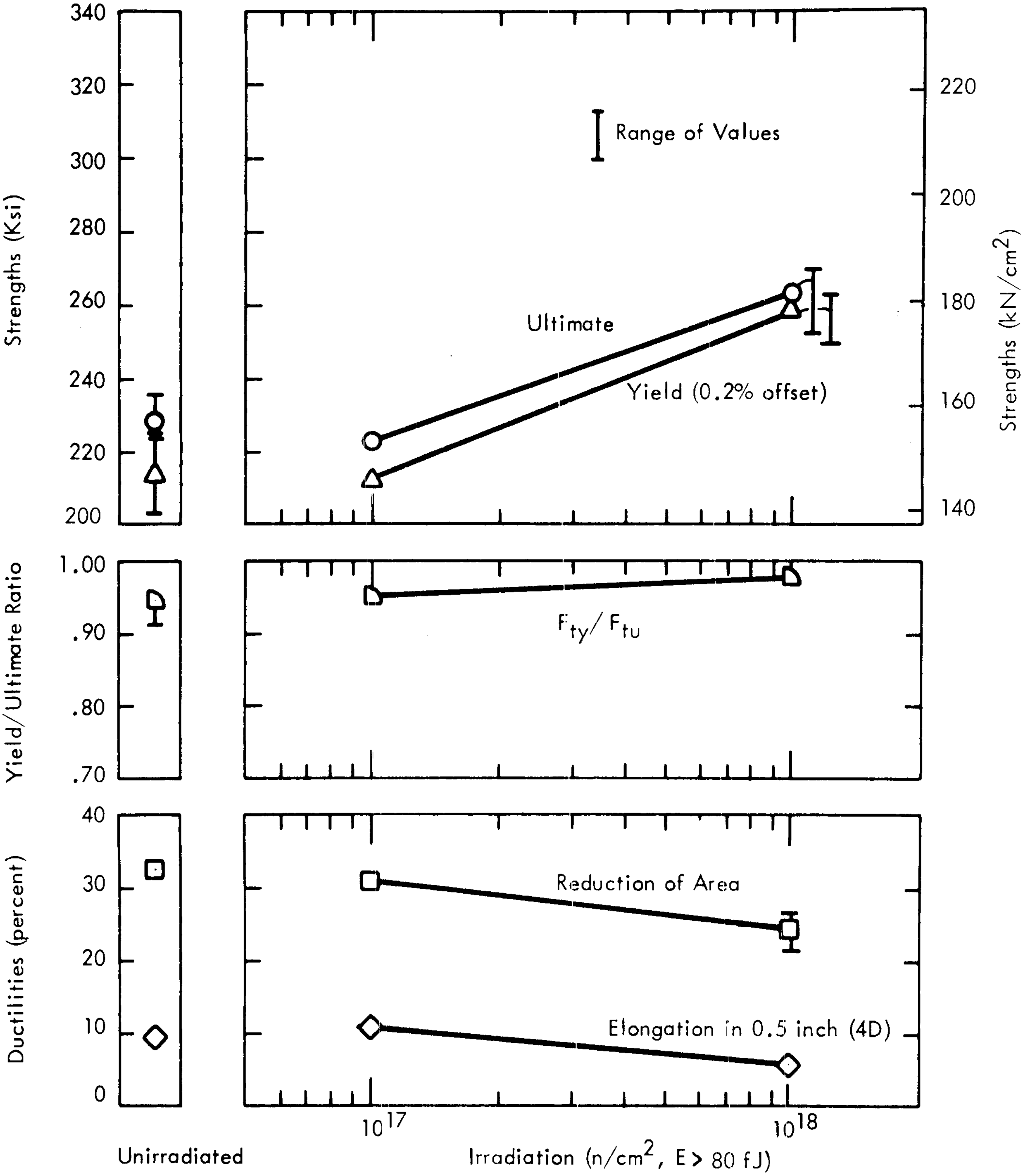

FIGURE 13 EFFECTS OF IRRADIATION AT 17°K ON TITANIUM 5 Al-2.5 Sn (ELI) (ANNEALED)

Specimen 8 Aa 55 Extra Low Interstitial

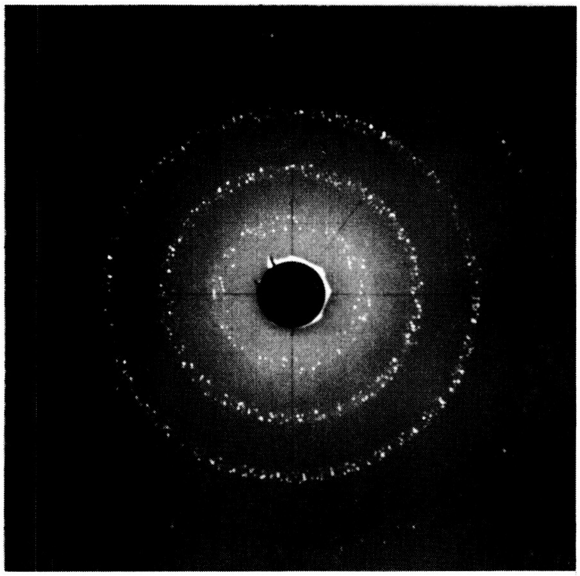

unstrained

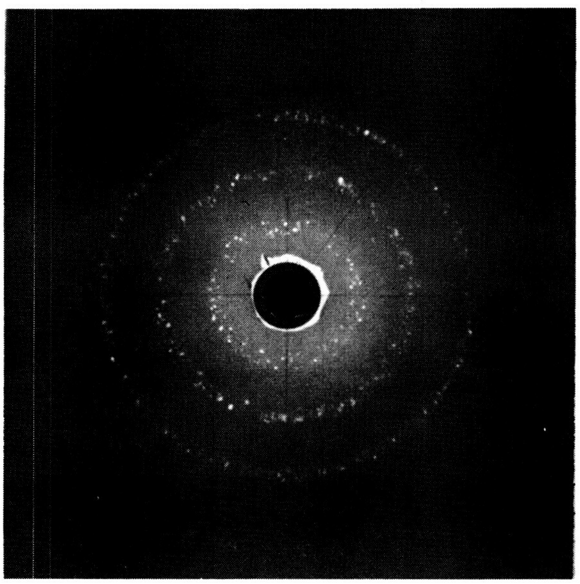

strained to failure

Specimen 3 Aa 63 Standard Interstitial

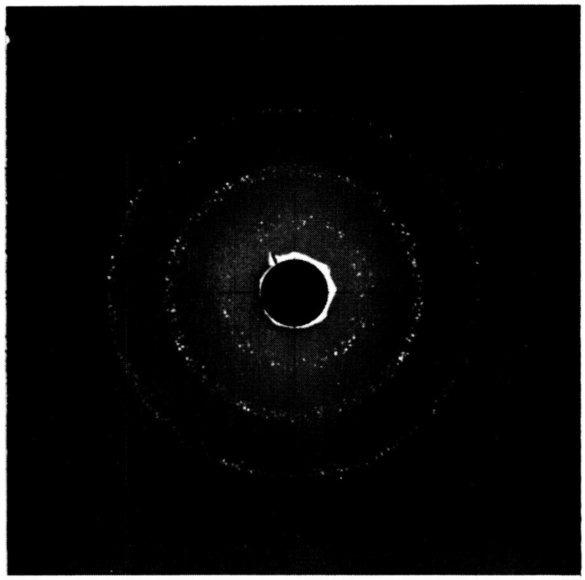

unstrained

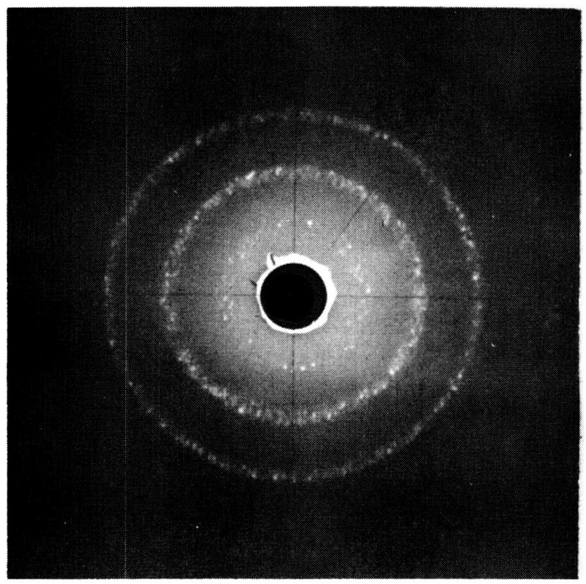

strained to failure

FIGURE 14 X-RAY DIFFRACTION PATTERNS (DEBYE RINGS) FOR TITANIUM 5% Al-2.5% Sn, TESTED IN TENSION AT 17°K FOLLOWING IRRADIATION AT 17°K TO 10^{18} n/cm^2

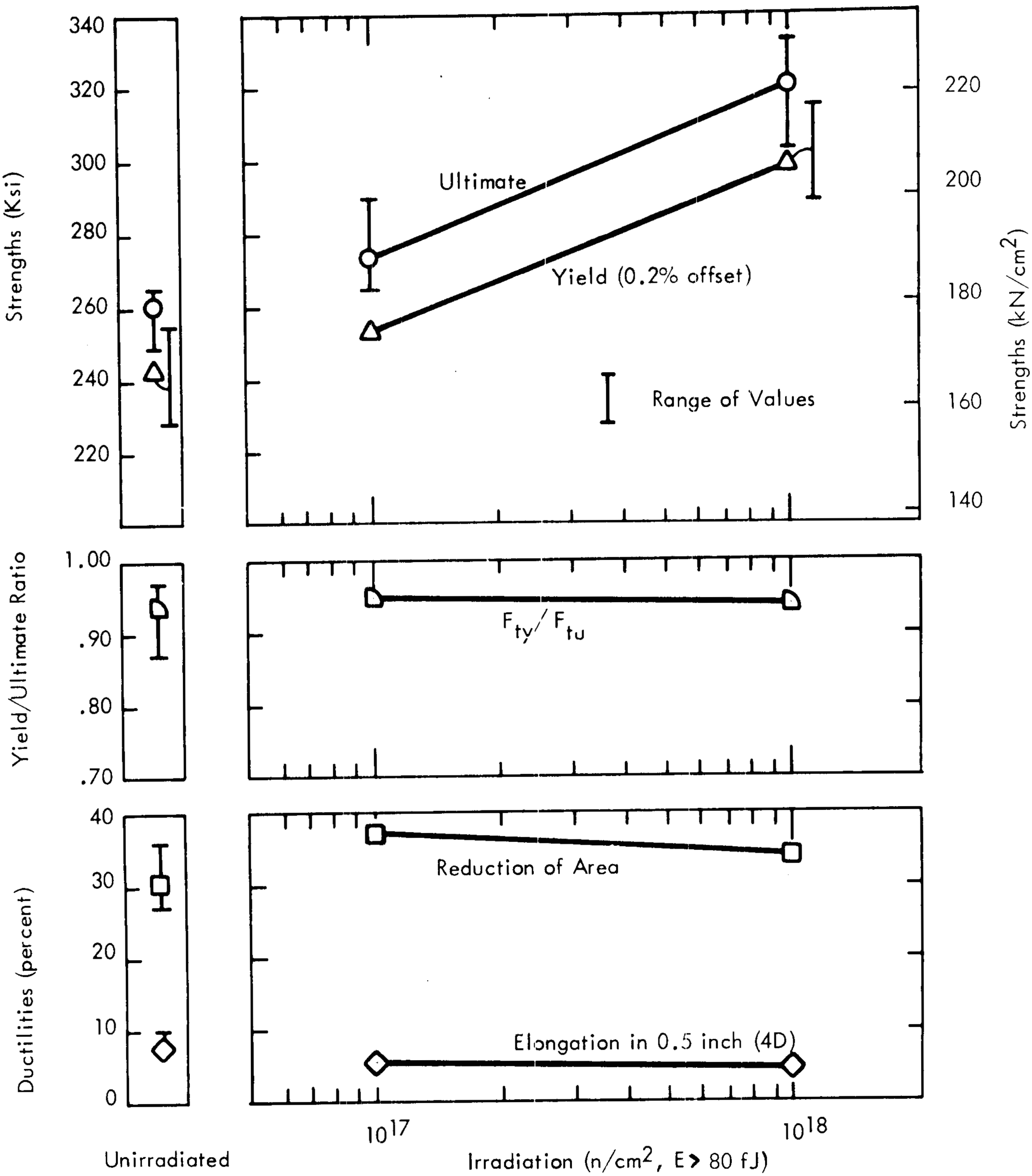

FIGURE 15 EFFECTS OF IRRADIATION AT 17°K ON TITANIUM 6 Al-4V (ANNEALED)

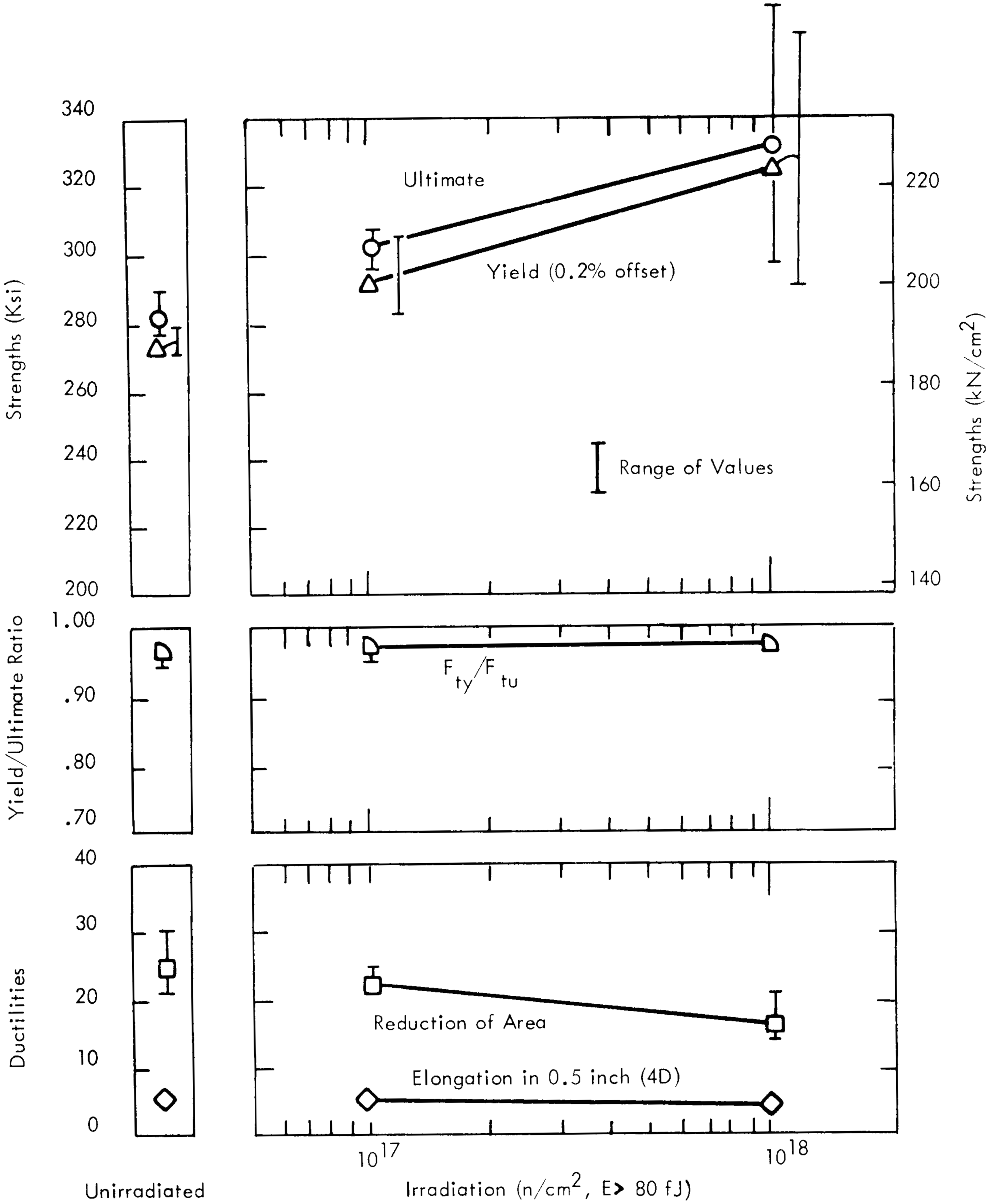

FIGURE 16 EFFECTS OF IRRADIATION AT 17°K ON TITANIUM 6 AL-4V (AGED)

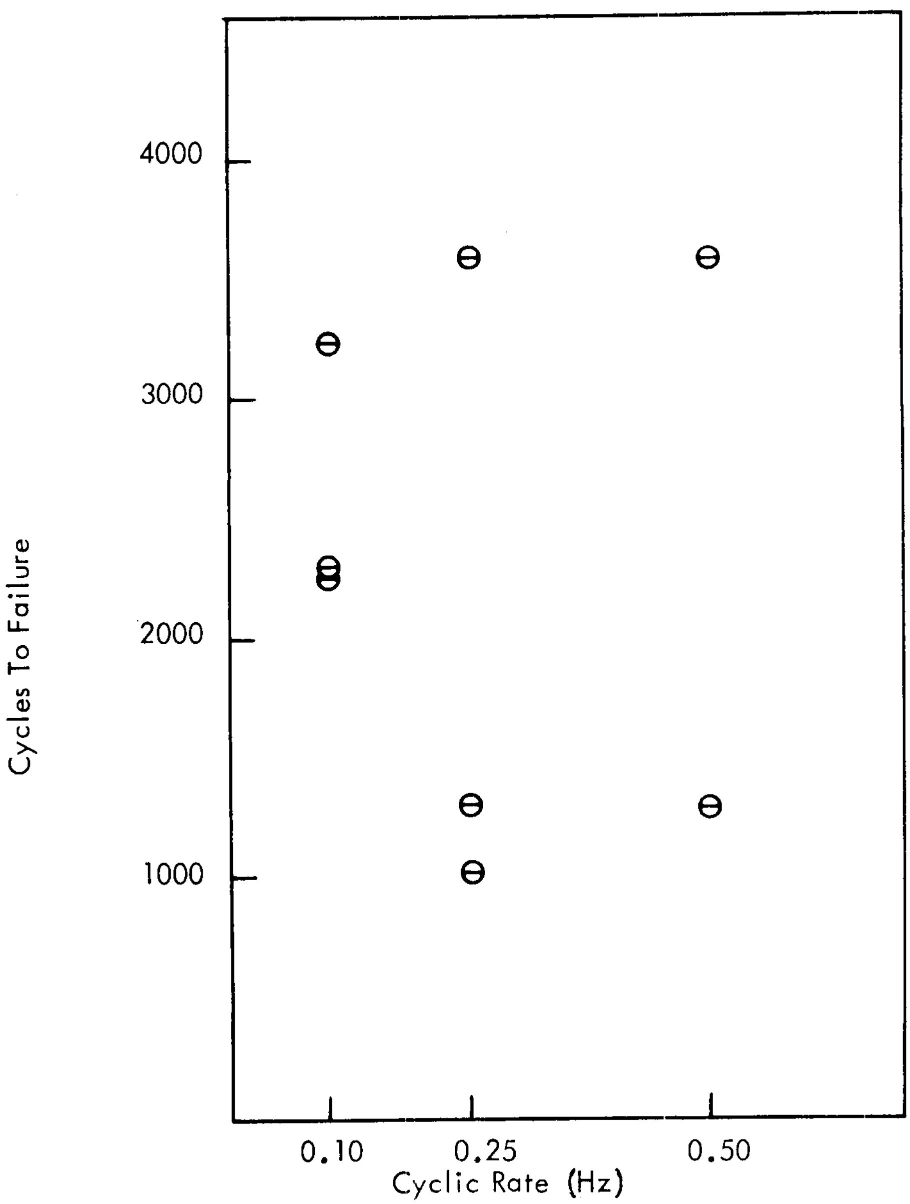

FIGURE 17 CYCLES TO FAILURE VS. CYCLIC LOAD RATE OF TITANIUM 55A AT 17°K NO IRRADIATION. TEST LOAD 90% OF NOMINAL F_{tu}; 152.5 Ksi, 105.1 kN/cm^2; TEST RATIO = -1

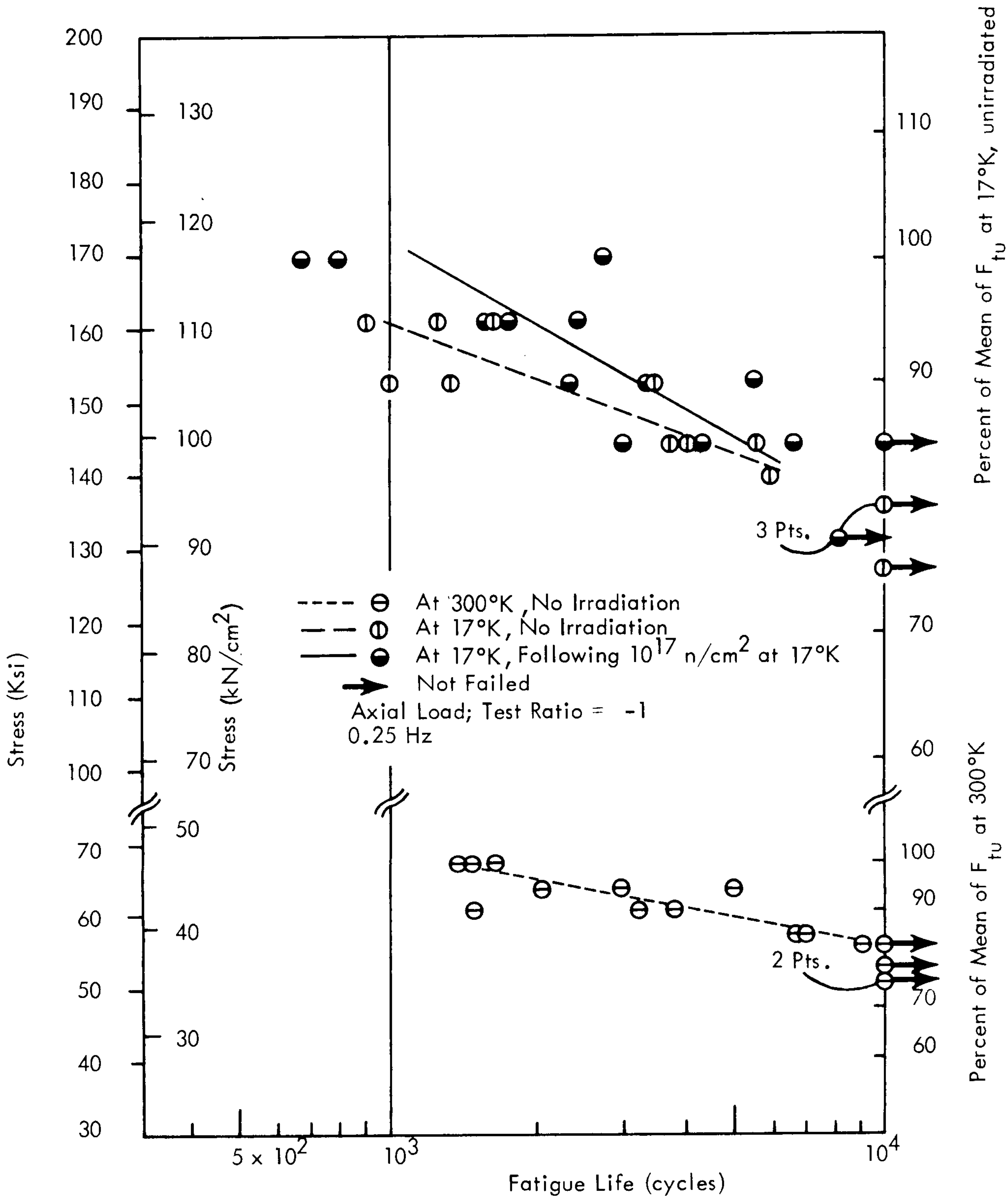

FIGURE 18 LOW-CYCLE FATIGUE STRENGTH OF TITANIUM 55A AT VARIOUS TEST CONDITIONS

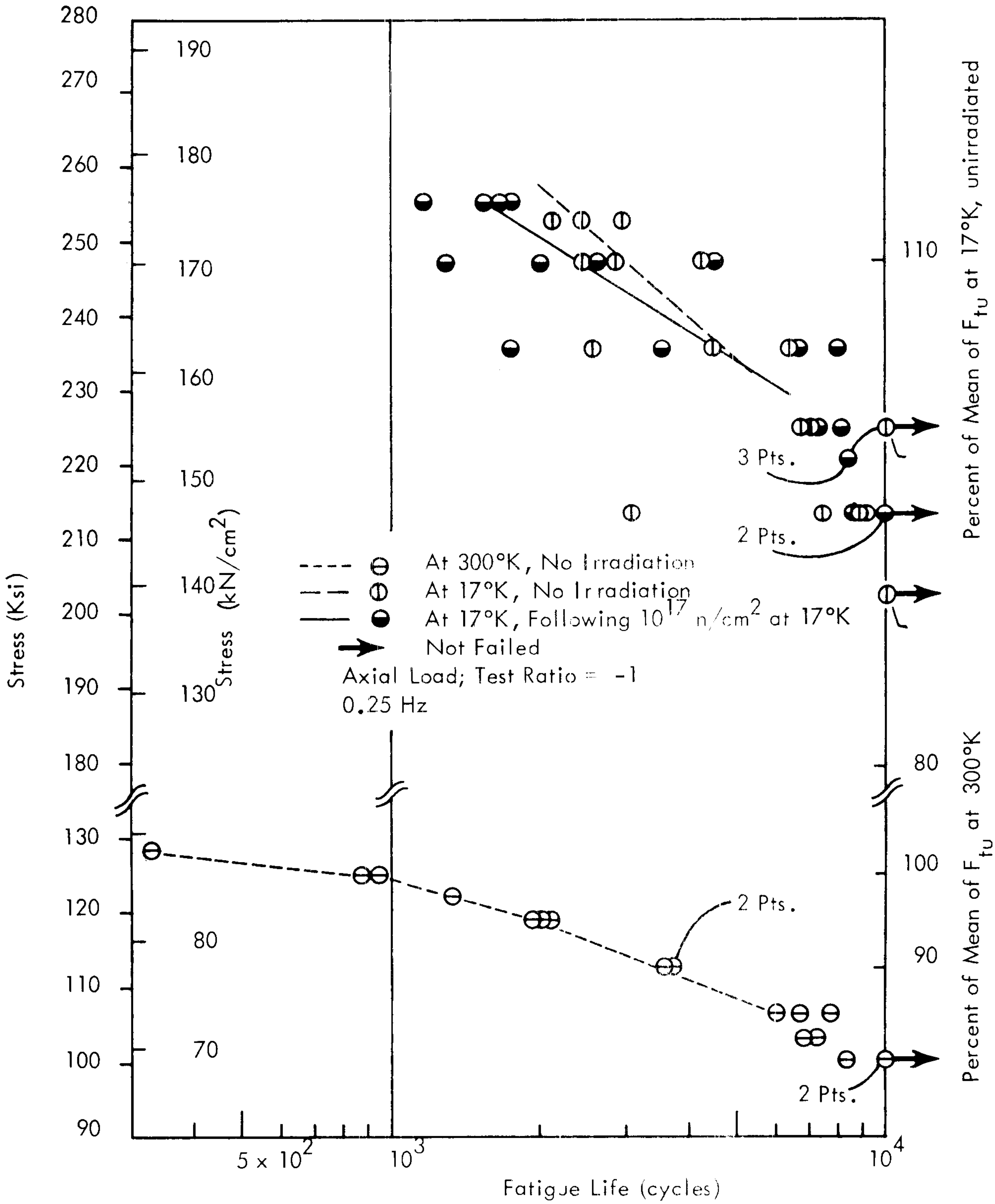

FIGURE 19 LOW-CYCLE FATIGUE STRENGTH OF TITANIUM 5 Al-2.5 Sn (Std. I) AT VARIOUS TEST CONDITIONS

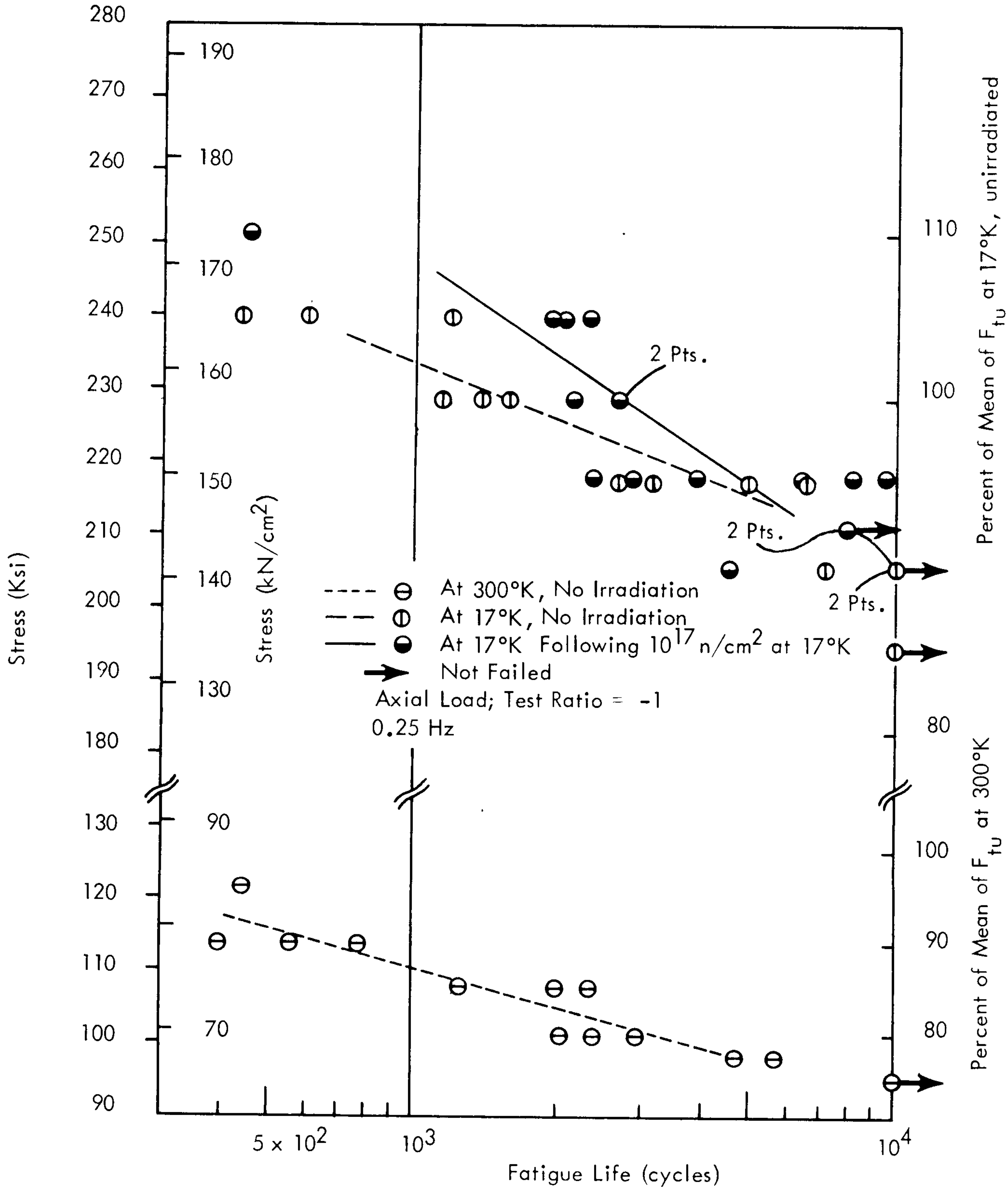

FIGURE 20 LOW-CYCLE FATIGUE STRENGTH OF TITANIUM 5 Al-2.5 Sn (ELI) AT VARIOUS TEST CONDITIONS

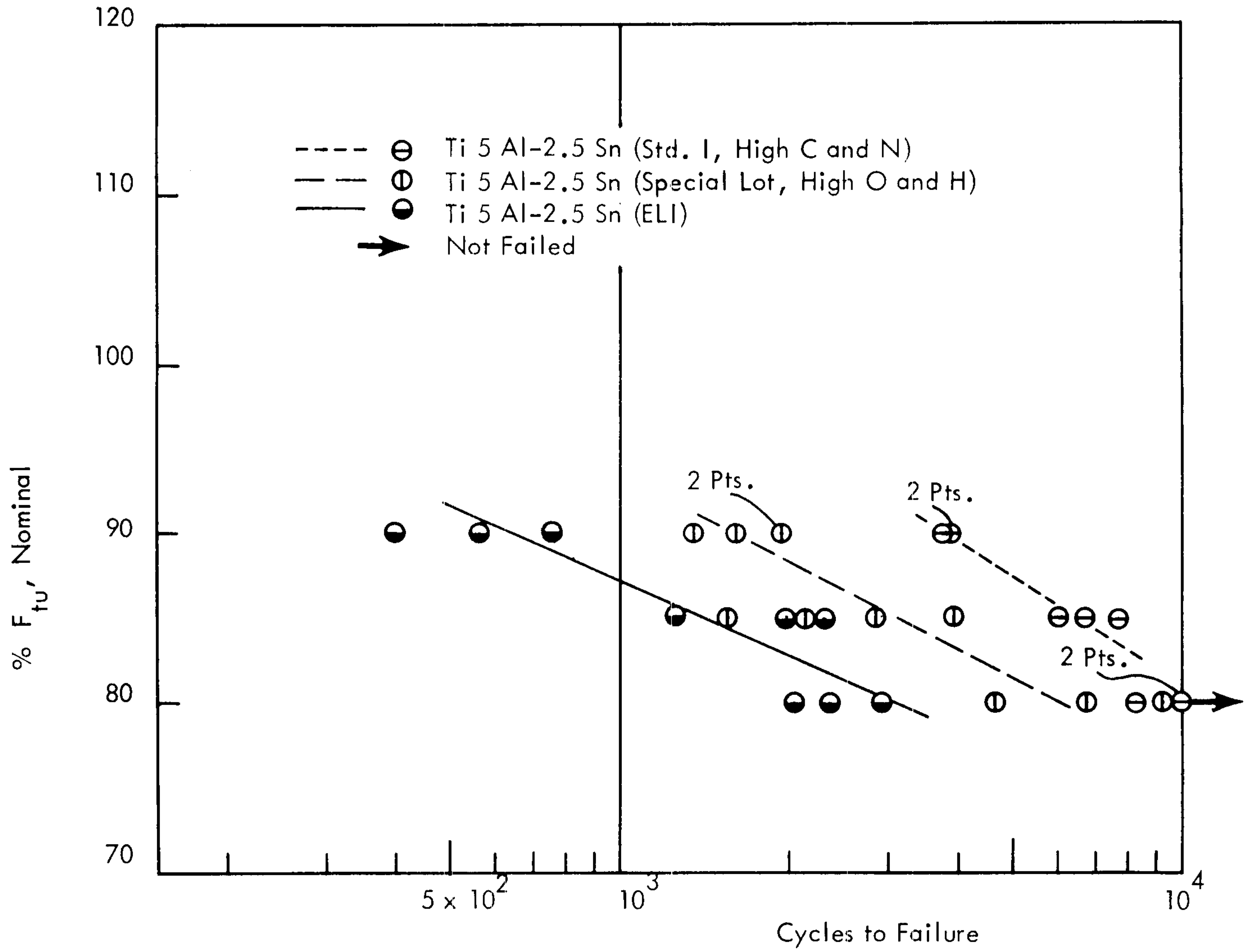

FIGURE 21 EFFECTS OF INTERSTITIAL ON LOW-CYCLE FATIGUE OF TITANIUM 5 Al-2.5 Sn AT 300°K, NO IRRADIATION

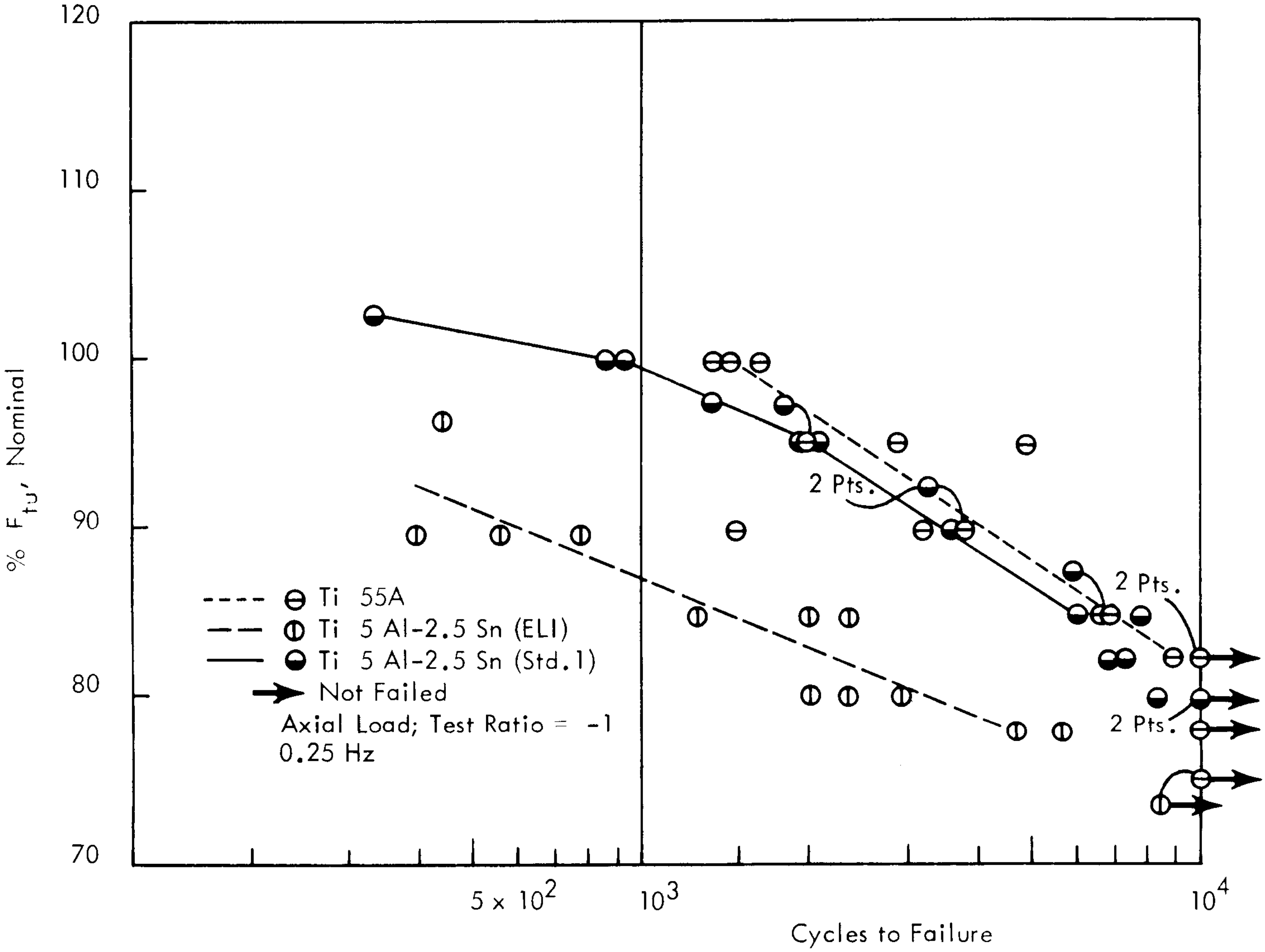

FIGURE 22 LOW-CYCLE FATIGUE STRENGTH OF VARIOUS TITANIUM ALLOYS AT 300°K, NO IRRADIATION

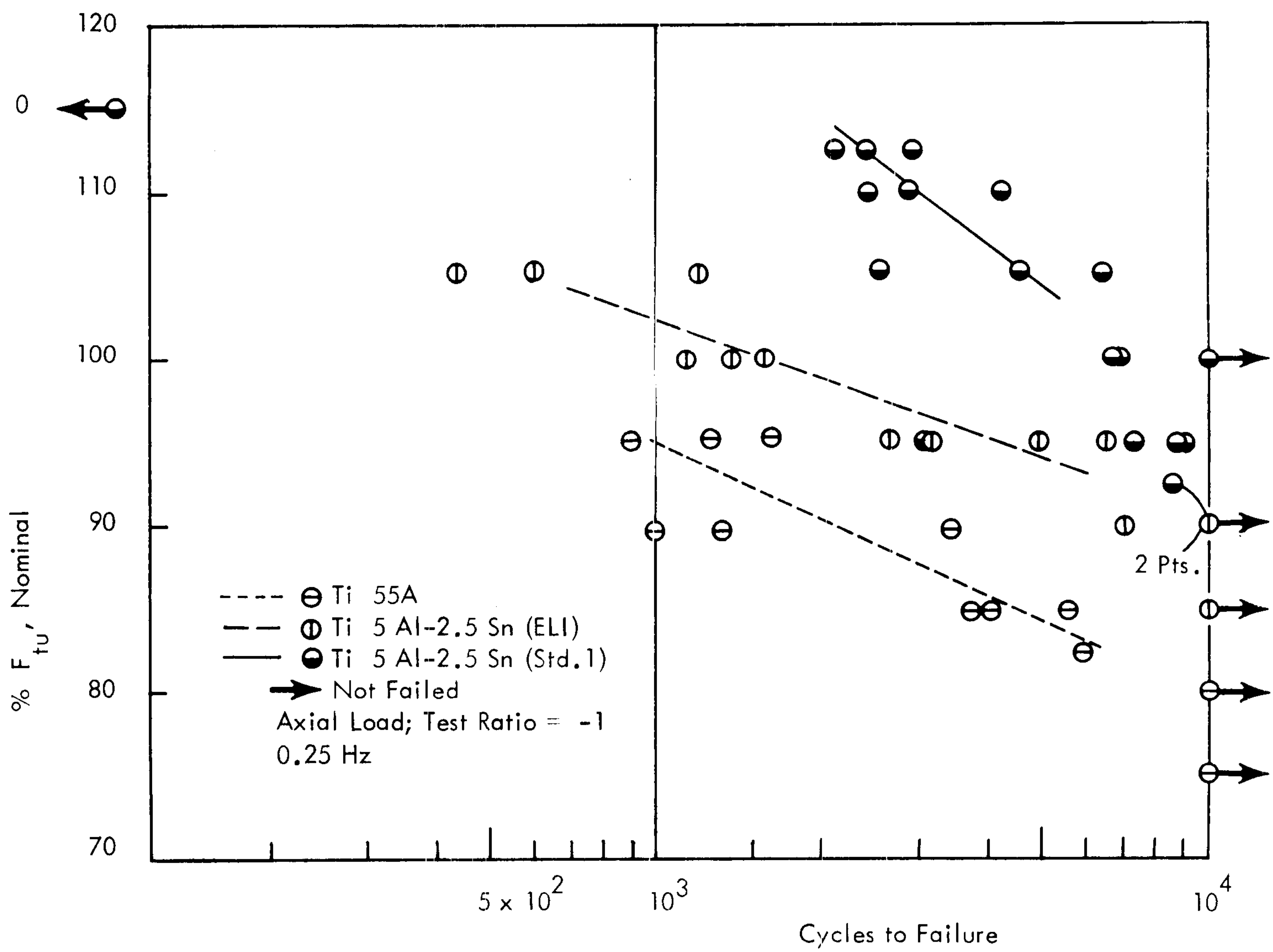

FIGURE 23 LOW-CYCLE FATIGUE STRENGTH OF VARIOUS TITANIUM ALLOYS AT 17°K, NO IRRADIATION

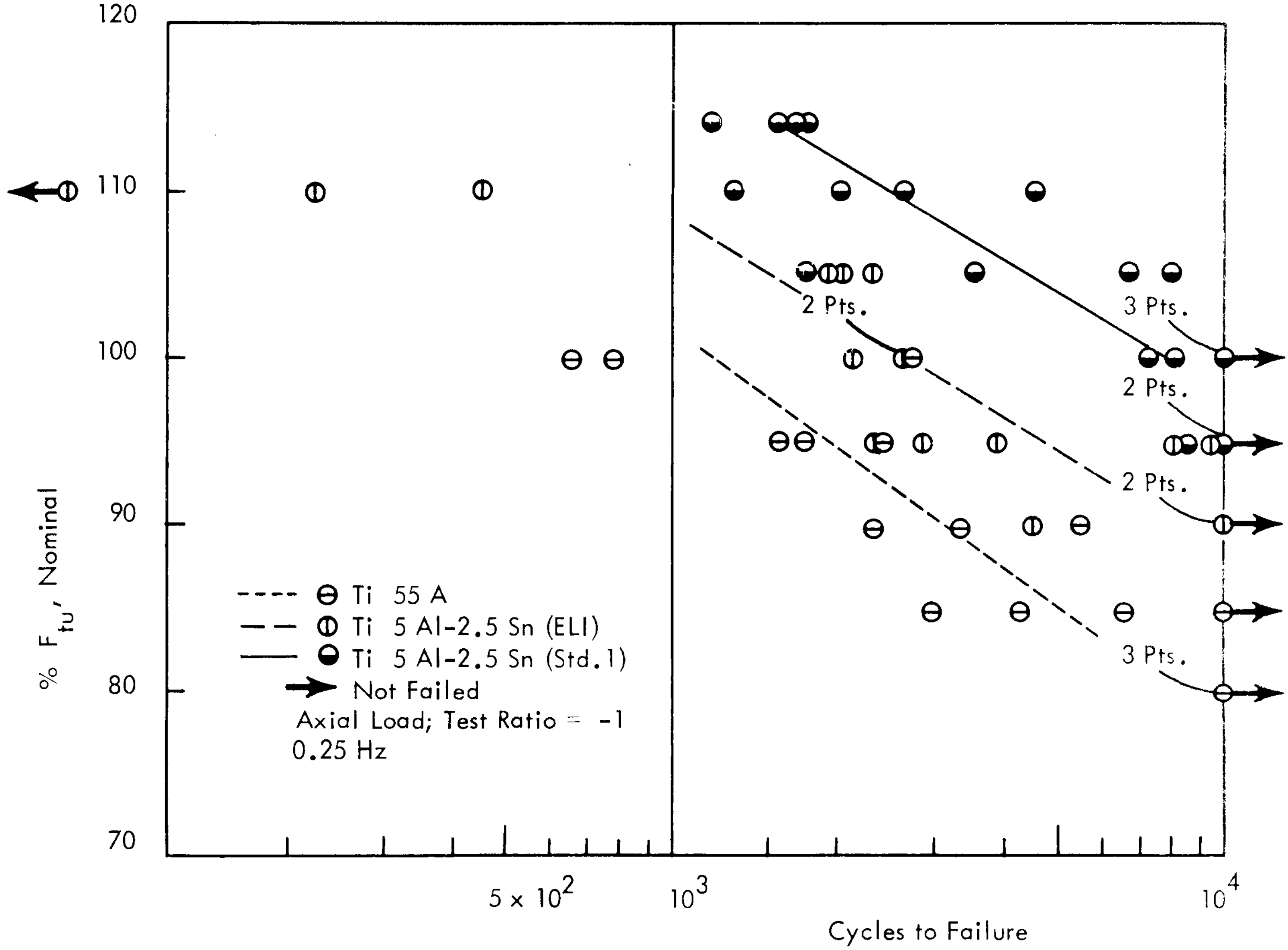

FIGURE 24 LOW-CYCLE FATIGUE STRENGTH OF VARIOUS TITANIUM ALLOYS AT 17°K, FOLLOWING 10^{17} n/cm^2 AT 17°K

APPENDIX A TENSILE TESTING METHOD

For tensile tests, the strain is determined from specimen elongation under load, measured using an extensometer developed for this application. This extensometer measures the increase of the separation between two knife edges initially 0.50 inch (1.27 cm) apart. The measurement is accomplished through the use of a linear variable differential transformer (LVDT) specially constructed to be resistant to radiation effects.

The signal generated by the LVDT is read out on the X axis of a Moseley X-Y Recorder used to plot a load-elongation curve for each specimen tested.

The extensometer was tested for reproducibility of signal at 17°K by repeatedly stressing an AISI 4130 steel test specimen to approximately 60% of its yield strength and comparing the modulus slope recorded for consistency.

The extensometers were verified and classified in accordance with ASTM Specification E-83-64T (ref. 3) using a Tuckerman optical strain gage as a primary standard. The error in indicated strain was less than 0.0001. This gives the extensometer an ASTM Classification of B-1, suitable for determination of modulus values as well as yield strength. However, this classification was obtained in a standards laboratory using precision techniques and this degree of accuracy cannot be expected following installation by remote means. As the extensometer is actually used, an ASTM Classification of B-2, suitable for determination of yield strength, but not of modulus, is probably a more realistic appraisal.

This extensometer has a range of reliable accuracy of approximately 0.010 in (0.025 cm) or some 2% of the specimen gage length. This is sufficient to record the elastic portion of the load-strain curve and the initial plastic portion to well beyond the yield strength (0.2% offset method). However, the strain cannot be measured immediately prior to failure except for rather brittle materials. During plastic behavior of the test specimen at strain levels beyond the capability of the extensometer, load is recorded against time on the X axis to provide a record of the loading pattern and to allow accurate determination of the fracture stress.

The strain rate, measured over 10 second intervals during the elastic behavior of the test specimen, is approximately 9×10^{-2} per sec. This method of measuring speed-of-testing confirms to ASTM E-8, paragraph 22 (ref. 3).

The load applied to the test specimens in the test loop is monitored by a proving ring type dynamometer using a linear variable differential transformer to measure the ring deflection resulting from loading. The transformer operates from a 2 kilocycle carrier oscillator and phase sensitive demodulator. The direct current output from this demodulator is fed through the X-Y Recorder where it is plotted on the Y axis as a direct measurement of stress.

Each dynamometer was calibrated prior to installation in the test loop by loading in series with a Morehouse vibrating reed proving ring calibrated by the National Bureau of Standards. The read out equipment associated with the test equipment was used to record dynamometer loading during calibration. The maximum difference in the load recorded by the dynamometer and the standard ring was less than 2%.

APPENDIX B FATIGUE TESTING METHOD

The basic test equipment used in this program discussed in the body of this report was described in reference .

The tensile/compression system, was modified in 1965-66 to provide the additional capability for low cyclic rate fatigue testing. This modification was performed under Contract NAS 3-7985 and this appendix constitutes the final report of the equipment modification phase of the effort authorized by that contract. The test system, after modification, provides the following operational parameters:

- Two single-specimen tension-compression test loops were modified to permit conducting in-pile axial tension-compression fatigue tests. Test loop requirements include the following:
  - Ability to maintain test specimen temperature within $\pm$ 0.5°K of the desired test temperature (17°K minimum) throughout irradiation to integrated flux levels equivalent to one power cycle of the Plum Brook Reactor;
  - Ability to vary frequency of cycle between 0.1 Hz and the maximum cyclic rate obtainable with equipment;
  - Ability to maintain constant frequency of cycle throughout any desired test time;
  - Ability to stop test automatically when specimen breaks;
  - Ability to be readily disassembled and assembled by remote means to replace test specimens;
  - Means for axial alignment of test specimen;
  - Means for measuring maximum and minimum tensile and/or compressive stress applied to the test specimen during a fatigue cycle;
  - Means for indicating number of cycles of stress applied to the test specimen.

Equipment alterations in two major areas were required to attain these objectives; the test loop was modified to permit cyclic loading in tension-compression with axial alignment to prevent introduction of bending moments on the test specimen and the load-control system was redesigned to facilitate cyclic reversals of load sign with precise control and to insure system reliability through many load cycles. Since a single test could require as many as 10^4 cyclic reversals, the reliability requirement for system operations is quite stringent.

B-1 FATIGUE TEST LOOP

The fatigue test loops were made by modification of tensile/compression test loops. The entire design was re-evaluated with regard to structural stability under cyclic loading conditions. Deflection of structural members under compressive and tensile specimen loading patterns were measured to determine if such deflections might influence the axiality of the applied force. No significant deflection was observed. A 5/16" (7.9 mm) diameter aluminum specimen was equipped with strain gages positioned parallel with the specimen axis at 90° (1.8 radians) circumferential intervals. At test loads of 3550 lb (15,790 newtons) the difference in measured strain indicated a differential fiber stress induced by bending moments of less than 7000 psi (4823 n/cm^2). Since this test load represents a stress of 239 Ksi (199,121 n/cm^2) on an actual specimen with a 1/8" (3.2 mm) diameter, the magnitude of the bending moment is within acceptable limits for axial load fatigue testing.

The tensile/compression was originally designed without consideration of reversal of loading direction during a test. Therefore, re-evaluation of the linkage in the push-pull rod mechanism was required to insure a smooth, impact free, transition between tensile and compression loads. Measurements of the lost motion in the linkage during load reversal was made; in the worst case the lost motion is - .020" (0.5 mm). This is considered negligable in this operation. Subsequent examination of oscilliscope patterns during cyclic loading confirm this opinion.

The specimen holders used in the tension/compression test loop rely on mated uni-directional spherical seats for specimen alignment. New holders using mating conical faces between the holder and a join nut were designed. The design, shown in figure B-1 uses the minimum number of parts to provide optimum alignment with minimum internal slack. Heat transfer studies were performed to insure that the heat leak through these holders was within the limits imposed by the temperature control requirements. The validity of these heat studies was demonstrated during the temperature control studies discussed in Appendix C.

The dynamometer design was specially modified to provide reliable load readings in the upper range of the machine capacity over the numerous cyclic load reversals required for fatigue testing capability. This modification was required as the result of operating experience discussed in section B-3 below.

B-2 FATIGUE LOAD CONTROL SYSTEM

The load control system available at the Plum Brook Reactor Facility test installation in HB-2 at the start of the program utilizes a positive displacement pump, with demineralized water as the working fluid, to operate the hydraulic actuator located in the test loop. To insure reliable servo-valve operation over the many cyclic load reversals inherent in fatigue testing, oil provides a much more suitable medium than water. However, the possibility of oil contamination of reactor coolant water must not exist. Therefore, a dual fluid system, shown schematically in figure 3, was constructed and installed. The electronic control was also modified, to incorporate a digital voltmeter to enhance the precision of dynamometer calibrations and load monitoring.

B-3 OPERATING EXPERIENCE

In the initial portion of the fatigue testing program the test load was monitored with the same 5000 lb (22,240 N) capacity dynamometer which has been extensively used for tensile testing with no significant shift in calibration. After about six months of testing an apparent discrepancy in test results between data being generated and prior test data was observed. Investigation of the load monitoring instrumentation revealed that the proving rings had developed fatigue cracks in the fillet joining the threaded connecting boss to the reinforcing pad on the end of the ring. A flourescent penetrant indication, under ultra-violet illumination, of this crack is presented in figure B-2. The cracked ring was broken by tensile loading to permit determination of the extent of the crack. The dark semi-elliptical area shown at the root of the boss, in figure B-2, represents the limit of crack propagation during cyclic loading. Re-examination of all test values generated with these proving rings and the operational/calibration histories of the instruments was undertaken to permit a statistical determination of the point where instrumental uncertainty reflected adversely on test data validity. It was determined that this particular proving ring produced accurate data for about 5×10^4 cyclic reversals of loads greater than 2500 lb (11,120 N); after that point a slight deviation of data values from earlier

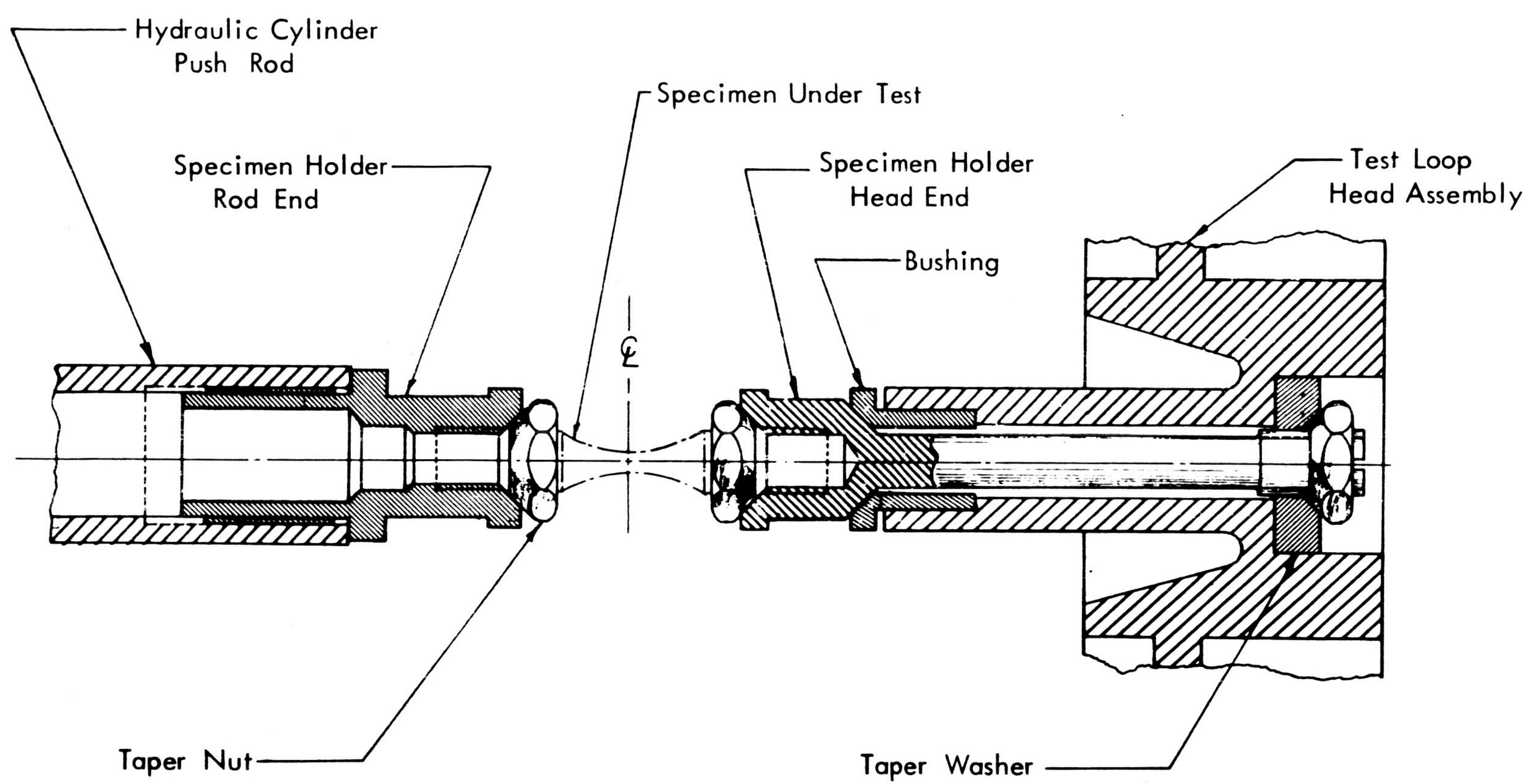

FIGURE B-1 SPECIMEN HOLDER DESIGN

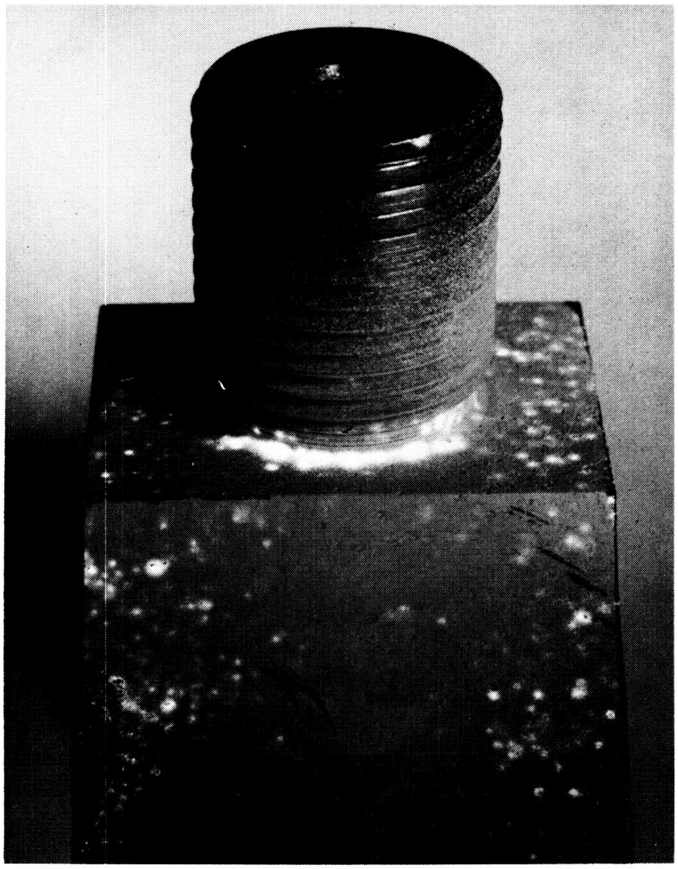

(a) Fluorescent penetrant indications

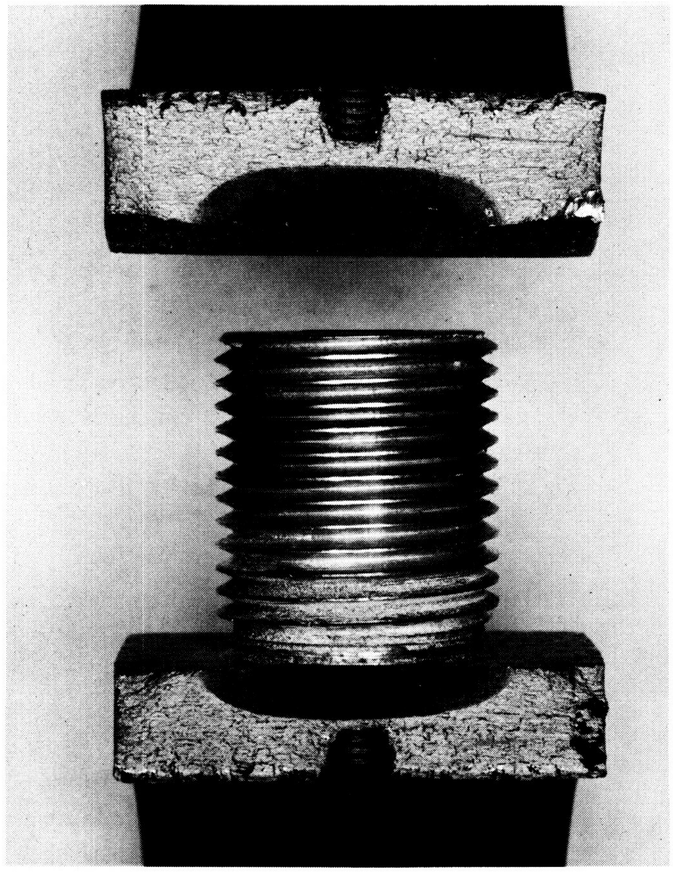

(b) Fractured faces of broken ring

FIGURE B-2 FAILED DYNAMOMETER PROVING RING test results was observable. The magnitude of the deviation increased with continued use. The crack closed during compressive loading without any appreciable effect on load measurement; opening of the crack during tensile loading increases the unit stress in that area of the proving ring to an extent that renders accurate tensile calibration impossible.

Forty-nine data points, eleven from specimens which had received irradiations of 10^{17} n/cm^2 and the remainder unirradiated, were discarded from the test data as of questionable accuracy. This number of rejected data points reflects a conservative approach to preclude the publication of possible erroneous and, therefore, misleading design information.

As an emergency measure, to permit resumptions of the fatigue testing program, dynamometers of a similar design but with a rated capacity of 10,000 lb (44,480 N) were obtained. One of these dynamometers was tested by repeated loadings of 3400 lbs (15,123 N) in tension and compression at cyclic rates up to 30 cpm using methods compatable with the procedures followed in the test program. This test load would apply a unit stress on an actual test specimen of about 120% of the ultimate tensile strength of any material-temperature condition in the anticipated test programs. The ring was recalibrated after 6.7 x 10^4 cyclic reversals with no evidence of signal shift. Cyclic loading was continued and the unit rechecked after 10^5 cycles. At this point, the calibration was at slightly over 3% variance with the initial calibration. Inspection of the proving ring showed indications of fatigue cracks similar to, but less in extent, than those encountered in the 5000 lb (22,240 N) rings. These tests demonstrated the adequacy of the 10,000 lb (44,480 N) capacity ring for a temporary corrective measure, subject to inspection and recalibration at suitable intervals dependent on actual test load levels used in the program.

Efforts were then directed to providing load monitoring instrumentation with a longer reliable operational life expectancy. After consultation with the manufacturer (The Schaevitz Engineering Company), it was decided to change the proving ring material to 17-7 PH stainless steel to prevent the formation of corrosion pits with notch-like stress concentration patterns and to increase the radius of the fillet blending the threaded connecting boss to the ring to reduce the stress concentration in the area where failures had occurred. These rings were fabricated and heat treated to the RH 950 condition for optimum fatigue life.

The rings were initially manufactured with 10,000 lb (44,480 N) rated capacity. One ring was tested as described above for the old design. The ring was recalibrated and inspected after 2.5 x 10^5 reversals of a 3400 lb (15,123 N) test load. No variation from initial calibration or evidence of crack nucleation was observed. The ring was then machined to a 5000 lb (22,240 N) capacity configuration to increase the sensitivity of response and retested. No changes in calibration or crack nucleation were observed after 1.5×10^5 cyclic reversals. Since the major portion of any anticipated fatigue testing program will be at load levels well below the test load level, this ring configuration will provide a long reliable operating life. Recalibrations at time intervals dependent on actual test loads will be included in standard operating procedures.

APPENDIX C MEASUREMENT AND CONTROL OF SPECIMEN TEMPERATURE

Direct measurement of the specimen temperature was not feasible because of:

(1) Possible alteration of the mechanical properties of the specimen during attachment of the sensing device.

(2) Mechanical difficulties in attaching sensing devices to the individual specimens using remote handling techniques.

(3) Possible erroneous results from protracted irradiation exposures.

(4) Possible erroneous results from mechanical damage to the sensor.

Therefore it was planned to monitor the test chamber temperature with a platinum resistance thermometer mounted in the test loop helium inlet duct just aft of the forward bulkhead. However, work reported by Coltman, et. al. (ref. 14) at ORNL indicated a gross change in the low temperature electrical resistance of platinum resulting from exposure to a fast neutron environment. This irradiation induced increase in resistivity is not completely removed by self-annealing at room temperature. Therefore, location of platinum resistance thermometers as originally planned would require recalibration after each irradiation. Even after recalibration, the sensors would have an uncertainty of measurement of about $\pm$ 10% at the test temperature.

For this reason, two platinum resistance thermometers were installed to monitor the temperature of the inlet and return helium streams in each test loop at a location remote from the fast neutron field. These pairs of sensors were located some thirty feet from the test zone, in the inlet and return legs of the refrigeration manifold.

Since this temperature control method does not provide direct measurement of specimen temperature, relationship between indicated sensor readings and specimen temperature was determined with thermocouples attached to typical specimens during the following test stages:

- Calibration of direct measuring thermocouples on instrumented specimens.

- Determination of temperature distribution across the gage length of each of the above specimens.

- Determination of correction to be applied to the control sensors to insure a temperature of 17°K *at the gage length mid-point.*

Instrumented specimens, both tensile and fatigue, were prepared for this program. Longitudinal slots were milled in each specimen and copper-constantan thermocouples were welded or soldered to the base of each slot at each end of the 1/2 inch (1.27 cm) gage length and at the mid-point of the gage length. After the thermocouples were mounted, the slots were filled with a suitable potting compound to prevent pertubations in the gas flow pattern and to increase the mechanical strength of the couple to specimen joints. Copper-constantan thermocouples were used since measurements at liquid helium temperature after a dose of 1×10^{18} n/cm^2, made at ORNL (ref. 15) showed no significant radiation induced measurement variations in this thermoelectric pair.

The wire used for the manufacture of these thermocouples was tested for homogeneity to minimize the effect of a Peltier emf on the Thomson emf generated by the finished instrument. This was assomplished by moving a liquid air bath along a closed loop of wire and measuring the emf generated at the two high temperature gradient interfaces. Any wire showing a change greater than 3 microvolts in a 1.5 foot (45.7 cm) length was rejected for use as thermocouple material.

The initial stage of the temperature correlation program, calibration of each of these thermocouples, was then undertaken. The instrumented specimens were individually packaged in aluminum foil with a platinum resistance bulb calibrated by the National Bureau of Standards serving as a primary standard. Each package was separately immersed in liquid nitrogen and the micro-voltage out-put from each thermocouple was recorded with the temperature measurement from the primary standard. This initial comparison at a known temperature was done to provide additional assurance against a systematic error.

After the liquid nitrogen check, each package was separately placed in the test zone inside the head of a test loop. The package was stabilized at several temperatures between liquid nitrogen and 17°K and emf readings for each couple were recorded against the temperature recorded by the primary standard. Actual temperature versus emf out-put curves were prepared for each thermocouple. At this point, the instrumented specimens were considered adequate for use as secondary, or working, standards.

After completion of the calibration, specimen temperature distribution measurements were made.

The instrumented specimens, now calibrated to serve as working standards, were individually installed in the normal test position in a test loop. The refrigeration system was stabilized at 17°K, 78°K, and 178°K out-of-pile, and the temperature was measured at each end and the midpoint of the specimen gage length from the emf out-put of each thermocouple with the individual calibration curves.

Initially, a variation of several degrees K were observed along the three test points. This was corrected by internal modification of the ducts which direct the helium across the specimen to increase the mass flow at the warmer locations.

After satisfactory temperature distribution was obtained across the gage length at 17°K, 78°K and 178°K out-of-pile, the test loop containing the instrumented specimen was brought to the "full forward" position in HB-2 to measure the effect of gamma heating on temperature distribution at full power reactor operation. The temperature of the test loop was again stabilized at the three temperatures of interest and brought to a steady-state, where the refrigeration capacity exactly balanced gamma heating. No appreciable increase in temperature differential between the test points was observed.

After completion of the temperature distribution tests, readings of the permanently installed temperature sensors of the refrigerator were taken which corresponded with the three specimen temperatures under in-pile steady-state conditions as measured with the secondary standard thermocouple. The use of these correction constants for each pair of permanent temperature sensors during each irradiation exposure assured the maintenance of specimen temperature under $\pm$ 0.56°k. The platinum resistance bulbs from the permanent temperature sensors were recalibrated by the manufacturer after the completion of the initial test program and gave readings within less than one degree of the initial calibrations.

Temperature distribution in an Aluminum 1099-H14 tensile specimen, together with refrigeration system operational parameters, are shown in tables C-I and C-II.

TABLE C-I IN-PILE TEMPERATURE CORRELATION DATA

	Specimen Temperatures (°K)			Refrig. Temperatures (°K)			Heater Loads		Expansion Engine	
Test Run	Fwd.	Mid.	Aft	Loop Inlet	Loop Return	Return Manifold	Main (watts)	Trim (watts)	Pressure Ratio	Speed (RPM)
(17°K)										
1	16.9	16.6	16.8	16.2	17.9	17.9	200	40	6.1:1	325
2	17.0	16.8	17.0	16.1	18.1	18.1	200	25	6.0:1	320
3	16.9	16.5	16.8	16.2	18.0	18.0	200	30	6.1:1	320
(39°K)										
1	39.0	38.9	38.9	37.6	42.5	42.5	1200	20	6.1:1	325
2	39.1	39.0	38.9	37.4	42.8	42.7	1100	35	6.0:1	325
(78°K)										
1	77.7	77.5	77.6	75.6	83.5	83.3	1050	25	5.9:1	250
2	78.3	78.0	78.2	75.5	83.3	83.0	1100	5	6.0:1	250
(178°K)										
1	178.7	178.2	178.0	176.4	184.3	184.4	1300	70	6.0:1	250
2	177.9	177.4	177.7	176.6	184.1	184.2	1300	25	6.0:1	260

TABLE C-2 OUT-OF-PILE TEMPERATURE CORRELATION DATA

Test Run	Specimen Temperatures (°K) Fwd.	Mid.	Aft	Refrig. Temperatures (°K) Loop Inlet	Loop Return	Return Manifold	Heater Loads Main (watts)	Trim (watts)	Expansion Engine Pressure Ratio	Speed RPM
(17°K)										
1	16.8	16.7	16.8	16.4	17.2	17.3	350	20	6.1:1	300
2	16.4	16.3	16.5	16.5	17.4	17.4	400	60	6.2:1	290
3	16.5	16.3	16.4	16.2	16.9	16.9	400	10	6.1:1	280
(39°K)										
1	39.0	38.9	39.2	37.7	40.0	40.0	1350	10	6.0:1	280
2	38.9	38.8	39.1	37.7	40.1	40.0	1250	60	6.2:1	270
(78°K)										
1	77.8	77.8	77.9	76.6	78.8	78.8	1600	35	6.1:1	260
2	78.0	77.9	78.1	76.9	79.2	79.1	1550	60	6.2:1	260
(178°K)										
1	177.6	177.6	177.7	176.5	178.9	178.7	1700	55	6.0:1	260
2	178.0	178.1	178.2	177.1	179.5	179.3	1650	25	6.0:1	270

APPENDIX D TENSILE TEST RESULTS, EFFECTS OF IRRADIATION, ALUMINUM 1099-H14, TESTED AT 17°K

TABLE D-1 TENSILE TEST RESULTS, EFFECTS OF IRRADIATION, ALUMINUM 1099-H14 TESTED AT 17°K

Specimen	Irradiation n/cm^2	F_{tu} Ksi	F_{tu} kN/cm^2	F_{ty} (0.2% offset) Ksi	F_{ty} (0.2% offset) kN/cm^2	F_{ty}/F_{tu}	Elongation in 0.5 in (4D) %	Reduction of Area %	Fracture Stress Ksi	Fracture Stress kN/cm^2	Modulus (#) E 10^3 Ksi	Modulus (#) E MN/cm^2
Range of 5[a]	None	30.0-39.3	20.6-27.1	6.0-8.2	4.1-5.7	0.17-0.27	60-63	61-76	110-110	76-76	7-12	5-8
Mean of 5[a]	None	33.78	23.3	7.21	4.97	0.216	61.4	69.2	110.0	75.8	11.0	7.6
8 Ba 147	5×10^{15}	44.9	31.0	19.8	13.7	0.44	56	63	94	65	12	8
8 Ba 165	5×10^{15}	47.8	33.0	20.8	14.3	0.44	53	67	116	80	7	5
8 Ba 188	5×10^{15}	45.6	31.4	20.2	13.9	0.44	55	68	108	74	16	11
Mean	5×10^{15}	46.10	31.79	20.27	13.98	0.440	54.7	66.0	106.0	73.1	12	8
8 Ba 153	7×10^{15}	38.3	26.4	17.4	12.0	0.45	55	67	81	56	10	7
8 Ba 131	4×10^{16}	50.0	34.5	28.9	19.9	0.58	42	50	85	59	19	13
8 Ba 155	5×10^{16}	46.9	32.3	31.3	21.6	0.67	45	56	80	55	15	10
8 Ba 113	5×10^{16}	50.9	35.1	34.7	23.9	0.68	40	47	81	56	17	12
8 Ba 161	5×10^{16}	51.2	25.0	36.2	25.0	0.71	41	55	84	58	12	8
Mean	5×10^{16}	49.67	34.2	34.07	23.5	0.687	42.0	52.7	81.7	56.3	15	10
8 Ba 87[a]	1×10^{17}	49.2	33.9	43.3	30.0	0.88	46	54	87	60	-	-
8 Ba 97	1×10^{17}	56.3	38.8	35.2	24.3	0.62	30	60	98	68	12	8
8 Ba 117	1×10^{17}	52.7	36.3	43.1	29.7	0.82	31	51	86	59	14	10
8 Ba 132	1×10^{17}	50.8	35.0	38.5	26.5	0.76	35	53	77	53	12	8
Mean	1×10^{17}	52.25	36.03	40.02	27.59	0.770	35.5	54.5	87.0	60.0	13	9
8 Ba 96	3×10^{17}	55.8	38.5	48.2	33.2	0.86	19	27	67	46	12	8
8 Ba 146	3×10^{17}	62.4	43.0	55.1	38.0	0.88	26	40	81	56	17	12
8 Ba 157	3×10^{17}	51.3	35.4	45.3	31.2	0.88	27	48	69	48	9	6
Mean	3×10^{17}	56.50	39.0	49.53	34.15	0.873	24.0	38.3	72.3	49.8	13	9

(a) From screening program (ref. 1)
(#) For comparison purposes only

\- Not determinable

APPENDIX E TENSILE TEST RESULTS, EFFECTS OF IRRADIATION TEMPERATURE, ALUMINUM 1099-H14, TESTED AT VARIOUS IRRADIATION TEMPERATURES AFTER 1×10^{17} n/cm^2 AND AT SAME TEMPERATURES WITH NO IRRADIATION

TABLE E-I

TENSILE TEST RESULTS, EFFECTS OF IRRADIATION TEMPERATURE, ALUMINUM 1099-H14, TESTED AT VARIOUS IRRADIATION TEMPERATURES AFTER 1 x 10^{17} n/cm^2 AND AT SAME TEMPERATURES WITH NO IRRADIATION

Specimen	Irradiation and Test Temp. °K	Irradiation n/cm^2	F_{tu} Ksi	F_{tu} kN/cm^2	F_{ty} (0.2% offset) Ksi	F_{ty} (0.2% offset) kN/cm^2	F_{ty}/F_{tu}	Elongation in 0.5 in (4D) %	Reduction of Area %	Fracture Stress Ksi	Fracture Stress kN/cm^2	Modulus (#) E 10^3 Ksi	Modulus (#) E MN/cm^2
Range of 4[c]	17-17*	10^{17} - 10^{17}	49.2-56.3	33.9-38.8	35.2-43.3	24.3-30.0	0.62-0.88	30-46	31-60	77-98	53-68	12-14	8-10
Mean of 4[c]	17*	1 x 10^{17}	52.25	36.03	40.02	27.59	0.770	35.5	54.5	87.0	60.0	13	9
8 Ba 162	78	1 x 10^{17}	25.9	17.9	18.9	13.0	0.73	42	74	-	-	9	6
8 Ba 167	78	1 x 10^{17}	26.8	18.5	20.6	14.2	0.77	42	74	55	38	7	5
8 Ba 170	78	1 x 10^{17}	23.6	16.3	16.2	11.2	0.69	42	74	-	-	4	3
Mean	78	1 x 10^{17}	25.43	17.57	18.57	12.80	0.730	42.0	74.0	55	38	7	5
8 Ba 135	178	1 x 10^{17}	16.2	11.2	14.6	10.1	0.90	27	79	21	14	5	3
8 Ba 145	178	1 x 10^{17}	17.2	11.9	16.3	11.2	0.95	28	78	-	-	9	6
8 Ba 156	178	1 x 10^{17}	14.5	10.0	12.8	8.8	0.88	28	78	35	24	10	7
Mean	178	1 x 10^{17}	15.97	11.01	14.57	10.04	0.910	27.7	78.3	28.0	19.3	8	6
8 Ba 179	300	1 x 10^{17}	12.2	8.4	11.7	8.1	0.96	17	72	-	-	4	3
8 Ba 135	300	1 x 10^{17}	11.9	8.2	9.7	6.7	0.82	19	76	-	-	3	2
8 Ba 190	300	1 x 10^{17}	12.4	8.5	11.9	8.2	0.96	17	74	-	-	12	8
Mean	300	1 x 10^{17}	12.17	8.39	11.10	7.65	0.913	17.7	74.0	-	-	6	4
8 Ba 136	78	None	21.5	14.8	14.0	9.7	0.65	48	78	41	28	8	6
8 Ba 138	78	None	21.0	14.5	13.1	9.0	0.62	48	78	41	28	4	3
8 Ba 138	78	None	21.1	14.5	13.9	9.6	0.66	46	82	54	37	6	4
Mean	78	None	21.20	14.62	13.67	9.43	0.643	47.3	79.3	45.3	31.2	6	4
8 Ba 149	178	None	13.9	9.6	11.9	8.2	0.86	28	82	46	32	8	6
8 Ba 150	178	None	13.3	9.2	11.5	7.9	0.86	27	84	41	28	6	4
8 Ba 151	178	None	14.4	9.9	12.7	8.8	0.88	28	81	42	29	10	7
Mean	178	None	13.87	9.57	12.03	8.29	0.867	27.7	82.3	43.0	29.6	8	6
Range of 5[a]	300	None	11.7-14.3	8.1-9.9	11.0-13.5	7.6-9.3	0.94-0.95	20-26	74-83	-	-	9-10	6-7
Mean of 5[a]	300	None	13.18	9.52	12.48	8.60	0.942	22.8	79.0	-	-	9	6

(a) From screening program (ref. 1)
(c) From table D-1

\- Not determinable
(#) For comparison purposes only
* Not annealed after irradiation

APPENDIX F TENSILE TEST RESULTS, EFFECTS OF ANNEALING AND TEST TEMPERATURE, ALUMINUM 1099-H14 (1×10^{17} n/cm^2 AT 17°K, ANNEALED AND TESTED AT VARIOUS TEMPERATURES) AND EFFECTS OF TEST TEMPERATURE WITH NO IRRADIATION

TABLE F-1

TENSILE TEST RESULTS, EFFECTS OF ANNEALING AND TEST TEMPERATURE, ALUMINUM 1099-H14 (1×10^{17} n/cm^2 AT 17°K, ANNEALED AND TESTED AT VARIOUS TEMPERATURES) AND EFFECTS OF TEST TEMPERATURE WITH NO IRRADIATION

Specimen	Annealing and Test Temp. °K	Irradiation n/cm^2	F_{tu} Ksi	F_{tu} kN/cm^2	F_{ty} (0.2% offset) Ksi	F_{ty} (0.2% offset) kN/cm^2	F_{ty}/F_{tu}	Elongation in 0.5 in (4D) %	Reduction of Area %	Fracture Stress Ksi	Fracture Stress kN/cm^2	Modulus (#) E 10^3 Ksi	Modulus (#) E MN/cm^2
Range of 4(c)	17-17 *	10^{17}- 10^{17}	49.2-56.3	33.9-38.8	35.2-43.3	24.3-30.0	0.62-0.88	30-46	31-60	77-98	53-68	12-14	8-10
Mean of 4(c)	17 *	1×10^{17}	52.25	36.03	40.02	27.59	0.770	35.5	54.5	87.0	60.0	13	9
8 Ba 126	78	1×10^{17}	28.7	19.8	22.8	15.7	0.79	29	61	-	-	-	-
8 Ba 121	78	1×10^{17}	26.7	18.4	20.4	14.1	0.76	39	76	37	26	16	11
8 Ba 173	78	1×10^{17}	26.8	18.5	19.2	13.2	0.72	46	73	41	28	-	-
Mean	78	1×10^{17}	27.40	18.89	20.80	14.34	0.757	38.0	70.0	39.0	26.9	16	11
8 Ba 106	178	1×10^{17}	16.6	11.4	15.9	11.0	0.96	29	85	-	-	14	10
8 Ba 177	178	1×10^{17}	16.4	11.3	13.7	9.4	0.84	28	81	-	-	4	3
8 Ba 114	178	1×10^{17}	16.8	11.6	15.5	10.7	0.92	23	78	-	-	9	6
Mean	178	1×10^{17}	16.60	11.45	15.03	10.36	0.907	26.7	81.3	-	-	9	6
8 Ba 160	300	1×10^{17}	11.9	8.2	11.5	7.9	0.97	20	75	27	19	7	5
8 Ba 163	300	1×10^{17}	11.7	8.0	10.7	7.4	0.91	20	75	33	23	4	3
8 Ba 164	300	1×10^{17}	12.0	8.3	11.7	8.1	0.98	22	77	27	19	12	8
Mean	300	1×10^{17}	11.87	8.18	11.30	7.79	0.953	20.7	75.7	29.0	20.0	8	6
8 Ba 125	78 (4)	None	22.9	15.8	13.9	9.6	0.61	46	73	48	33	8	6
8 Ba 144	78 (4)	None	22.8	15.7	15.1	10.4	0.66	47*	83*	-	-	4	3
8 Ba 154	78 (4)	None	21.1	14.5	13.9	9.6	0.66	47	83	61	42	19	13
Mean	78	None	22.27	15.36	14.30	9.86	0.643	46.7	79.7	54.5	37.6	10	7
8 Ba 127	178 (4)	None	15.8	10.9	15.1	10.4	0.96	22	61	25	17	9	6
8 Ba 128	178 (4)	None	15.1	10.4	13.6	9.4	0.90	25	71	33	23	8	6
8 Ba 129	178 (4)	None	14.6	10.1	12.8	8.8	0.88	23	71	30	21	12	8
Mean	178	None	15.17	10.46	13.83	9.54	0.913	23.3	67.7	29.3	20.2	10	7
8 Ba 120	300 (4)	None	12.5	8.6	11.2	7.7	0.90	20	63	-	-	8	6
8 Ba 122	300 (4)	None	13.0	9.0	12.5	8.6	0.96	22	67	24	16	8	6
8 Ba 124	300 (4)	None	13.4	9.2	13.2	9.1	0.99	19	61	23	16	11	8
Mean	300	None	12.97	8.94	12.30	8.48	0.950	20.3	63.7	23.5	16.2	9	6

(c) From table D-1
(#) For comparison purposes only
(4) Stabilized at 17°K before stabilizing and testing at indicated temperature

\- Not determinable
* Not annealed after irradiation

APPENDIX G TENSILE TEST RESULTS, EFFECTS OF ANNEALING, ALUMINUM 1099-H14 (1×10^{17} n/cm^2 AT 17°K, ANNEALED AT VARIOUS TEMPERATURES, TESTED AT 17°K)

TABLE G-I TENSILE TEST RESULTS, EFFECTS OF ANNEALING, ALUMINUM 1099-H14 (1×10^{17} n/cm^2 AT 17°K, ANNEALED AT VARIOUS TEMPERATURES, TESTED AT 17°K)

Specimen	Annealing Temp. °K	Irradiation n/cm^2	F_{tu} Ksi	F_{tu} kN/cm^2	F_{ty} (0.2% offset) Ksi	F_{ty} (0.2% offset) kN/cm^2	F_{ty}/F_{tu}	Elongation in 0.5 in (4D) %	Reduction of Area %	Fracture Stress Ksi	Fracture Stress kN/cm^2	Modulus (#) E 10^3 Ksi	Modulus (#) E MN/cm^2
Range of 4(c)	Not	10^{17} - 10^{17}	49.2-56.3	33.9-38.8	35.2-43.3	24.3-30.0	0.62-0.88	30-46	31-60	77-98	53-68	12-14	8-10
Mean of 4(c)	Annealed	1×10^{17}	52.25	36.03	40.02	27.59	0.770	35.5	54.5	87.0	60.0	13	9
8 Ba 140	78	1×10^{17}	45.2	31.2	28.9	19.9	0.64	39	53	64	44	14	10
8 Ba 178	78	1×10^{17}	54.5	37.6	34.4	23.7	0.63	43	58	93	64	15	10
8 Ba 181	78	1×10^{17}	46.1	31.8	28.5	19.7	0.62	46	58	84	58	16	11
Mean	78	1×10^{17}	48.60	33.51	30.60	21.10	0.630	42.7	56.3	80.3	55.4	15	10
8 Ba 186	178	1×10^{17}	44.2	30.5	23.9	16.5	0.54	47	62	85	59	18	12
8 Ba 189	178	1×10^{17}	44.4	37.6	24.1	16.6	0.54	43	59	76	52	-	-
8 Ba 200	178	1×10^{17}	37.4	31.8	16.5	11.4	0.44	58	62	78	54	12	8
Mean	178	1×10^{17}	42.00	33.51	21.50	14.82	0.50	49.3	61.0	79.7	55.0	14	10
8 Ba 187	300	1×10^{17}	45.5	31.4	16.2	11.2	0.36	63	61	96	66	3	2
8 Ba 193	300	1×10^{17}	43.4	29.9	15.9	11.0	0.37	58	58	75	52	13	9
8 Ba 198	300	1×10^{17}	40.4	27.9	10.4	7.2	0.26	58	59	79	54	3	2
Mean	300	1×10^{17}	43.10	29.72	14.17	9.77	0.330	59.7	59.3	83.3	57.4	6	4
8 Ba 107	17 (1)	None	40.0	27.6	10.7	7.4	0.27	55	67	99	68	13	9
8 Ba 112	17 (1)	None	38.0	26.2	16.6	11.4	0.44	55	56	66	46	11	8
8 Ba 115	17 (1)	None	39.8	27.4	14.5	10.0	0.36	49	57	70	48	7	5
Mean	17	None	39.27	27.08	13.93	9.60	0.357	53.0	60.0	78.3	54.0	10	7
8 Ba 130	17 (2)	None	38.6	26.6	15.8	11.0	0.41	61	61	86	59	12	8
8 Ba 142	17 (2)	None	37.4	25.8	12.9	8.9	0.34	56	65	76	52	6	4
8 Ba 148	17 (2)	None	37.8	26.1	14.7	10.1	0.39	56	64	79	54	10	7
Mean	17	None	37.93	26.15	14.47	9.98	0.380	57.7	63.3	80.3	55.4	9	6
8 Ba 99	17 (3)	None	38.3	26.4	15.1	10.4	0.39	59	70	91	63	11	8
8 Ba 101	17 (3)	None	39.5	27.2	15.3	10.5	0.39	57	68	94	65	-	-
8 Ba 110	17 (3)	None	43.1	29.7	17.3	11.9	0.40	54	62	86	59	14	10
Mean	17	None	40.30	27.79	15.90	10.96	0.393	56.7	66.7	90.3	62.3	13	9

(c) From table D-1
(#) For comparison purposes only
- Not determinable

(1) Stabilized at 17°K and then at 78°K before stabilizing and testing at 17°K
(2) Stabilized at 17°K and then at 178°K before stabilizing and testing at 17°K
(3) Stabilized at 17°K and then at 300°K before stabilizing and testing at 17°K

APPENDIX H TENSILE TEST RESULTS, EFFECTS OF IRRADIATION TITANIUM 55A, TESTED AT 17°K

TABLE H-1 TENSILE TEST RESULTS, TITANIUM 55A (ANNEALED)

Specimen	Temp. °K	Irradiation n/cm^2	F_{tu} Ksi	F_{tu} kN/cm^2	F_{ty} (0.2% offset) Ksi	F_{ty} (0.2% offset) kN/cm^2	F_{ty}/F_{tu}	Elongation in 0.5 in (4D) %	Reduction of Area %	Fracture Stress Ksi	Fracture Stress kN/cm^2	Modulus (#) E 10^3 Ksi	Modulus (#) E MN/cm^2
Range of 5[a]	300	None	65.1-69.4	44.9-47.9	47.5-63.3	32.8-43.6	0.73-0.91	25-33	59-65	-	-	12-14	8-10
Mean of 5[a]	300	None	67.0	46.20	53.5	36.89	0.798	30.0	62.3	-	-	14	10
Range of 5[a]	17	None	167-172	115.1-118.6	118-124	81.4-85.5	0.71-0.73	33-34	51-54	-	-	16-20	11-14
Mean of 5[a]	17	None	169.4	116.8	122.0	84.12	0.722	33.3	53.0	-	-	18	12
Range of 3[a]	17	1×10^{17}	180-216	124.1-148.9	128-136	88.3-93.8	0.63-0.73	32-36	52-54	-	-	17-25	12-17
Mean of 3[a]	17	1×10^{17}	192.3	132.6	131.7	90.8	0.690	34.0	53.0	-	-	18	12
1 Aa 200	17	6×10^{17}	203	140	154	106	0.75	29	45	370	255	20	14
1 Aa 203	17	6×10^{17}	204	141	158	109	0.78	29	46	380	262	19	13
1 Aa 153	17	6×10^{17}	211	145	154	106	0.73	27	38	341	235	15	10
Mean	17	6×10^{17}	206.0	142.0	155.3	107.1	0.753	28.3	43.0	363.7	250.8	18	12
1 Aa 152	17	1×10^{18}	213	147	159	110	0.74	30	49	420	290	12	8
1 Aa 205	17	1×10^{18}	216	149	171	118	0.79	29	44	387	267	22	15
1 Aa 206	17	1×10^{18}	223	154	181	125	0.81	19	38	358	247	-	-
Mean	17	1×10^{18}	217.3	149.8	170.3	117.4	0.780	26.0	43.7	388.3	267.7	17	12

(a) From screening program (ref. 1)

(#) For comparison purposes only

\- Not determinable

APPENDIX I TENSILE TEST RESULTS, EFFECTS OF IRRADIATION, TITANIUM 5 Al-2.5 Sn, TESTED AT 17°K

TABLE I-1 TENSILE TEST RESULTS, TITANIUM 5 AL-2.5 Sn (STD. 1) (ANNEALED)

Specimen	Temp. °K	Irradiation n/cm^2	F_{tu} Ksi	F_{tu} kN/cm^2	F_{ty} (0.2% offset) Ksi	F_{ty} (0.2% offset) kN/cm^2	F_{ty}/F_{tu}	Elongation in 0.5 in (4D) %	Reduction of Area %	Fracture Stress Ksi	Fracture Stress kN/cm^2	Modulus (#) E 10^3 Ksi	Modulus (#) E MN/cm^2
Range of 5[a]	300	None	124-127	85.5-87.6	112-121	77.2-83.4	0.90-0.98	23-24	48-52	-	-	12-16	8-11
Mean of 5[a]	300	None	125.2	86.33	114.8	79.15	0.920	23.3	50.7	-	-	15	10
Range of 5[a]	17	None	213-231	147-159	200-215	138-148	0.87-0.95	12-18	21-35	298	205	18-18	12-12
Mean of 5[a]	17	None	224.8	155.0	205.2	141.5	0.915	13.8	30.0	298	205	18	12
Range of 3[a]	17	1×10^{17}	222-257	153-177	211-231	145-159	0.82-0.97	9-14	36	-	-	15-21	10-14
Mean of 3[a]	17	1×10^{17}	239.0	164.8	218.0	150.3	0.913	11.5	36	-	-	18	12
3 Aa 64[x]	17	5×10^{17}	254.9	175.8	-	-	-	8	29	360.0	248.2	-	-
3 Aa 71[x]	17	8.5×10^{17}	240.8	166.0	231.6	159.7	0.96	6	25	322.9	222.6	20	14
3 Aa 73	17	1×10^{18}	211.8	145.5	205.3	141.6	0.97	8	34	322.0	222.0	20	14
3 Aa 168	17	1×10^{18}	226.8	156.4	220.6	152.1	0.99	8	34	342.7	236.3	20	14
3 Aa 167	17	1×10^{18}	250.8	172.9	248.2	171.1	0.99	7	27	342.1	235.9	16	11
3 Aa 169	17	1×10^{18}	270.8	186.7	262.8	181.2	0.97	8	33	386.8	266.7	22	15
3 Aa 63	17	1×10^{18}	289.2	199.4	279.9	193.0	0.97	6	21	368.2	253.9	25	17
Mean	17	1×10^{18}	250.0	172.4	243.4	167.8	0.974	7.4	29.8	352.4	243.0	21	14

(a) From screening program (ref. 1)
(x) Irradiation terminated prematurely by irrecoverable reactor scram

(#) For comparison purposes only
\- Not determinable

TABLE I-2 TENSILE TEST RESULTS, TITANIUM 5 AL-2.5 Sn (ELI) (ANNEALED)

Specimen	Temp. °K	Irradiation n/cm^2	F_{tu} Ksi	F_{tu} kN/cm^2	F_{ty} (0.2% offset) Ksi	F_{ty} (0.2% offset) kN/cm^2	F_{ty}/F_{tu}	Elongation in 0.5 in (4D) %	Reduction of Area %	Fracture Stress Ksi	Fracture Stress kN/cm^2	Modulus (#) E 10^3 Ksi	Modulus (#) E MN/cm^2
Range of 5(a)	300	None	118-133	81.3-91.7	104-119	71.7-82	0.88-0.91	12-19	39-46	169-171	116-118	15-20	10-14
Mean of 5(a)	300	None	126.4	87.15	113.4	78.19	0.896	16.0	42.2	170.0	117.2	15	10
Range of 5(a)	17	None	225-236	155-163	203-225	140-155	0.92-0.96	8-11	32-33	-	-	-	-
Mean of 5(a)	17	None	228.4	157.5	214.2	147.7	0.948	9.7	32.3	-	-	-	-
Range of 3(a)	17	1×10^{17}	222-225	153-155	211-215	145-148	0.95-0.96	11	31	-	-	17-18	12-12
Mean of 3(a)	17	1×10^{17}	223.3	154.0	213.0	146.7	0.953	11.0	31.0	-	-	18	12
8 Aa 49	17	1×10^{18}	268.0	184.8	262.1	180.7	0.98	6	22	-	-	22	15
8 Aa 55	17	1×10^{18}	270.9	186.8	263.1	181.4	0.97	6	25	359	248	23	16
8 Aa 60	17	1×10^{18}	252.6	174.2	250.0	172.4	0.99	6	27	347	239	22	15
Mean	17	1×10^{18}	263.8	181.9	258.4	178.2	0.980	6.0	24.7	353.0	243.4	22	15

(a) From screening program (ref. 1)
(#) For comparison purposes only

\- Not determinable

APPENDIX J TENSILE TEST RESULTS, EFFECTS OF IRRADIATION, TITANIUM 6 Al-4 V, TESTED AT 17°K

TABLE J-1 TENSILE TEST RESULTS, TITANIUM 6 AL-4 V (ANNEALED)

Specimen	Temp. °K	Irradiation n/cm^2	F_{tu} Ksi	F_{tu} kN/cm^2	F_{ty} (0.2% offset) Ksi	F_{ty} (0.2% offset) kN/cm^2	F_{ty}/F_{tu}	Elongation in 0.5 in (4D) %	Reduction of Area %	Fracture Stress Ksi	Fracture Stress kN/cm^2	Modulus (#) E 10^3 Ksi	Modulus (#) E MN/cm^2
Range of 5[a]	300	None	142-145	97.9-100	134-141	92.4-97.2	0.94-0.97	13-14	42-48	-	-	14-15	10-10
Mean of 5[a]	300	None	144.0	99.29	137.8	95.01	0.957	13.8	45.0	-	-	15	10
Range of 5[a]	17	None	249-265	172-183	228-255	157-176	0.87-0.97	7-10	27.36	-	-	17-17	12-12
Mean of 5[a]	17	None	260.4	79.5	243.2	167.7	0.934	7.6	30.4	-	-	17	12
Range of 3[a]	17	1×10^{17}	265-290	183-200	254	175	0.95	5-6	37-38	-	-	-	-
Mean of 3[a]	17	1×10^{17}	273.7	188.7	254	175	0.95	5.7	37.3	-	-	-	-
2 Ac 54	17	1×10^{18}	302.7	208.7	289.4	199.5	0.96	4	34	456	314	20	14
2 Ac 55	17	1×10^{18}	332.9	229.5	314.5	216.8	0.95	4	34	506	349	25	17
2 Ac 56	17	1×10^{18}	325.0	224.1	294.7	203.1	0.91	6	34	494	341	32	22
Mean	17	1×10^{18}	320.2	220.8	299.5	206.5	0.940	4.7	34.0	485	334.6	26	17

(a) From screening program (ref. 1)
(#) For comparison purposes only

\- Not determinable

TABLE J-2 TENSILE TEST RESULTS, TITANIUM 6 AL-4 V (AGED)

Specimen	Temp. °K	Irradiation n/cm^2	F_{tu} Ksi	F_{tu} kN/cm^2	F_{ty} (0.2% offset) Ksi	F_{ty} (0.2% offset) kN/cm^2	F_{ty}/F_{tu}	Elongation in 0.5 in (4D) %	Reduction of Area %	Fracture Stress Ksi	Fracture Stress kN/cm^2	Modulus (#) E 10^3 Ksi	Modulus (#) E MN/cm^2
Range of 5[(a)]	300	None	161-170	111-117	155-161	107-117	0.92-0.97	13-19	53-55	-	-	14-18	10-12
Mean of 5[(a)]	300	None	167.6	115.6	158.6	109.4	0.946	16.5	54.0	-	-	16	11
Range of 5[(a)]	17	None	277-286	191-197	273-279	188-192	0.95-0.99	5-7	22-31	-	-	17-19	12-13
Mean of 5[(a)]	17	None	282.2	194.6	275.0	189.6	0.976	6.4	25.4	-	-	18	12
Range of 3[(a)]	17	1×10^{17}	296-308	204-212	281-305	194-210	0.95-0.99	5	21-24	-	-	20	14
Mean of 3[(a)]	17	1×10^{17}	302.3	208.4	293.3	202.2	0.970	5	22.4	-	-	20	14
2 Aa 78	17	1×10^{18}	296.1	204.2	289.5	199.6	0.98	5	21	375	259	20	14
2 Aa 87	17	1×10^{18}	324.8	223.9	-	-	-	4	13	375	259	15	10
2 Aa 89	17	1×10^{18}	325.2	224.2	319.0	220.0	0.98	5	16	387	267	19	13
2 Aa 82	17	1×10^{18}	328.3	226.4	322.1	222.1	0.98	5	14	382	263	20	14
2 Aa 81	17	1×10^{18}	373.2	257.3	365.5	252.0	0.98	3	13	381	263	22	15
Mean	17	1×10^{18}	329.5	227.2	324.0	223.4	0.983	4.4	15.4	380.0	262.0	19	13

(a) From screening program (ref. 1)
(#) For comparison purposes only

- Not determinable

ELECTRON FRACTOGRAPHS OF FATIGUE FRACTURE SURFACES

The following figures show typical fractographs obtained from failed TI-55A test specimens. The environmental conditions and load pattern for each specimen accompany the figures, together with a limited discussion of the salent features observed.

All photographs were taken at a magnification of 28,800 lines/inch 30 Lo and frequent calibration frames were included. The initial figure in this section, figure K-1, reproduces a typical calibration frame for technique verification; fractographs follow. The terminology used in describing the fractographs conforms to that used elsewhere (ref. 16).

The increase of the frequency of tear dimples at cryogenic temperatures is observable in other fractographs published in the Handbook. The lack of detail observable in the fractographs of irradiated specimens, including the absence of fatigue striations may be the result of the action of radioactive emmenations from the specimen on the replicating plastic during replication.

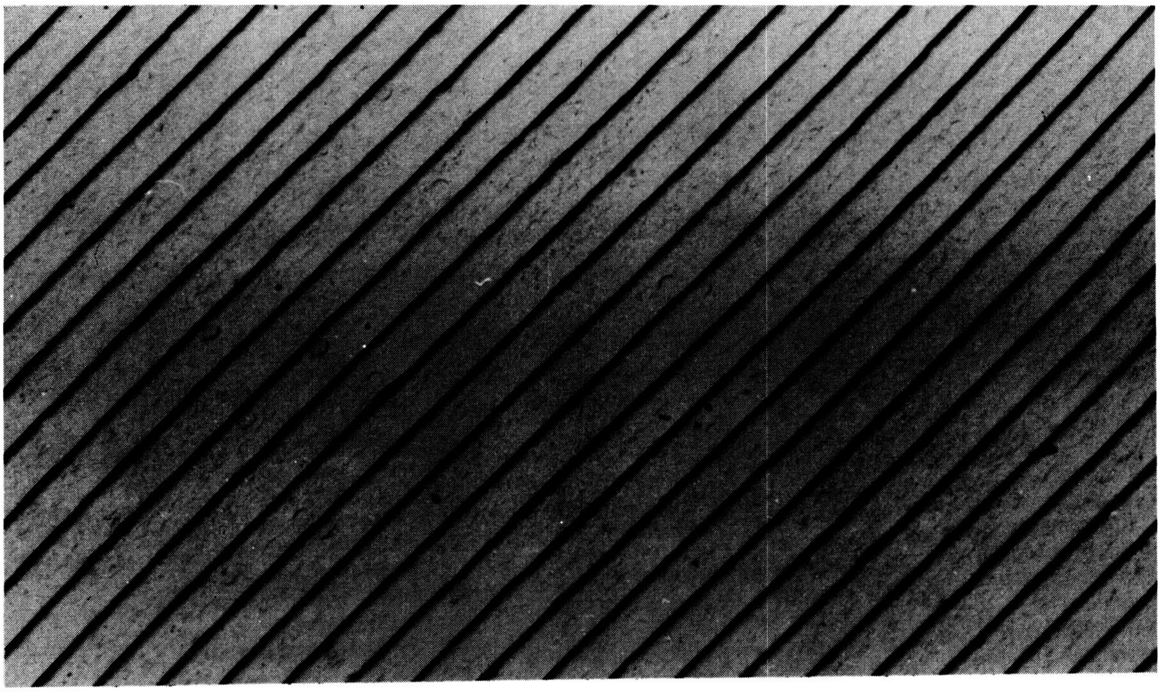

FIGURE K-1 CALIBRATION FRAME 28,800 LINES/INCH

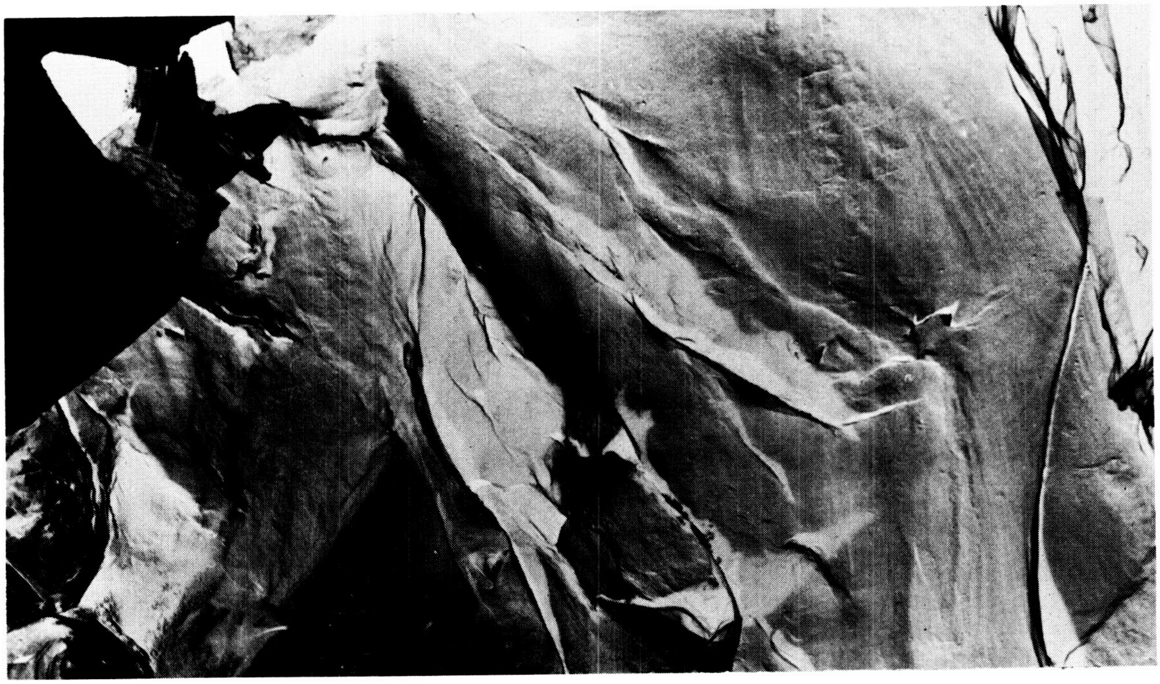

(a) Tensile portion of fracture showing stretching resulting from glide plane decohesion during ductile cleavage

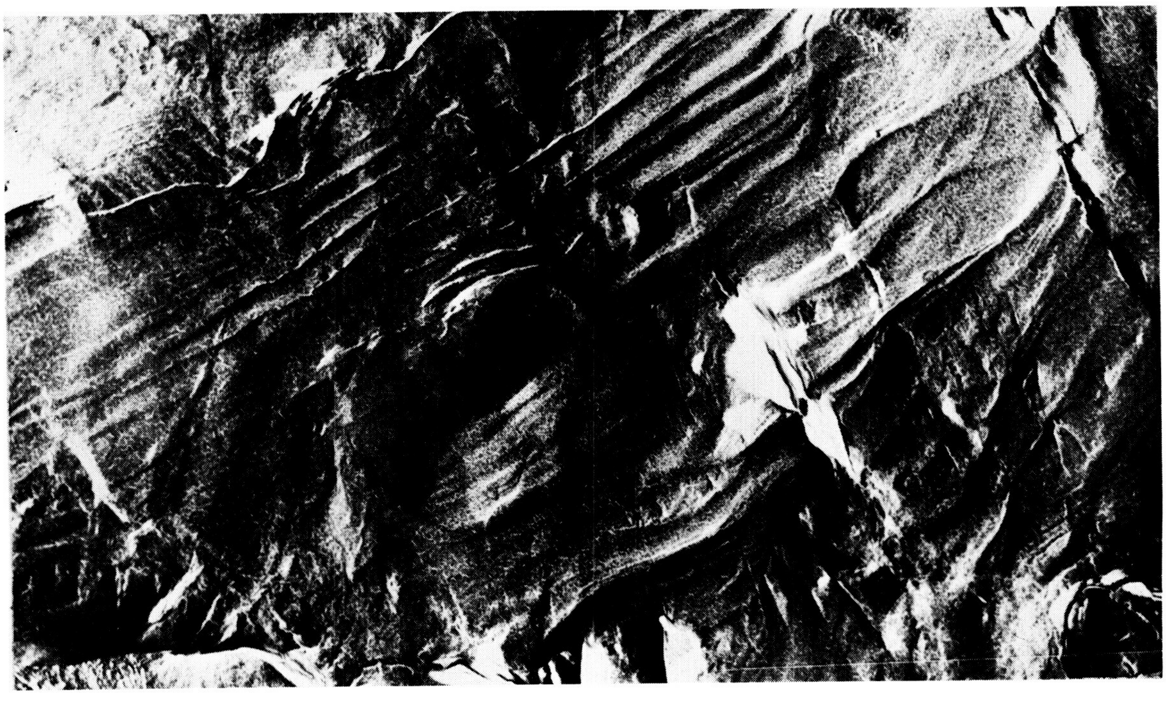

(b) Fatigue Striations

FIGURE K-2 FRACTOGRAPHS OF TITANIUM 55A SPECIMEN 1 Aa 247 FAILED IN AXIAL FATIGUE, TEST RATIO -1, 0.25 Hz TEST CONDITIONS: 300°K UNIRRADIATED; TEST LOAD: 100% NOMINAL F_{tu}; 67.0 Ksi; 46.2 kN/cm^2; 1479 CYCLES TO FAILURE

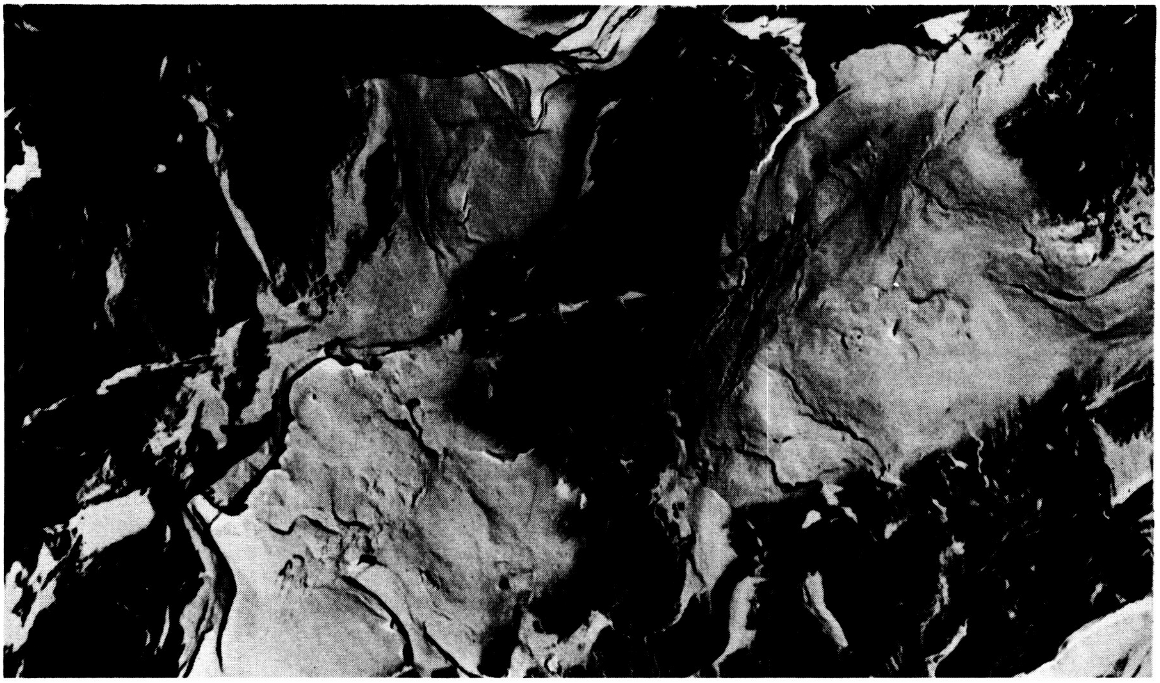

(a) Tensile portion of fracture showing stretching with residual serpentine glide in lower central area

(b) Fatigue striations

FIGURE K-3 FRACTOGRAPHS OF TITANIUM 55A SPECIMEN 1 Aa 241 FAILED IN AXIAL FATIGUE, TEST RATIO -1, 0.25 Hz TEST CONDITIONS: 300°K UNIRRADIATED; TEST LOAD: 95% NOMINAL F_{tu}; 63.6 Ksi; 43.9 kN/cm^2; 2905 CYCLES TO FAILURE

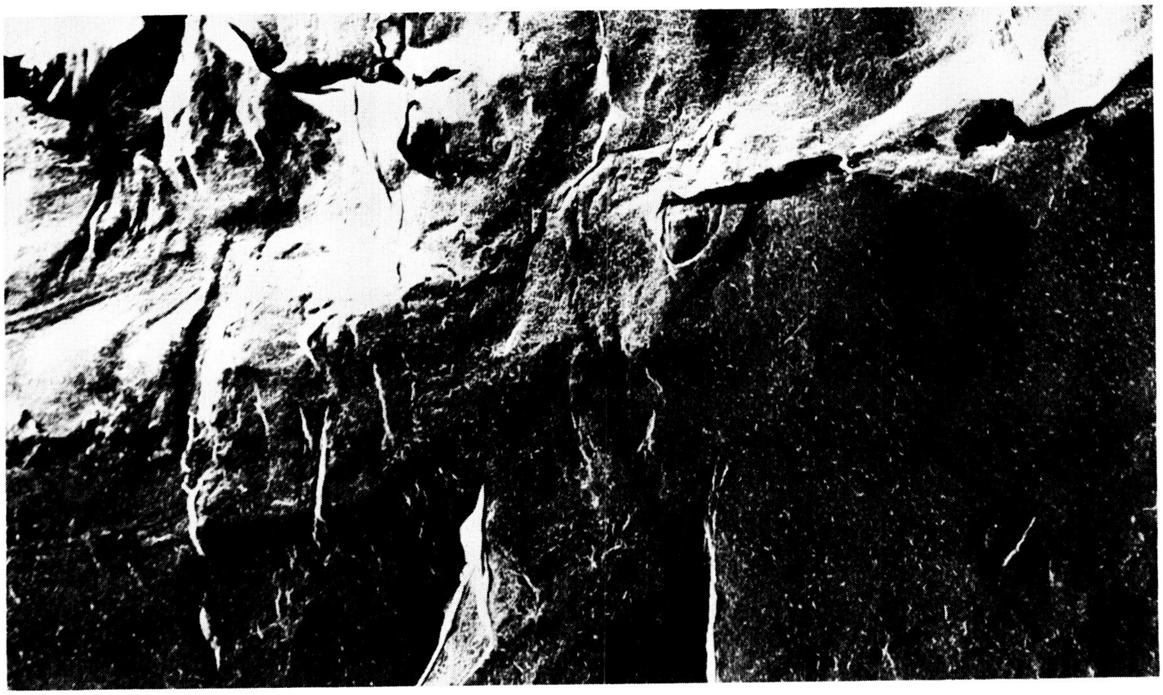

(a) Tensile portion of fracture showing evidence of quasi-cleavage in predominantly stretched area

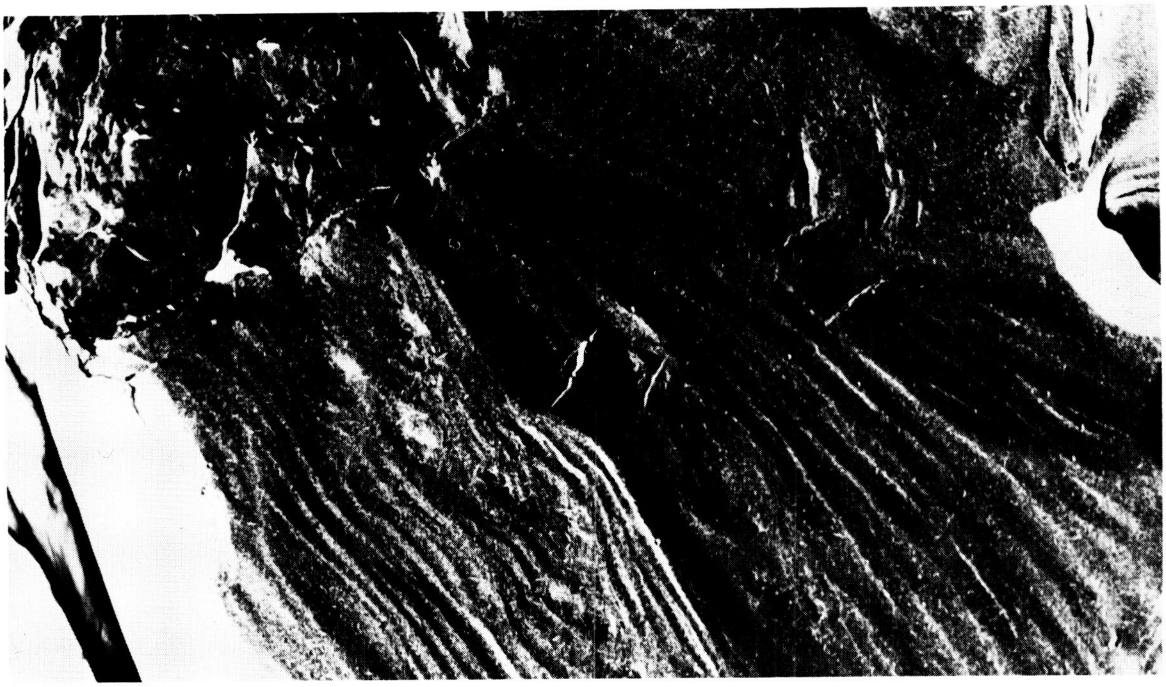

(b) Fatigue striations

FIGURE K-4 FRACTOGRAPHS OF TITANIUM 55A SPECIMEN 1 Aa 223 FAILED IN AXIAL FATIGUE, TEST RATIO -1, 0.25 Hz TEST CONDITIONS: 300°K UNIRRADIATED; TEST LOAD: 90% NOMINAL F_{tu}; 60.3 Ksi; 41.6 kN/cm^2; 3198 CYCLES TO FAILURE

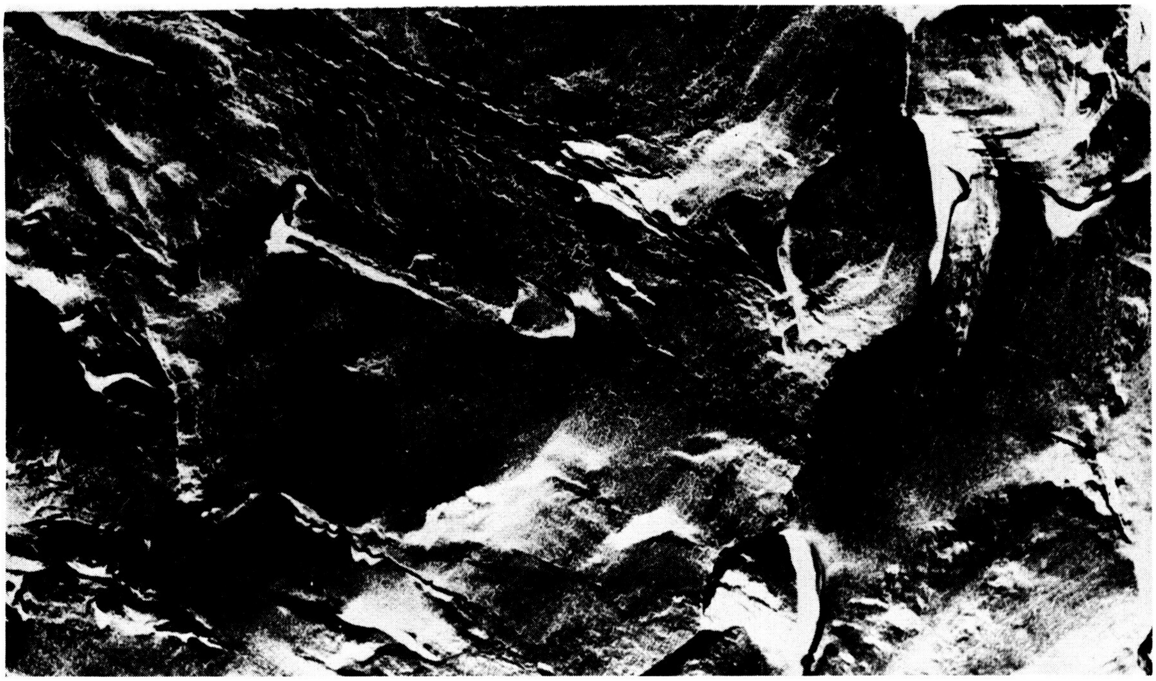

(a) Tensile portion of fracture showing pronounced cleavage steps and occasional equi-axed dimples indicative of micro-void coalescence

(b) Fatigue striations, also showing deformed dimples indicative of tensile shear

FIGURE K-5 FRACTOGRAPHS OF TITANIUM 55A SPECIMEN 1 Aa 239 FAILED IN AXIAL FATIGUE, TEST RATIO -1, 0.25 Hz TEST CONDITIONS: 300°K UNIRRADIATED; TEST LOAD: 85% NOMINAL F_{tu}; 57.0 Ksi; 39.3 kN/cm^2; 6587 CYCLES TO FAILURE

(a) Tensile portion of fracture showing feathering associated with quasi-cleavage

(b) Fatigue striations, largely obscured by super-imposed tear dimples

FIGURE K-6 FRACTOGRAPHS OF TITANIUM 55A SPECIMEN 1 Aa 267 FAILED IN AXIAL FATIGUE, TEST RATIO -1,0.25 Hz TEST CONDITIONS: 17°K UNIRRADIATED; TEST LOAD: 95% NOMINAL F_{tu}; 160.9 Ksi; 110.9 kN/cm^2; 1260 CYCLES TO FAILURE

(a) Tensile portion of fracture showing large equi-axed dimples from micro-void coalescence and small tear dimples

(b) Fatigue striations and super-imposed tear dimples

FIGURE K-7 FRACTOGRAPHS OF TITANIUM 55A SPECIMEN 1 Aa 248 FAILED IN AXIAL FATIGUE, TEST RATIO -1, 0.25 Hz TEST CONDITIONS: 17°K UNIRRADIATED; TEST LOAD: 90% NOMINAL F_{tu}; 152.5 Ksi; 105.1 kN/cm^2; 3589 CYCLES TO FAILURE

(a) Tensile portion of fracture showing large equi-axed dimples from micro-void coalescence and small tear dimples

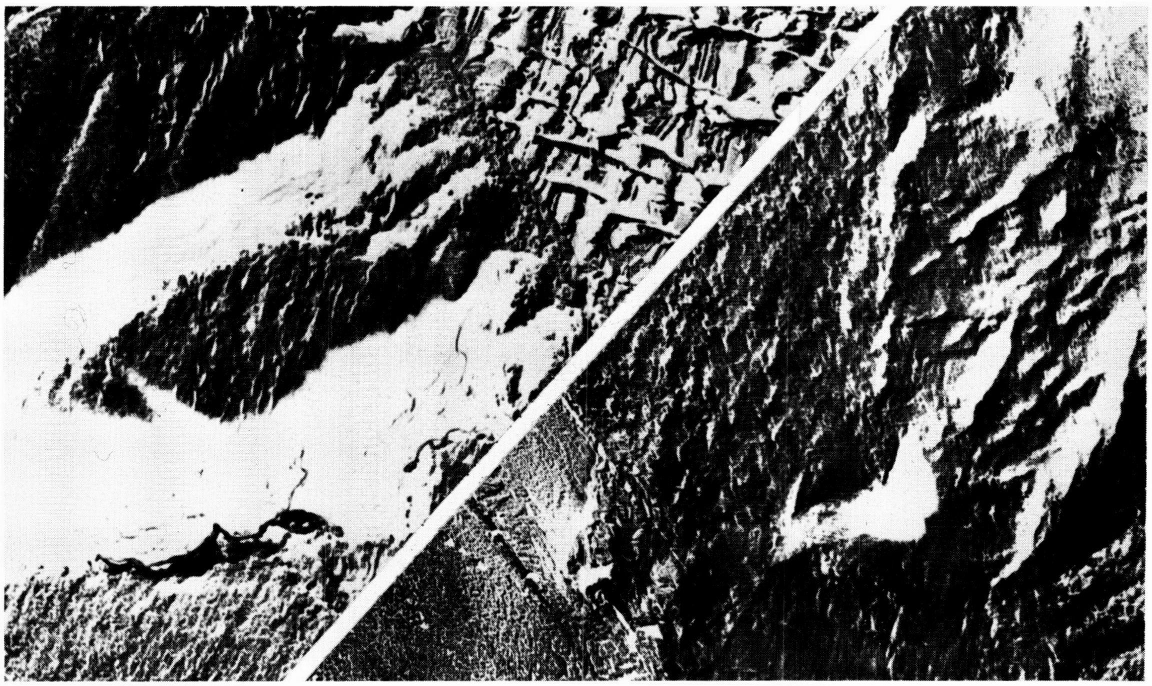

(b) Fatigue striations partially obscured by rub marks, possibly indicative of crack nucleation at microscopic stress concentration caused by material inhomogeneity

FIGURE K-8 FRACTOGRAPHS OF TITANIUM 55A SPECIMEN 1 Aa 250 FAILED IN AXIAL FATIGUE, TEST RATIO -1, 0.25 Hz TEST CONDITIONS: 17°K UNIRRADIATED; TEST LOAD: 90% NOMINAL F_{tu}; 152.5 Ksi; 105.1 kN/cm^2; 1322 CYCLES TO FAILURE

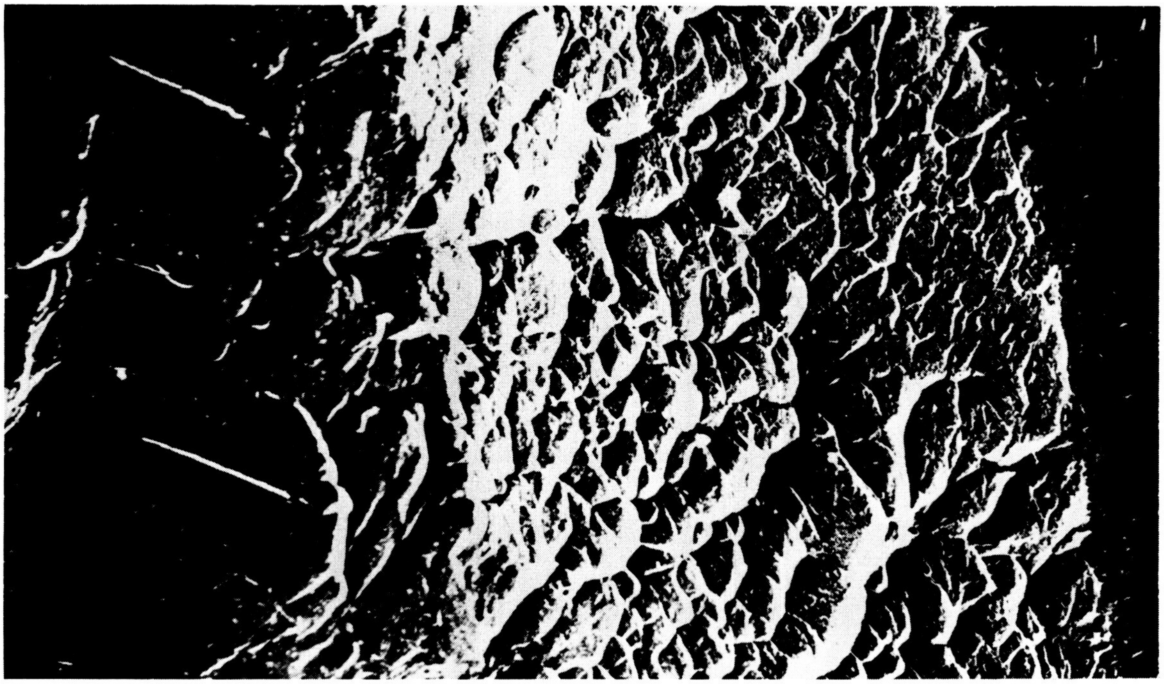

(a) Tensile portion of fracture showing area of tensile shear dimples adjacent between two zones of equi-axed dimples from micro-void coalescence

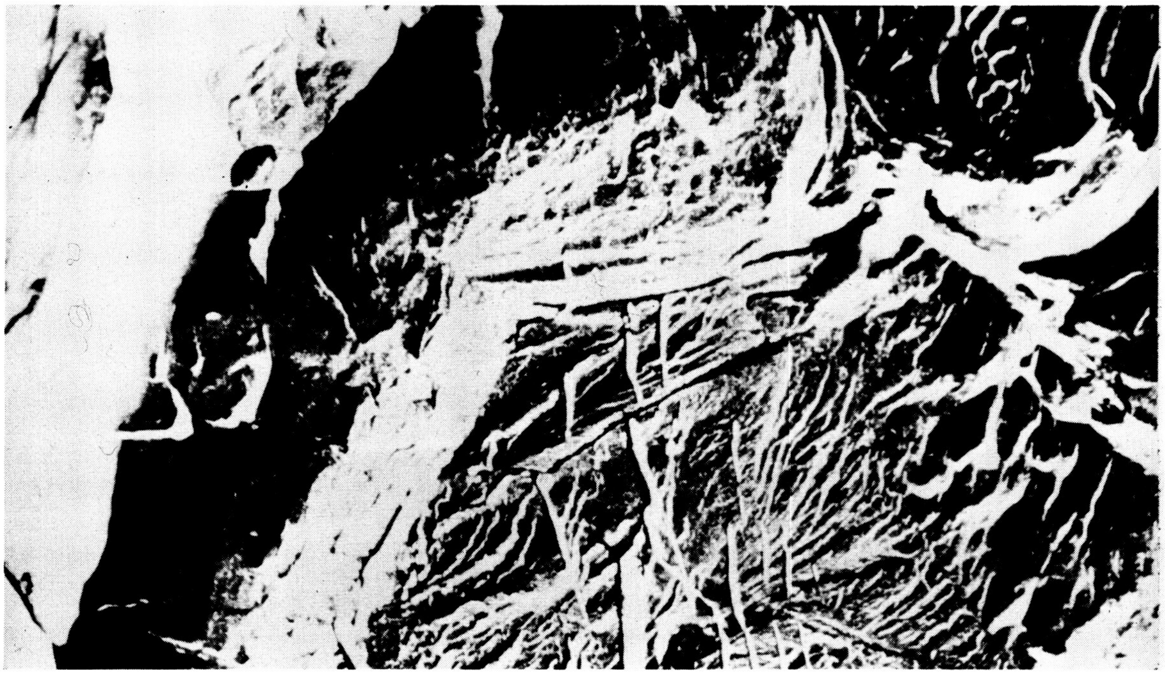

(b) Fatigue striations on two levels of crack propagation connected by tensile tear

FIGURE K-9 FRACTOGRAPHS OF TITANIUM 55A SPECIMEN 1 Aa 255 FAILED IN AXIAL FATIGUE, TEST RATIO -1, 0.25 Hz TEST CONDITIONS: 17°K UNIRRADIATED; TEST LOAD: 85% NOMINAL F_{tu}; 144.0 Ksi; 99.2 kN/cm^2; 3725 CYCLES TO FAILURE

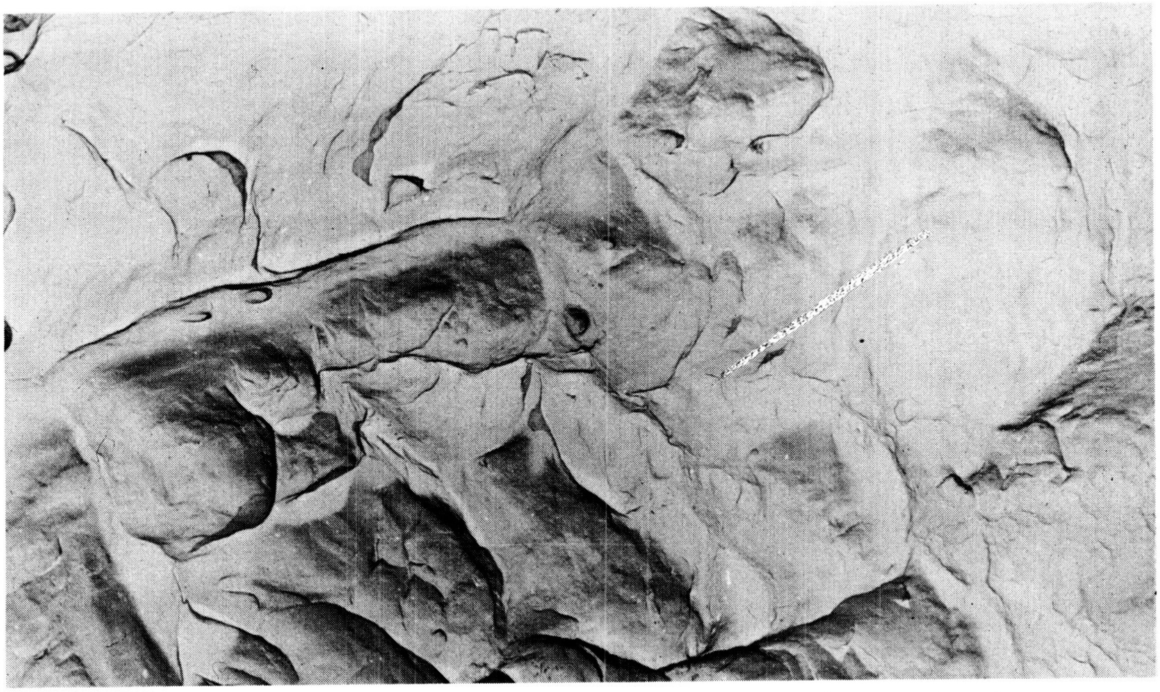

(a) No Fatigue striations observed, views of two areas of fractured surface showing dimples and cleavage feathers are shown

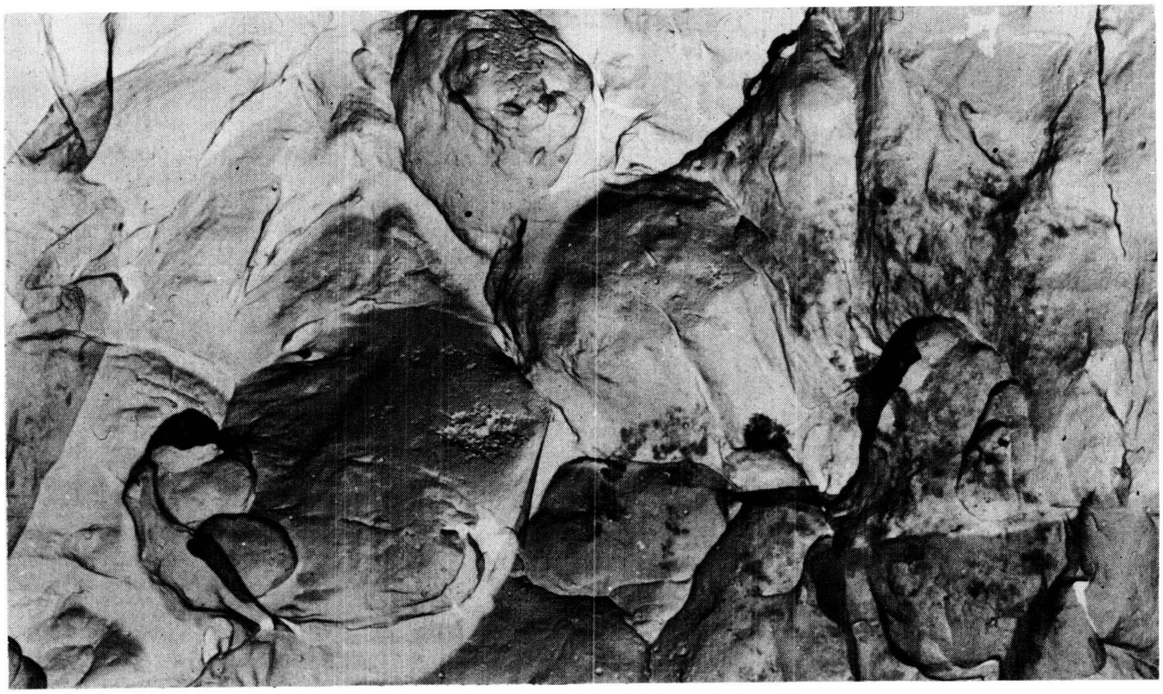

(b) No fatigue striations observed, views of two areas of fractured surface showing dimples and cleavage feathers are shown

FIGURE K-10 FRACTOGRAPHS OF TITANIUM 55A SPECIMEN 1 Aa 260 FAILED IN AXIAL FATIGUE, TEST RATIO -1, 0.25 Hz TEST CONDITIONS: 17°K AFTER IRRADIATION TO 10^{17} n/cm^2 at 17°K TEST LOAD: 100% NOMINAL F_{tu}; 169.4 Ksi; 116.8 kN/cm^2; 799 CYCLES TO FAILURE

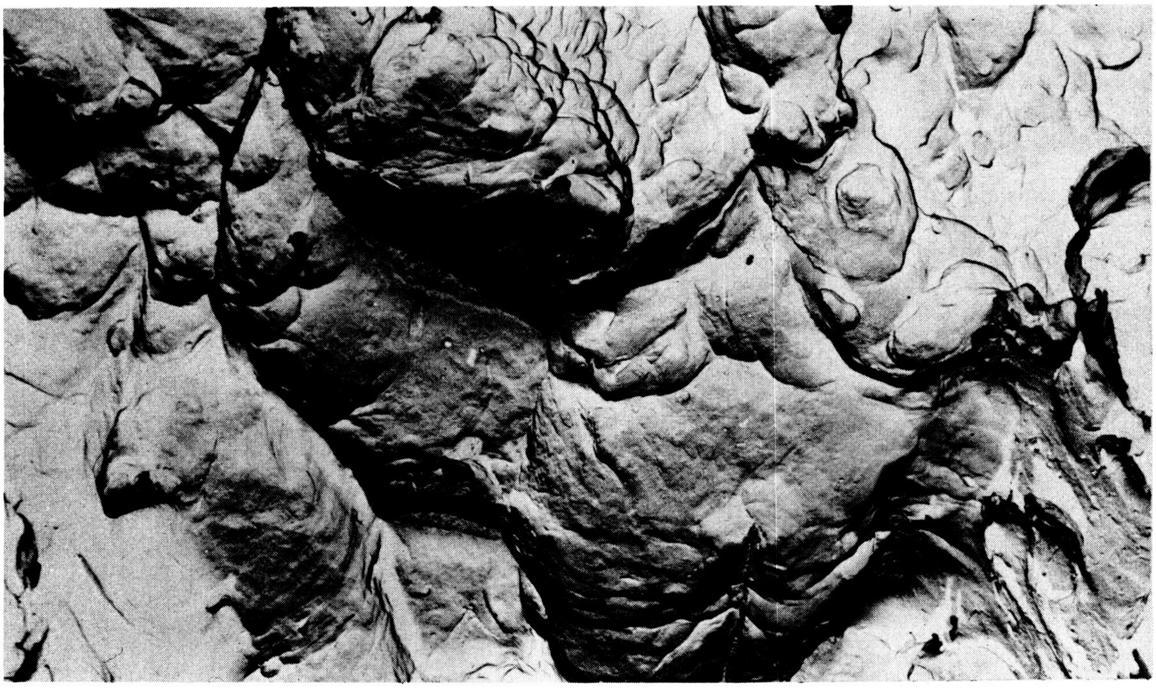

(a) No fatigue striations observed, views of two areas of fractured surface showing dimples and rub marks are shown

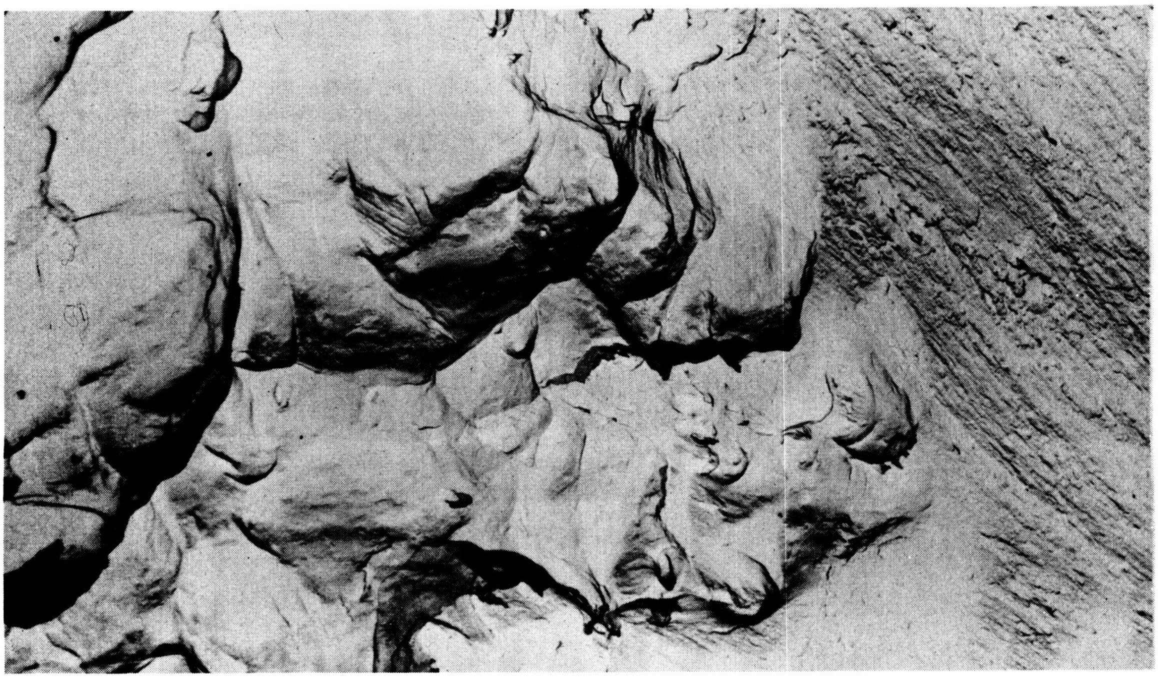

(b) No fatigue striations observed, views of two areas of fractured surface showing dimples and rub marks are shown

FIGURE K-11 FRACTOGRAPHS OF TITANIUM 55A SPECIMEN 1 Aa 253 FAILED IN AXIAL FATIGUE, TEST RATIO -1, 0.25 Hz TEST CONDITIONS: 17°K AFTER IRRADIATION TO 10^{17} n/cm^2 at 17°K TEST LOAD: 95% NOMINAL F_{tu}; 160.9 Ksi; 110.9 kN/cm^2; 1748 CYCLES TO FAILURE

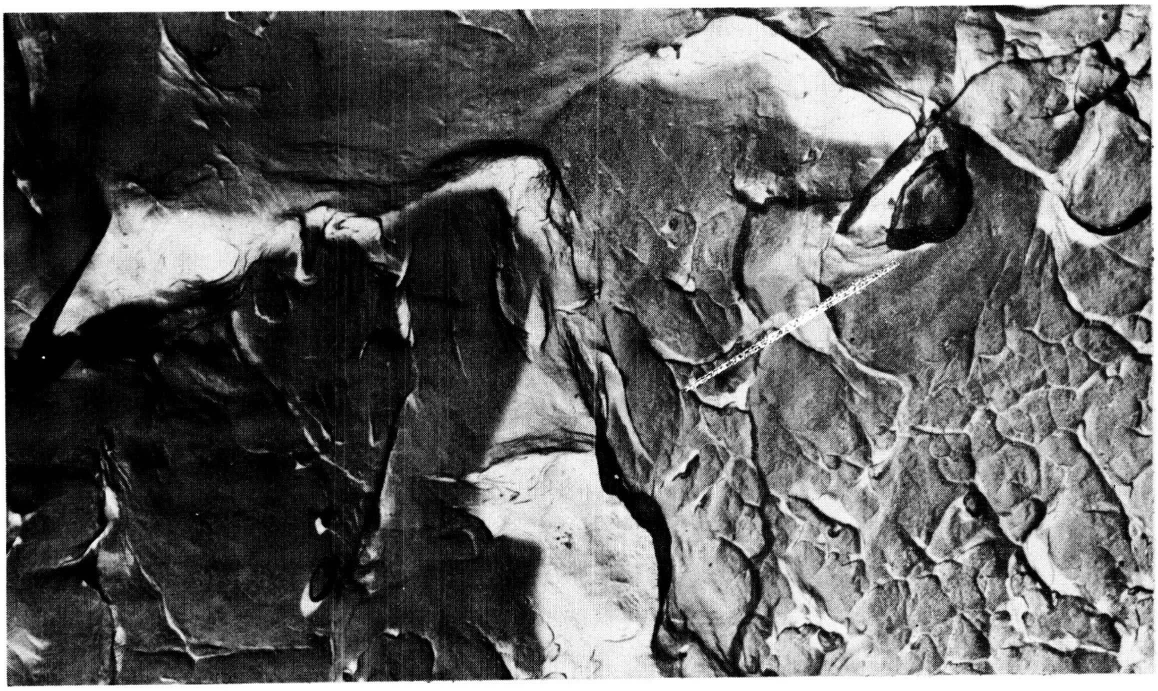

(a) No fatigue striations observed, views of two areas of fractured surface showing dimples and stretched areas are shown

(b) No fatigue striations observed, views of two areas of fractured surface showing dimples and stretched areas are shown

FIGURE K-12 FRACTOGRAPHS OF TITANIUM 55A SPECIMEN 1 Aa 244 FAILED IN AXIAL FATIGUE, TEST RATIO -1, 0.25 Hz TEST CONDITIONS: 17°K AFTER IRRADIATION TO 10^{17} n/cm^2 at 17°K TEST LOAD: 90% NOMINAL F_{tu}; 152.5 Ksi; 105.1 kN/cm^2; 3436 CYCLES TO FAILURE

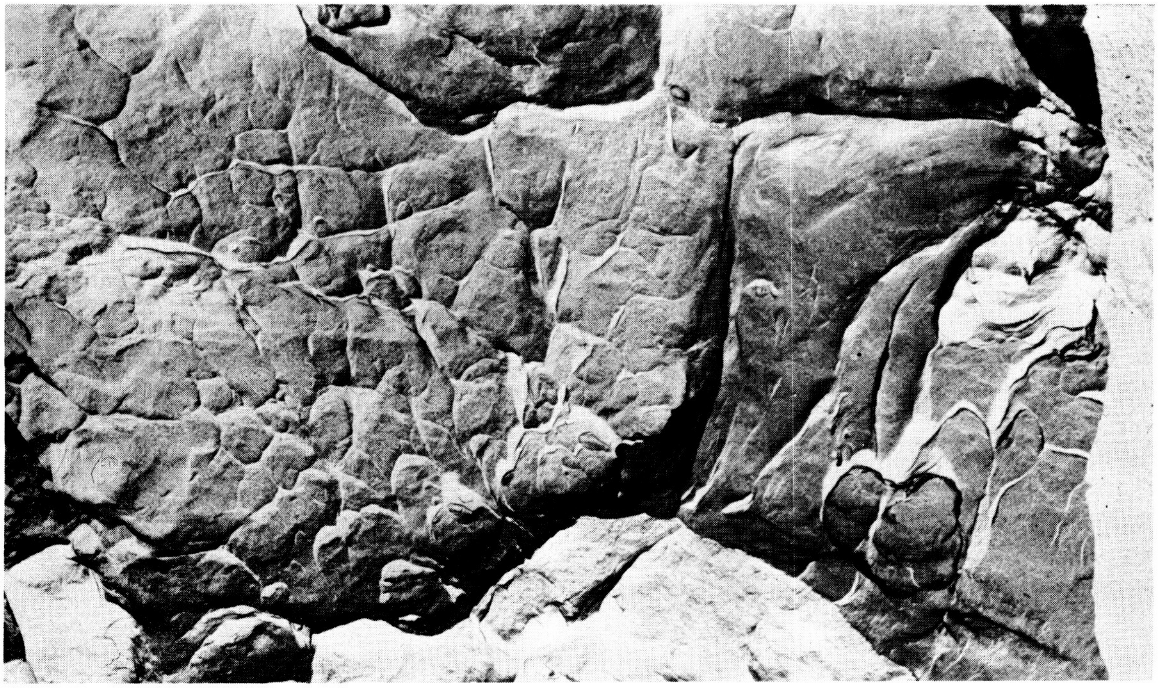

(a) No fatigue striations observed, views of two areas of fractured surface showing dimples and stretched areas are shown

(b) No fatigue striations observed, views of two areas of fractured surface showing dimples and stretched areas are shown

FIGURE K-13 FRACTOGRAPHS OF TITANIUM 55A SPECIMEN 1 Aa 245 FAILED IN AXIAL FATIGUE, TEST RATIO -1, 0.25 Hz TEST CONDITIONS: 17°K AFTER IRRADIATION TO 10^{18} n/cm^2 at 17°K TEST LOAD: 85% NOMINAL F_{tu}; 144.0 Ksi; 99.2 kN/cm^2; 4279 CYCLES TO FAILURE

TABLE K-1

FATIGUE TEST RESULTS, TITANIUM 55A-ANNEALED
(Axial Load; Test Ratio = -1; 0.25 Hz)
Tested at 300°K No Irradiation

STRESS			SPECIMEN	CYCLES TO FAILURE
Ksi	kN/cm^2	%F_{tu} *		
67.0	46.2	100	1 Aa 275	1643
			1 Aa 274	1476
			1 Aa 276	1395
63.6	43.9	95	1 Aa 240	4945
			1 Aa 241	2905
			1 Aa 264	2006
60.3	41.6	90	1 Aa 263	3764
			1 Aa 223	3198
			1 Aa 273	1498
57.0	39.3	85	1 Aa 242	6873
			1 Aa 239	6587
55.3	38.1	82 1/2	1 Aa 279	10000 (not failed)
			1 Aa 278	9051
52.3	36.1	78	1 Aa 238	10000 (not failed)
50.3	34.7	75	1 Aa 220	10000 (not failed)
			1 Aa 224	10000 (not failed)

* Mean at 300°K, unirradiated (ref. 1)

TABLE K-2

FATIGUE TEST RESULTS, TITANIUM 55A-ANNEALED
(Axial Load; Test Ratio = -1; 0.25 Hz)
Tested at 17°K, No Irradiation

STRESS			SPECIMEN	CYCLES TO FAILURE
Ksi	kN/cm^2	$\%F_{tu}$*		
160.9	110.9	95	1 Aa 256	1619
			1 Aa 267	1260
			1 Aa 268	903
152.5	105.1	90	1 Aa 248	3589
			1 Aa 250	1322
			1 Aa 266	1001
144.0	99.2	85	1 Aa 265	5576
			1 Aa 257	4035
			1 Aa 255	3725
139.8	96.4	82 1/2	1 Aa 269	5912
135.5	93.4	80	1 Aa 249	10000 (not failed)
127.1	87.6	75	1 Aa 247	10000 (not failed)

* Mean at 17°K, unirradiated (ref. 1).

TABLE K-3

FATIGUE TEST RESULTS, TITANIUM 55A-ANNEALED
(Axial Load; Test Ratio = -1; 0.25 Hz)
Tested at 17°K, Irradiated

STRESS Ksi	STRESS kN/cm^2	STRESS $\%F_{tu}$*	SPECIMEN	CYCLES TO FAILURE	NEUTRON FLUX Rate**(1)	NEUTRON FLUX Accum (2)
Tested After Irradiation to 10^{17} n/cm^2 at 17°K:						
169.4	116.8	100	1 Aa 290	2740		
			1 Aa 260	799		
			1 Aa 277	740		
			1 Aa 315	647		
160.9	110.9	95	1 Aa 280	2401		
			1 Aa 253	1748		
			1 Aa 271	1568		
152.5	105.1	90	1 Aa 270	5498		
			1 Aa 244	3436		
			1 Aa 252	2329		
144.0	99.2	85	1 Aa 329	10000 (not failed)		
			1 Aa 258	6562		
			1 Aa 245	4279		
			1 Aa 251	2964		
135.5	93.4	80	1 Aa 259	10000 (not failed)		
			1 Aa 289	10000 (not failed)		
			1 Aa 291	10000 (not failed)		
Tested During Irradiation at 17°K						
160.9	110.9	95	1 Aa 313	2105	2.4	2.7
152.5	105.1	90	1 Aa 254	2709	2.2	2.5
135.5	93.4	80	1 Aa 281	5762	2.1	5.2

* Mean at 17°K, unirradiated (ref. 1)
** Average over irradiation period

(1) $\times 10^{-12}$ n/cm^2 sec
(2) $\times 10^{-16}$ n/cm^2

APPENDIX L FATIGUE TEST RESULTS, TITANIUM 5 Al-2.5 Sn

TABLE L-1

FATIGUE TEST RESULTS, TITANIUM
5 Al-2.5 Sn (Std. I)
(Axial Load; Test Ratio = -1; 0.25 Hz)
Tested at 300°K, No Irradiation

STRESS			SPECIMEN	CYCLES TO FAILURE
Ksi	kN/cm^2	$\%F_{tu}$*		
128.3	88.5	102 1/2	3 Aa 95	327
125.2	86.3	100	3 Aa 90	949
			3 Aa 91	875
122.1	84.2	97 1/2	3 Aa 86	1333
118.9	82.0	95	3 Aa 87	2132
			3 Aa 85	2024
			3 Aa 75	1937
112.7	77.7	90	3 Aa 80	3758
			3 Aa 76	3756
			3 Aa 77	3544
106.4	73.4	85	3 Aa 78	7724
			3 Aa 82	6716
			3 Aa 79	6066
103.3	71.2	82 1/2	3 Aa 89	7229
			3 Aa 88	6968
100.2	69.1	80	3 Aa 84	10000 (not failed)
			3 Aa 83	10000 (not failed)
			3 Aa 93	8308

* Mean at 300°K, unirradiated (ref. 1)

TABLE L-2

FATIGUE TEST RESULTS, TITANIUM
5 Al-2.5 Sn (Std. I)
(Axial Load; Test Ratio = -1; 0.25 Hz)
Tested at 17°K, No Irradiation

STRESS Ksi	STRESS kN/cm^2	STRESS $\%F_{tu}$*	SPECIMEN	CYCLES TO FAILURE
258.5	178.2	115	3 Aa 122	Failed on Ramp
252.9	174.4	112.5	3 Aa 109	2946
			3 Aa 110	2450
			3 Aa 106	2136
247.3	170.5	110	3 Aa 96	4272
			3 Aa 108	2873
			3 Aa 104	2449
236.0	162.7	105	3 Aa 121	6441
			3 Aa 101	4565
			3 Aa 105	2579
224.8	155.0	100	3 Aa 92	10000 (not failed)
			3 Aa 123	7161
			3 Aa 124	6774
213.6	147.2	95	3 Aa 151	9238
			3 Aa 174	9004
			3 Aa 173	7544
			3 Aa 175	3206
202.3	139.5	90	3 Aa 97	10000 (not failed)

* Mean at 17°K, unirradiated (ref. 1)

TABLE L-3 FATIGUE TEST RESULTS, TITANIUM 5 Al-2.5 Sn (Std. I) (Axial Load; Test Ratio = -1; 0.25 Hz) Tested at 17°K Following Irradiation to 10^{17} n/cm^2 at 17°K

STRESS Ksi	kN/cm^2	%F_{tu}*	SPECIMEN	CYCLES TO FAILURE
256.3	176.7	114	3 Aa 144	1780
			3 Aa 149	1685
			3 Aa 171	1560
			3 Aa 145	1169
247.3	170.5	110	3 Aa 140	4577
			3 Aa 146	2641
			3 Aa 158	2012
			3 Aa 147	1308
236.0	162.7	105	3 Aa 160	7968
			3 Aa 141	6753
			3 Aa 148	3567
			3 Aa 139	1749
224.8	155.0	100	3 Aa 142	10000 (not failed)
			3 Aa 161	10000 (not failed)
			3 Aa 159	10000 (not failed)
			3 Aa 138	8100
			3 Aa 172	7298
213.6	147.3	95	3 Aa 156	10000 (not failed)
			3 Aa 157	10000 (not failed)
			3 Aa 155	8970

* Mean at 17°K, unirradiated (ref. 1)

TABLE L-4

FATIGUE TEST RESULTS, TITANIUM
5 Al-2.5 Sn (ELI)
(Axial Load; Test Ratio = -1, 0.25 Hz)
Tested at 300°K, No Irradiation

STRESS Ksi	kN/cm^2	%F_{tu}*	SPECIMEN	CYCLES TO FAILURE
121.3	83.6	96	8 Aa 63	446
113.8	78.5	90	8 Aa 70	764
			8 Aa 69	557
			8 Aa 71	394
107.4	74.1	85	8 Aa 72	2306
			8 Aa 67	1991
			8 Aa 73	1249
101.1	69.7	80	8 Aa 65	2928
			8 Aa 68	2387
			8 Aa 74	2036
98.0	67.6	77 1/2	8 Aa 75	5653
			8 Aa 76	4674
94.8	65.4	75	8 Aa 64	10000 (not failed)

* Mean at 300°K, unirradiated (ref. 1)

TABLE L-5

FATIGUE TEST RESULTS, TITANIUM
5 Al-2.5 Sn (ELI)
(Axial Load; Test Ratio = -1; 0.25 Hz)
Tested at 17°K, No Irradiation

STRESS			SPECIMEN	CYCLES TO FAILURE
Ksi	kN/cm^2	$\%F_{tu}$*		
239.8	165.3	105	8 Aa 94	1180
			8 Aa 85	593
			8 Aa 92	433
228.4	157.5	100	8 Aa 93	1551
			8 Aa 84	1374
			8 Aa 88	1114
217.0	149.6	95	8 Aa 89	6502
			8 Aa 87	4965
			8 Aa 83	3147
			8 Aa 135	2659
205.6	141.8	90	8 Aa 86	10000 (not failed)
			8 Aa 91	10000 (not failed)
			8 Aa 82	7152
194.1	133.8	85	8 Aa 81	10000 (not failed)

* Mean at 17°K, unirradiated (ref. 1)

TABLE L-6

FATIGUE TEST RESULTS, TITANIUM
5 Al-2.5 Sn (ELI)
(Axial Load; Test Ratio = -1; 0.25 Hz)
Tested at 17°K Following Irradiation
to 10^{17} n/cm^2 at 17°K

STRESS Ksi	kN/cm^2	%F_{tu}*	SPECIMEN	CYCLES TO FAILURE
251.2	173.2	110	8 Aa 137	453
			8 Aa 138	225
			8 Aa 136	64
			8 Aa 141	**
239.8	165.3	106	8 Aa 101	2295
			8 Aa 127	2049
			8 Aa 126	1923
228.4	157.5	100	8 Aa 124	2685
			8 Aa 97	2636
			8 Aa 125	2119
217.8	150.2	95	8 Aa 140	9523
			8 Aa 139	8085
			8 Aa 130	6467
			8 Aa 98	3841
			8 Aa 96	2823
			8 Aa 128	2355
215.6	148.7	90	8 Aa 132	10000 (not failed)
			8 Aa 129	10000 (not failed)
			8 Aa 100	4447

* Mean at 17°K, unirradiated

** Failed at end of ramp on initial application of full tensile load

TABLE L-7 FATIGUE DATA, TITANIUM ALLOY 5 Al-2.5 Sn AT 300°K

STRESS % Nom F_{tu}	MATERIAL CLASS	SPECIMEN NUMBER	CYCLES TO FAILURE
90	Std. I	3 Aa 80	3758
	(1.12 at %)	3 Aa 76	3756
	High C & N	3 Aa 77	3544
	Special Lot	3 Ad 4	1944
	(1.30 at %)	3 Ad 3	1917
	High O & H	3 Ad 8	1602
		3 Ad 2	1368
	ELI	8 Aa 70	764
	(0.62 at %)	8 Aa 69	557
		8 Aa 71	394
85	Std. I	3 Aa 78	7724
	(1.12 at %)	3 Aa 82	6716
	High C & N	3 Aa 79	6066
	Special Lot	3 Ad 5	3903
	(1.30 at %)	3 Ad 6	2833
	High O & H	3 Ad 1	2143
		3 Ad 7	1557
	ELI	8 Aa 72	2306
	(0.62 at %)	8 Aa 67	1991
		8 Aa 73	1249
80	Std. I	3 Aa 84	10000 (not failed)
	(1.12 at %)	3 Aa 83	10000 (not failed)
	High C & N	3 Aa 93	8308
	Special Lot	3 Ad 9	9361
	(1.30 at %)	3 Ad 11	6800
	High O & H	3 Ad 10	4667
	ELI	8 Aa 65	2928
	(0.62 at %)	8 Aa 68	2387
		8 Aa 74	2036

APPENDIX M REFERENCES

1. Lockheed Nuclear Products: Effect of Nuclear Radiation on Materials at Cryogenic Temperatures; Final Report, Contracts NASw-114 and NAS3-7987, NASA CR-54881; LAC ER-8434, 1966.

2. Lockheed Nuclear Products: Pedigrees of Metals and Alloys, NASw-114; LAC ER-5542, 1962 (Addendum, 1963).

3. Anon: ASTM Standards, The American Society for Testing Materials, 1966.

4. Coffin, L. F. Jr.: Low Cycle Fatigue: A Review; Appl. Mat. Res., Vol. 1, No. 3, October 1962.

5. Manson, S. S. : "Fatigue: A Complex Subject - Some Simple Approximations", NASA TM-X-52084 (1965). (William M. Murray lecture presented to the Society for Experimental Stress Analysis, Cleveland, Ohio, October 30, 1964).

6. Shen, H.; Podlaseck, S. E. ; and Kramer, I.R.: Effect of Vacuum on the Fatigue Life of Aluminum; Acta Met., Vol. 14, March 1966.

7. Cryogenics Materials Data Handbook, Technical Document Report No. ML-TDR-64-280.

8. Dieter, George E. Jr.: Mechanical Metallurgy, McGraw-Hill Book Co., Inc., 1961.

9. Wilkov, M.A. and Shield, R.: Crack Initiation in Fatigue of Metals, Air Force Office of Scientific Research Scientific Report AFOSR560-65, EMRL-RM 1012, May 1966.

10. Coffin, L.F. Jr.: Low Cycle Fatigue, Met. Eng. Quart., November 1963.

11. Brinkman, J.A. and Wiedersich, H.: Flow and Fracture of Metals and Alloys in Nuclear Environments, ASTM Special Technical Publication No. 380, 1965.

12. Holmes, D.K.: The Interaction of Radiation with Solids, John Wiley and Sons, 1964.

13. Barnes, R.S.: Flow and Fracture of Metals and Alloys in Nuclear Environments, ASTM Special Technical Publication No. 380, 1965.

14. Coltman, R.R.; Klabunde, C.G.; McDonald, D.C. and Redman, J.K.: Reactor Damage in Pure Metals, J. Appl. Phys. Vol. 33, No. 12, December 1962.

15. Coltman, R.R.: Private Communication, 1962

16. Phillips, A.; Kerlins, V.; and Whitson, B.V.: Electron Fractography Handbook, U. S. Air Force, ML-TDR-64-416.

APPENDIX N DISTRIBUTION

NASA-Lewis Research Center (3)
21000 Brookpark Road
Cleveland, Ohio 44135
Attention: Charles L. Younger (NSD)

NASA-Lewis Research Center (1)
21000 Brookpark Road
Cleveland, Ohio 44135
Attention: T. J. Flanagan (P&SD)

NASA-Lewis Research Center (1)
21000 Brookpark Road
Cleveland, Ohio 44135
Attention: Norman T. Musial

NASA-Scientific & Technical
Information Facility (6)
Box 5700
Bethesda, Maryland 20014
Attention: NASA Representative
(CRT)

NASA-Lewis Research Center (2)
21000 Brookpark Road
Cleveland, Ohio 44135
Attention: Library

NASA-Lewis Research Center (1)
21000 Brookpark Road
Cleveland, Ohio 44135
Attention: Report Control Office

U. S. Atomic Energy Commission (3)
Technical Reports Library
Washington, D.C.

U. S. Atomic Energy Commission (1)
Division of Technical Information
Extension
P. O. Box 62
Oak Ridge, Tennessee 37831

National Aeronautics & Space
Administration (1)
Washington, D.C. 20546
Attention: George C. Deutsch
(Code RRM)

National Aeronautics & Space
Administration (1)
Washington, D.C. 20546
Attention: David Novik, Chief
(Code RNV)

AEC-NASA Space Nuclear Propulsion
Office (2)
U. S. Atomic Energy Commission
Washington, D.C. 20545
Attention: F. C. Schwenk

AEC-NASA Space Nuclear Propulsion
Office (1)
U. S. Atomic Energy Commission
Washington, D.C. 20545
Attention: J. E. Morrissey

National Aeronautics & Space
Administration (1)
Space Nuclear Propulsion Office-
Cleveland
Lewis Research Center
21000 Brookpark Road
Cleveland, Ohio 44135
Attention: L. C. Corrington

NASA-Lewis Research Center (3)
21000 Brookpark Road
Cleveland, Ohio 44135
Attention: M.H. Krasner,
Mail Stop 49-2

NASA-Lewis Research Center (1)
21000 Brookpark Road
Cleveland, Ohio 44135
Attention: H.J. Heppler, Jr.

NASA-Lewis Research Center (2)
21000 Brookpark Road
Cleveland, Ohio 44135
Attention: Dr. John C. Liwosz

NASA-Plum Brook Station (3)
Sandusky, Ohio 44870
Attention: Don B. Crandall

NASA-Lewis Research Center (1)
21000 Brookpark Road
Cleveland, Ohio 44135
Attention: Office of Reliability &
Quality Assurance

NASA-Ames Research Center (1)
Moffett Field, California 94035
Attention: Library

NASA-Flight Research Center (1)
P.O. Box 273
Edwards, California 93523
Attention: Library

NASA-Goddard Space Flight Center (1)
Greenbelt, Maryland 20771
Attention: Library

Jet Propulsion Laboratory (1)
4800 Oak Grove Drive
Pasadena, California 91103
Attention: Library

NASA-Langley Research Center (1)
Langley Station
Hampton, Virginia 23365
Attention: Library

NASA-Manned Spacecraft Center (1)
Houston, Texas 77001
Attention: Library

NASA-Western Operations (1)
150 Pico Boulevard
Santa Monica, California 90406
Attention: Library

NASA-Marshall Space Flight Center (1)
Huntsville, Alabama 35812
Attention: Library

NASA-Marshall Space Flight Center (1)
Huntsville, Alabama 35812
Attention: W.Y. Jordan, P&VE-FN

NASA-Marshall Space Flight Center (1)
Huntsville, Alabama 35812
Attention: Dr. W.R. Lucas,
M-P & VE-M

NASA-Marshall Space Flight Center (1)
Huntsville, Alabama 35812
Attention: R.D. Shelton, M-RP-N

Aerojet-General Corporation (1)
P.O. Box 1947
Sacramento, California
Attention: W.A. Greenhow, Manager
Radiation Effects Program
Department 7431

Aerojet-General Corporation (2)
P.O. Box 1947
Sacramento, California
Attention: C.K. Soppet, Manager
Nuclear Operations

Aerojet- General Corporation (3)
P.O. Box 296
Azusa, California
Attention: C.N. Trent, Associate Director
NERVA Operations

Aerojet-General Corporation (1)
P.O. Box 1947
Sacramento, California
Attention: Dr. W. Weleff

Aerojet-General Nucleonics (1)
A Division of Aerojet-General
Corporation
P.O. Box 77
San Ramon, California 94583
Attention: G. A. Linenberger,
General Manager

Aluminum Company of America (1)
P.O. Box 1012
New Kensington, Pennsylvania
Attention: Edwin H. Spuhler

Argonne National Laboratories (1)
P.O. Box 299
Lemont, Illinois
Attention: T. H. Blewitt

Argonne National Laboratory (1)
Library Services Dept. 203-CE 125
9700 South Cass Avenue
Argonne, Illinois 60440
Attention: Report Section

Arthur D. Little Company, Inc. (1)
Acorn Park
Cambridge, Massachusetts
Attention: Charles A. Schulte

Atomics International (4)
P.O. Box 309
Canoga Park, California
Attention: F. E. Farhat, Librarian

Battelle Memorial Institute (1)
505 King Avenue
Columbus, Ohio 43201
Attention: D.J. Hammon, Radiation
Effects Information Center

Battelle Memorial Institute (1)
505 King Avenue
Columbus, Ohio 43201
Attention: Roger J. Runck

Battelle Memorial Institute (1)
Northwest Laboratories
326 Building, 300 Area
Richland, Washington 99352
Attention: Dr. T. T. Claudson

Battelle-Northwest (1)
P.O. Box 999
Richland, Washington 99352
Attention: Spencer H. Bush

Beech Aircraft Corporation (1)
P.O. Box 631
Boulder, Colorado 80301
Attention: Technical Library

The Bendix Corporation (1)
Research Laboratory Division
Southfield, Michigan
Attention: Frank W. Poblenz,
Library Services

The Boeing Company (1)
Aerospace Group
P.O. Box 3707
Seattle, Washington 98124
Attention: Ruth E. Peerenboom,
Processes Supervisor

Brookhaven National Laboratory (1)
Upton Long Island, New York 11973
Attention: D.H. Gurinsky

Brookhaven National Laboratory (1)
Upton Long Island, New York 11973
Attention: Paul W. Levy, Department of Physics

Bureau of Naval Weapons (1)
Washington, D.C.
Attention: J.H. Terry, Captain, RRNU

California Institute of Technology (1)
1201 East California Street
Pasadena, California 91109
Attention: General Library

Carbone Company (1)
Toonton, New Jersey
Attention: E.P. Eaton

Carpenter Steel Company (1)
P.O. Box 662
Reading, Pennsylvania
Attention: Neil J. Culp

Department of the Army (1)
United States Army Munitions Command
Frankford Arsenal
Philadelphia, Pennsylvania
Attention: Librarian

Douglas Aircraft Company, Inc. (2)
Missile & Space Systems Division
3000 Ocean Park Blvd.
Santa Monica, California 90406
Attention: A2-260 Library

General Dynamics/Convair (1)
P.O. Box 1128
San Diego, California 92112
Attention: A. Hurlich, Manager Materials & Processes Section, Mail Zone 572-00

General Dynamics/Fort Worth (1)
P.O. Box 748
Fort Worth, Texas 76101
Attention: Mr. Bob Vollmer, Administrative Assistant President's Office

General Electric Company (1)
Nuclear Materials & Propulsion Operation
P.O. Box 132
Cincinnati, Ohio 45215
Attention: J.W. Stephenson

Hughes Aircraft Company (1)
Nucleonics Division
Fullerton, California
Attention: Dr. A.M. Liebschutz

IIT Research Institute (1)
10 W. 35th Street
Chicago 16, Illinois
Attention: D.J. McPherson, Vice President

International Nickel Company, Inc. (1)
Huntington Alloy Products Division
Huntington, West Virginia
Attention: E.B. Fernsler

Kaman Aircraft Corporation (1)
Kaman Nuclear Division
Colorado Springs, Colorado
Attention: Mary G. Brown, Librarian

Lockheed-California Company (1)
P.O. Box 551
Burbank, California 91503
Attention: Dr. Lewis Larmore

Lockheed-California Company (2)
Burbank, California 91503
Attention: Central Library, Bldg. 63 Scientific & Technical Information Center

Lockheed-California Company (1)
Burbank, California 91503
Attention: H.B. Wiley,
Engineering Research

Lockheed-Georgia Company (1)
Nuclear Laboratory
P.O. Box 128
Dawsonville, Georgia
Attention: Dr. M.M. Miller, Manager
Nuclear Aerospace Division

Lockheed-Georgia Company (15)
P.O. Box 2155
Sandusky, Ohio 44870
Attention: C. A. Schwanbeck

Lockheed-Georgia Company (1)
Nuclear Laboratory
P.O. Box 128
Dawsonville, Georgia
Attention: Information Center

Lockheed Missiles & Space Company (1)
3251 Hanover Street
Palo Alto, California
Attention: John C. McDonald,
Materials Research Staff

Lockheed Missiles & Space Company (2)
3251 Hanover Street
Palo Alto, California
Attention: Sci-Tech Information Center

Lockheed Aircraft Corporation
Lockheed Missiles & Space Company (1)
P.O. Box 551, Burbank, California
Attention: M.A. Steinberg

Lockheed Missiles & Space Company (1)
Sunnyvale, California
Attention: H.F. Plank, Nuclear Space
Programs

Los Alamos Scientific Laboratory (1)
P.O. Box 1663
Los Alamos, New Mexico 87544
Attention: Glen A. Graves

Los Alamos Scientific Laboratory (3)
P.O. Box 1663
Los Alamos, New Mexico 87544
Attention: Report Library

The Martin Company (1)
P.O. Box 179
Denver, Colorado 80201
Attention: F.R. Schwartzberg, G0534

Mechanical Properties Data Center (1)
Suttons Bay, Michigan 49682
Attention: Matthew J. Kanold,
Administrative Assistant

National Bureau of Standards (1)
Boulder, Colorado 80302
Attention: Cryogenic Data Center

National Bureau of Standards (1)
Cryogenic Engineering Laboratory
Boulder, Colorado 80302
Attention: R.P. Reed

North American Aviation (1)
Rocketdyne Division
6633 Canoga Avenue
Canoga Park, California
Attention: Technical Information Center

North American Aviation, Inc. (1)
Space & Information Systems Division
12214 Lakewood Blvd.
Downey, California 90241
Attention: Technical Information Center
D/41-096-410, AJ01
For: T. M. Littman, D/141-093-33

Northrop Corporation (1)
Norair Division
3901 W. Broadway
Hawthorne, California
Attention: Technical Information 3343-32

Oak Ridge National Laboratory (1)
Oak Ridge, Tennessee 37831
Attention: D.S. Billington

Ohio State University Libraries (1)
Serial Division
1858 Neil Avenue
Columbus, Ohio 43210

Pennsylvania State University (1)
105 Hammond Building
University Park, Pennsylvania 16802
Attention: Mr. Joseph Marin, Engineering Mechanics Department

Picatinny Arsenal (1)
Technical Information Section, SMUPA-VA6
Dover, New Jersey 07801
Attention: Commanding Officer

Purdue University (1)
Lafayette, Indiana
Attention: Librarian

Pure Carbon Company (1)
Wellsville Street
Saint Marys, Pennsylvania
Attention: Robert Paxon

Reynolds Metals Company (1)
6601 West Broad Street
Richmond, Virginia
Attention: L. E. Householder

Rice University (1)
P.O. Box 1892
Houston, Texas 77001
Attention: The Fondren Library

Rocketdyne (1)
A Division of North American Aviation, Inc.
6633 Canoga Avenue
Canoga Park, California
Attention: Mr. G.A. Fairboirn, D/596-174Z-2

Sandia Corporation (1)
P.O. Box 5800
Sandia Base
Albuquerque, New Mexico 87115
Attention: Technical Library

Southeastern Research Insitute (1)
Birmingham, Alabama
Attention: J.R. Kattus

Special Metals, Inc. (1)
New Hartford, New York
Attention: Robert Neilsen

Titanium Metals Corporation of America (1)
233 Broadway
New York, New York
Attention: E.F. Erbin, Staff

TRW Systems (1)
Technical Information Center
One Space Park
Redondo Beach, California 90278

U.S. Air Force (1)
Air Force Weapons Laboratory
Kirtland AFB, New Mexico 87117
Attention: Technical Library (WLIL)

U.S. Air Force (1)
AF Materials Laboratory, Research & Technology Division, AFSC
Wright-Patterson AFB, Ohio 45433
Attention: Harold M. Hormann

U.S. Air Force (1)
Foreign Technology Division, TDEPR
Wright-Patterson AFB, Ohio 45433
Attention: Lt. Schauffle

U.S. Air Force (1)
AFML (MAAM) (1A)
Wright-Patterson AFB, Ohio 45433

U.S. Army Materials Research Agency (1)
Watertown Arsenal
Watertown, Massachusetts
Attention: T.S. DeSisto

U.S. Naval Research Laboratory (1)
Washington, D.C. 20390
Attention: Dr. Albert V.H. Masket, Mechanics Division, Code 6204

U.S. Naval Research Laboratory (1)
Washington, D.C. 20390
Attention: L.E. Steele, Head, Reactor Materials Branch, Metallurgy Division

United States Steel Corporation (1)
Monroeville, Pennsylvania
Attention: Waldo Rall

University of California (1)
Lawrence Radiation Laboratory
Berkeley, California
Attention: Technical Information Division

University of California (1)
Lawrence Radiation Laboratory
P.O. Box 808
Livermore, California
Attention: Technical Information Division

University of California (1)
Los Alamos Scientific Laboratory
P.O. Box 1663
Los Alamos, New Mexico 87544
Attention: W.L. Kirk

University of California (1)
405 Hilgard Avenue
Los Angeles, California 90024
Attention: Engineering & Mathematical Sciences Library

University of California (1)
University Research Library
Los Angeles, California 90024
Attention: Serials Department

University of Chicago (1)
5640 Ellis
Chicago, Illinois 60637
Attention: Institute of Metals Library

University of Colorado (1)
Engineering Research Center
Boulder, Colorado
Attention: K.D. Timmerhaus, Associate Dean of Engineering

University of Georgia Libraries (2)
Athens, Georgia 30601
Attention: Acquisitions Division

University of Michigan (1)
Ann Arbor, Michigan 48104
Attention: Robert G. Carter, University Library

Westinghouse Electric Corporation (1)
Astronuclear Laboratory
P.O. Box 10864
Pittsburgh, Pennsylvania 15235
Attention: Dr. D.E. Thomas, Manager Materials Department

Westinghouse Electric Corporation (1)
Metallurgical Division
Pittsburgh, Pennsylvania 15235
Attention: E.T. Wessel, Research & Development Center

ABSTRACT

Strain hardened high purity aluminum (1099-H14) and several titanium alloys were tested in tension after irradiation exposures to several fluences and, in the case of aluminum, with varying cryogenic thermal histories. Low cycle fatigue tests were performed on unalloyed titanium and Titanium 5% Al-2.5% Sn, with varying interstitial contents, at 17°K after irradiation exposure to 10^{17} n/cm^2 (fast). The test data are reported and a number of conclusions are drawn.